Solving the Static Resource Allocation Problems in Next Generation Optical Networks

March 2024

Jiading Wang

Solving the Static Resource Allocation Problems in Next Generation Optical Networks

Graduate School of Science and Technology

Degree Programs in Systems and Information Engineering

University of Tsukuba

March 2024

Jiading Wang

Abstract

In recent years, with the proliferation of emerging Internet services such as high-definition video, online education, remote work, cloud computing, etc., network traffic is also growing explosively. As a result, the demand for network bandwidth is also growing, which directly contributes to the technology advancement of physical devices for optical networks. In order to cope with the growing network traffic and bandwidth demand, from the deployment of traditional wavelength switched optical networks (WSONs) in the early 2000s, thanks to the technology advancement of physical devices, the optical network architecture has gone through several significant evolutions.

As the highly representative optical network architectures of next generation optical networks, spectrally flexible elastic optical networks (EONs) and spectrally and spatially flexible space division multiplexing elastic optical networks (SDM-EONs) are the focus in our work. Different from traditional WSONs, which have been fully commercialized currently, EONs employ flexible wavelength assignment technology with smaller spectral granularity to improve the efficiency and flexibility of diverse traffic transmission. On the other hand, SDM-EONs are considered to be one of the most promising network architectures to meet the rapid growth of Internet traffic by adding spatial dimensions to EONs via space division multiplexing (SDM) technology, leading to a significant increase in transmission capacity.

In this thesis, we begin with an introduction to the evolution history of optical network architectures and the resource allocation problems needing to be solved in each generation of architectures. Through a review of previous work related to the resource allocation problems, our contributions to static resource allocation in EONs and SDM-EONs are clarified. After that, we discuss the related background technologies and assumptions needed to be used in this thesis in detail for several typical optical network architectures. Next, we focus on the static resource allocation problem in EONs, in order to better understand the characteristics of various types of mathematical optimization models for this problems in next generation optical networks. Specifically, we divide the models for the problem in EONs into four types based on different perspectives for routing and spectrum assignment. Afterwards, we analyze and summarize the characteristics of each model, and propose a series of improved methods to enhance the computational performance of each model. This work can be a reference for mathematical modeling of the optical network resource allocation problems in different generations. In addition, we extend the node-type model from EONs to make it applicable to the problem in SDM-EONs. Since the model has a large number of constraints and variables and is difficult to solve directly, we proposed three exact algorithms based on model decomposition to better solve it. Moreover, it is shown via simulation experiments that our model can provide a more accurate solution compared to the model in previous work. This work will assist network operators in designing more efficient and reasonable resource supply schemes in network planning for SDM-EONs.

Acknowledgements

I would like to express my sincere gratitude to my doctoral advisor, Professor Maiko Shigeno, from the Institute of Systems and Information Engineering at the University of Tsukuba, Japan. Throughout my entire graduate school journey, she has provided me with invaluable academic guidance, encouragement, and support. Her dedication to scholarly pursuits, along with her caring and considerate approach towards students, not only inspired my academic research but also influenced my daily life.

I also extend my thanks to Professor Akiko Yoshise, another esteemed faculty member from the Institute of Systems and Information Engineering at the University of Tsukuba, who served as my master's advisor and co-guided me during my doctoral studies. Her rigorous and conscientious academic attitude has consistently motivated and propelled me forward.

I am deeply grateful to several other professors in the adviser group and the reviewer group who provided unique and valuable insights during the review of my thesis. Their thoughtful feedback has significantly contributed to the improvement of my work.

Special appreciation goes to my friends and fellow students for their unwavering support and assistance throughout my doctoral journey. Their camaraderie has been a source of strength and motivation.

I would like to express my deep gratitude to the Japan Science and Technology Agency (JST) for the research grants and financial support, which played a crucial role in the successful completion of my doctoral studies.

Lastly, I want to convey my deepest thanks to my beloved wife, Wan Lau, and my parents. Their love, understanding, and unwavering support over the years have been the pillars of my success in obtaining a doctoral degree. I am truly grateful for their presence in my life.

Contents

List of Figures

List of Tables

List of Abbreviations

16QAM	16-ary quadrature amplitude modulation
8QAM	8-ary quadrature amplitude modulation
ASLC-MD	All space lane change model decomposition
BDM	Bandwidth division multiplexing
BPSK	Binary phase-shift keying
BVT	Bandwidth-variable transceiver
BV-WSS	Bandwidth-variable wavelength selective switch
BV-WXC	Bandwidth-variable wavelength cross-connect
B&S ROADM	Broadcast-and-select reconfigurable optical add-drop multiplexer
CO-OFDM	Coherent optical orthogonal frequency division multiplexing
DAC	Digital-to-analog converter
DAT	Distance adaptive transmission
DMD	Direct model decomposition
DWDM	Dense wavelength division multiplexing
DP	Dual-polarization
DP-16QAM	Dual-polarization 16-ary quadrature amplitude modulation
DP-8QAM	Dual-polarization 8-ary quadrature amplitude modulation
DP-BPSK	Dual-polarization binary phase-shift keying
DP-QPSK	Dual-polarization quadrature phase-shift keying
DSP	Digital signal processor
EON	Elastic optical network
EDFA	Erbium-doped fiber amplifier
FB	Fiber bundle
FIFO	Fan-in and fan-out
FMF	Few-mode fiber

FMFB	Few-mode fiber bundle
FM-MCF	Few-mode multi-core fiber
FrJ-Sw	Fractional joint switching
FS	Frequency slot
GB	Guard band
Gbaud	Giga baud
Gbps	Giga bits per second
GHz	Giga hertz
Hz	Hertz
ILP	Integer linear programming
In-Sw	Independent switching
IoT	Internet of things
IQ-MOD	In-phase and quadrature modulator
ITU-T	International Telecommunication Union Telecommunication Standardization Sector
J-Sw	Joint switching
KSP	K-shortest path
LS	Laser source
MB	Multi-band
MB-EON	Multi-band elastic optical network
MB-SDM-EON	Multi-band space division multiplexing elastic optical network
MCF	Multi-core fiber
MIMO	Multi-input and multi-output
MMF	Multi-mode fiber
N-WDM	Nyquist wavelength division multiplexing
OC	Optical carrier
OCh	Optical channel
OFDM	Orthogonal frequency division multiplexing
OSNR	Optical signal-to-noise ratio
O-E-O	Optical-electrical-optical
Pbps	Peta bits per second
QoT	Quality of transmission

QPSK	Quadrature phase-shift keying
RCSA	Routing, core, and spectrum assignment
RMSA	Routing, modulation format and spectrum assignment
RMSSA	Routing, modulation format, space and spectrum assignment
ROADM	Reconfigurable optical add-drop multiplexer
RSA	Routing and spectrum assignment
RSSA	Routing, space and spectrum assignment
RWA	Routing and wavelength assignment
Rx	Receiver
R&S ROADM	Route-and-select reconfigurable optical add-drop multiplexer
SCN	Spatial channel network
SDM	Space division multiplexing
SDM-EON	Space division multiplexing elastic optical network
SL	Space lane
SLC	Space lane change
SMF	Single-mode fiber
SMFB	Single-mode fiber bundle
SM-MCF	Single-mode multi-core fiber
Spa SpCh	Spatial super channel
SpCh	Super channel
Spe SpCh	Spectral super channel
Spe & Spa SpCh	Spectral and spatial super channel
SSLC-MD	Semi space lane change model decomposition
Tbps	Tera bits per second
TDM	Time division multiplexing
Tx	Transmitter
WDM	Wavelength division multiplexing
WSON	Wavelength switched optical network
WSS	Wavelength selective switch
WXC	Wavelength cross-connect
XT	Intercore crosstalk

Chapter 1

Introduction

In recent years, the rapid growth of data-intensive applications such as cloud computing, multimedia streaming, and internet of things (IoT) has led to an unprecedented demand for high-speed and efficient communication networks. Optical networks have emerged as a promising solution to meet these escalating bandwidth requirements due to their inherent characteristics of high capacity and low latency.

As shown in Fig. 1.1, since the beginning of this century, technologies of optical networks have shown an unprecedented high-speed development trend [1]. Among them, wavelength division multiplexing (WDM) -based wavelength switched optical network (WSON) has been widely used in various current optical network scenarios, while elastic optical network (EON) and space division multiplexing elastic optical network (SDM-EON) are widely noticed as promising next-generation optical networks due to their larger network capacity and higher spectral flexibility. However, due to the varying characteristics of new optical network architectures, in order to ensure the optimal utilization of network resources while meeting the stringent quality of transmission (QoT) requirements of different applications, we need to design efficient resource allocation schemes to correspond to the challenges posed by the new architectures.

In this chapter, we briefly introduce the static resource allocation problems and summarize our contributions to the research in this field. Finally, we state the structure of this thesis.

1.1 Static resource allocation problems in optical networks

Thanks to technological advances in physical devices, optical network architectures have evolved rapidly. However, the new architectures have created a wide variety of new network resources and restrictions on resource utilization. As a result, the resource allocation methods in the existing architecture will be difficult to adapt to the new architectures.

Figure 1.1: Evolution of optical transmission system over the last few decades.

Therefore, designing efficient and reasonable resource utilization schemes has become an important task that next generation optical network architectures must address in their applications.

Resource allocation problems in optical networks, such as routing and wavelength assignment (RWA) in WSONs, routing and spectrum assignment (RSA) or routing, modulation format and spectrum assignment (RMSA) in EONs, and routing, space and spectrum assignment (RSSA) or routing, modulation format, space and spectrum assignment (RMSSA) in SDM-EONs, can be divided into static (e.g., [2–21]) and dynamic scenarios (e.g., [8,22–27]). In static scenarios, all connection requests are known in advance, and the objectives are usually to determine the network design required to accommodate all known connection requests or to minimize the amount of resources required for various sets of known connection requests. In contrast, in dynamic scenarios, we deal with connection requests that occur and disappear based on the passage of time. We typically simulate actual connection situations and study how to design the network and distribute connection requests so that connection requests are served in real time [28].

To solve resource allocation problems in optical networks, mathematical optimization techniques are generally adopted. These techniques can be classified into two approaches. One approach is to find the exact optimal solution (e.g., [2–4, 7, 8]). When we formulate the problem as an integer linear programming (ILP) problem, we can solve it exactly by using solvers [15, 16]. If we employ such an approach, modeling and formulating the problem as an ILP depend on the efficiency of solving it. The scales of the instances that can be solved in a reasonable time by this approach are often much smaller than those in real application scenarios, making the approach suitable for static scenarios where an exact optimal solution is required and there is enough time for investigation. In contrast, using heuristic algorithms enables finding better solutions within a relatively short time (e.g., [8, 17, 18, 29]). In particular, in the dynamic case, since the network is in the practical stage and the QoT is important, the scalability of the approach and the response time to each connection request are prioritized [8]. Moreover, it is also often difficult to find high-quality solutions in reasonable time for solving large-scale instances in static scenarios. Therefore, if we require a fast and reasonable resource allocation scheme rather than an exact optimal solution, in this case, heuristic algorithms are usually used to solve the optimization problem quickly, instead of using an ILP model to find an exact solution.

In this thesis, we focus on the static RSA/RMSA and RMSSA problems for two next generation optical networks, EONs and SDM-EONs, which are widely noticed and anticipated in recent years. We selected EONs and SDM-EONs for our study as they are established architectures with extensive research support. While other architectures of next generation

optical networks are also promising, EONs and SDM-EONs offer a robust foundation for optical network research. Studying these architectures provides core insights that benefit future research. Furthermore, the main reason for focusing on the static scenario of resource allocation is that it plays a critical role in the initial design and planning of next generation optical networks. While dynamic scenarios are important and reflect real-time network conditions, understanding the static resource allocation in the planning phase is essential. Researching resource allocation problems in static scenarios for EONs and SDM-EONs is crucial for understanding their performance, developing theoretical foundations, aiding network planning and design, facilitating comparisons, and directly improving resource allocation efficiency in specific applications. By addressing the static scenarios, this research aims to develop insights and mathematical optimization models that can inform both static and dynamic resource allocation strategies, contributing to the long-term efficiency and performance of next generation optical networks.

1.2 Motivations and contributions

1.2.1 Contribution to the RSA/RMSA problem

The RSA/RMSA problem in EONs has garnered significant attention, and several works have focused on solving it using ILP models [2–14, 29]. In this thesis, we present a comprehensive summary of mathematical optimization models for the static RSA/RMSA problem from two distinct perspectives: routing and spectrum assignment.

Regarding routing, the models can be categorized into node-type and path-type, while spectrum assignment models fall into slot-type and channel-type classifications. Furthermore, the consideration of multiple modulation formats is essential in EONs, where DAT is used to dynamically select the optimal modulation level for signals [5]. By combining routing and spectrum assignment models with modulation format considerations, we identify four primary types of mathematical optimization models: node/slot, node/channel, path/slot, and path/channel.

Various types of ILP models have been discussed in previous works on different optical networks with or without considering multiple modulation formats, as shown in Table 1.1. To the best of our knowledge, as shown in the table 1.1, while there are many researches using or comparing several models, this research is the first work to have a unified discussion of all four models, which contributes to a better understanding of the characteristics of the various types of models. Moreover, in order to analyze the characteristics of each model, we formulate these four models respectively for the RSA problem considering the modulation formats (i.e., the RMSA problem) in Chapter 3.

Table 1.1: Related models considered in previous works.

Refs.	Models				Modulation
	path/slot	path/channel	node/slot	node/channel	
[2, 4, 9, 10, 13, 29]	Y	N	N	N	Y
[3]	N	Y	N	Y	N
[15, 17, 19]	N	Y	N	N	Y
[5]	Y	Y	Y	N	Y
[8]	N	Y	N	Y	N
[14]	N	N	Y	Y	Y
[16]	Y	Y	N	N	Y
[12]	Y	Y	N	Y	N
our work	Y	Y	Y	Y	Y

For instance, Christodoulopoulos et al. [2] formulated an RMSA problem model, which aligns with our path/slot model. Their work also proposed a decomposition method that breaks down the RSA problem with modulation formats into two constituent subproblems.

Velasco et al. [3] pioneered a channel-based ILP model for the RSA problem without considering modulation formats, and they compared it with a slot-based model. On the other hand, Walkowiak et al. [11] presented a path/channel model, slightly different from Velasco et al.'s model, as it considered the RSA problem with modulation formats. This model is similar to our path/channel model.

Cai et al. [7] proposed a node-type model for the RSA problem without considering modulation formats, which shares similarities with our node/slot model. Additionally, Velasco et al. [8] formulated a node-link model using precomputed slots for the RSA problem without considering modulation formats, which is similar to our node/channel model. It is notable that both our node/slot and node/channel models for RMSA problem in this thesis are original since there are few previous works that formulated node-type models in the context of considering modulation formats.

To better comprehend the characteristics of each model type and enhance their applicability in emerging optical switching networks like SDM-EONs, we systematically classify and summarize previous works on the static RSA/RMSA problem for EONs. Additionally, we aim to improve the computational performance of each model type according to their unique characteristics and discern the differences between them.

By conducting a thorough analysis and comparison of these models, our research contributes to a deeper understanding of the RSA/RMSA problem and provides valuable insights to optimize and adapt these models for newer generations of optical switching net-

works, ensuring efficient resource allocation and enhanced performance in evolving EON environments.

1.2.2 Contribution to the RMSSA problem

As we stated in the last subsection, ILP models for the resource allocation problems in optical networks can be classified into path-type models (e.g., [2,4]), which select paths from a set of candidate paths, and node-type models (e.g., [8, 14]), which consider all available paths according to the modeling approaches on routing [28]. Notably, for a path-type model that employs a set of candidate paths, the solutions obtained by the model are exact if the set of candidate paths considers all available paths, which we call all-path-type; and the solutions obtained by the model are not necessarily exact if the set of candidate paths includes only a part of the available paths, which we call k-path-type. To the best of our knowledge, the vast majority of previous works employing the path-type models uses the k-path-type. Moreover, for RMSA or RMSSA problems that consider multiple modulation formats, ILP models are correspondingly complicated.

In addition, space lane change (SLC) is a nonnegligible transmission technique in SDM-EONs. Specifically, with the adoption of SLC technology, connection requests can disregard spatial continuity restrictions and use different spatial dimensions on different links of a light path. Although SLC can further increase the routing flexibility at the same spatial switching granularity to enable higher spectral efficiency, it consumes higher equipment costs due to its deployment of wavelength selective switches (WSSs) with higher port counts. In Table 1.2, we categorize previous works based on whether the SLC technique is applied to the resource allocation problem.

Table 1.2: Previous works with and without space lane change technology.

References	Space lane change
[9, 16, 30–51]	Y
[12, 21, 31, 45, 48, 52–63]	N

For static scenarios, based on the conclusions in previous works Yang et al. [9, 25], it can be observed that the savings in spectrum resources that SLC can bring are negligible compared to its equipment cost. Therefore, in our work, the RMSSA problem without considering SLC is discussed for static scenarios.

There are three types of SpChs in SDM-EONs i.e., spectral (Spe), spatial (Spa), and spectral and spatial (Spe & Spa) SpChs, which correspond to three switching paradigms, i.e., independent switching (In-Sw), fractional joint switching (FrJ-Sw), and joint switching

Table 1.3: Previous works in consideration of different switching paradigms and SpChs.

References	Switching paradigm	Super channel
[30–58, 61, 63–71]	Ind-Sw	Spe
[24, 33, 34, 52, 54, 55, 61, 64–67, 72, 73]	J-Sw	Spa
[33, 34, 52, 54, 55, 64–67, 72]	FrJ-Sw	Spe & Spa

(J-Sw), respectively. Table 1.3 shows the previous works that considered different switching paradigms and SpChs. In our work, all the above mentioned SpChs and switching paradigms will be considered.

In our previous work on RSA/RMSA, analyzing the characteristics of various types of models, it is easy to conclude that the node-type ILP models can provide theoretically optimal solutions to these problems, which will be very significant for designing a reasonable resource allocation scheme to minimize the cost in the design phase of optical networks. However, how to solve the node-type model efficiently is also a challenge because of its high complexity. Therefore, for the RMSSA problem in SDM-EONs, we consider a node-type model and discuss how it can be solved in a reasonable time.

Table 1.4: Related problems considered in previous works that formulated ILP models for SDM-EONs.

Refs.	SLC	Models		SpCh types			Modulation
		(k)-path	node	Spe	Spa	Spe & Spa	
[20]	N	Y	N	Y	N	N	Y
[37, 63]	N	Y	N	Y	N	N	N
[21]	N	Y	N	N	N	Y	Y
[40]	N	Y	N	Y	Y	Y	N
[50, 51]	Y	Y	N	Y	N	N	Y
[19]	Y	Y	N	Y	N	Y	Y
[41]	Y	N	Y	Y	N	N	Y
[12]	Y	Y	Y	Y	N	N	N
[25]	N	Y	N	Y	Y	Y	Y
[9, 16]	Y	Y	N	Y	Y	Y	Y
our work	N	N	Y	Y	Y	Y	Y

To the best of our knowledge, in the static scenarios of SDM-EONs, there is not yet any work that solves the RMSSA problem, which involves multiple modulation formats by formulating node-type ILP models. In our work, considering the limitations of the role of SLC in static scenarios, a novel non-SLC node-type ILP model considering all three

types of SpChs is proposed, several computational methods to speed up the model and a heuristic algorithm for addressing large-scale instances are discussed. This part is detailed in Chapter IV. Furthermore, this model can provide better solutions than the k-path-type models in Refs. [9, 16]. Table 1.4 shows the difference between our work and previous works that formulated ILP models to describe the resource allocation problems for optical networks. In Table 1.4, (k)-path and node represent the path-type and node-type models with arbitrary types of spectrum assignment, respectively. Besides, the three SpChs, Spe, Spa and Spe & Spa, and the switching paradigms corresponding to them, will be specifically introduced in Chapter 2.

With our research, we aim to make substantial contributions to the field of RMSSA problems in SDM-EONs, paving the way for efficient and cost-effective resource allocation schemes in the context of static scenarios. By focusing on node-type ILP models and addressing the challenges posed by multiple modulation formats, our work seeks to advance the state-of-the-art in optical network design and optimization.

1.3 Structure of this thesis

This thesis consists of five chapters.

In Chapter 1, the research background, significance, and contribution of this thesis are explained as an overview.

In Chapter 2, we present in detail the background knowledge and key technologies in the three generations of optical networks, WSON, EON and SDM-EON, as well as their resource allocation problems.

In Chapter 3, we classify the mathematical optimization models in the previous works for the RSA/RMSA problem in EONs into four types (namely, path/slot, path/channel, node/slot, and node/channel models) according to the two perspectives of routing and spectrum assignment. Moreover, we analyze and summarize the characteristics of each model and propose a series of improved methods to enhance the computational performance of each model. Finally, we verify the effectiveness of the improved methods and analyze the differences between the models by comparative simulation experiments.

In Chapter 4, we propose a node-type ILP model without SLC for the RMSSA problem in SDM-EON, based on the node/slot model of the RMSA problem in EON in Chapter 3. To better solve this model, we propose three exact algorithms based on model decomposition (namely, DMD, ASLC-MD, and SSLC-MD algorithms) and examine their performance through comparative simulation experiments. In addition, we also compared our node-type model with the k-path-type one in the previous works Refs. [9, 16].

In Chapter 5, we summarize this research and describe the possible future works.

Chapter 2

Background knowledge and key technologies

The rapid development of optical communication began with a significant breakthrough in the 1970s when Corning Inc. of the USA successfully developed the world's first practical silicon optical fiber. This achievement marked the beginning of utilizing optical fibers for communication purposes, propelling the swift evolution of optical networks. The advent of the first optical fiber system in 1976 in Atlantic, USA laid the foundation for addressing the increasing demand for high-bandwidth network applications [74].

Optical networks are composed of optical fibers and equipment deployed along the fibers to manipulate light signals. This configuration allows for the utilization of light as a medium for data transmission, making it an ideal solution for handling the ever-growing data requirements of modern communication systems. The functionality of optical networks is intricately linked to the physics of light and the technologies used to manage optical flow. As a result, breakthroughs in optical technologies have led to several landmark evolutions in optical network architectures.

This chapter provides an overview of the evolutionary history of optical network architectures and their corresponding features. Each network architecture is characterized by unique properties and supported by specific physical devices. We delve into the relationship between these factors and the challenges posed to the network optimization problem. Specifically, we begin with an introduction of the basics of optical transmission. Then, we overview the relevant background technologies and resource allocation problems in the three representative generations of optical network architectures, which are WSON, EON, and SDM-EON, respectively.

2.1 Optical transmission

2.1.1 Evolution of optical networks

An optical network consists of optical fibers carrying optical channels (OChs) and the devices deployed along the fibers to process the light. Thanks to the development of breakthrough technologies, optical networks have undergone several milestones in their evolution.

In this century, optical networks have rapidly evolved into six typical architectures as shown in Fig. 2.1 to address the growing requirements of traffic. Among them, the earliest and currently active architecture is wavelength switched optical network (WSON), which employs wavelength division multiplexing (WDM) technology to carry different connection requests simultaneously [75–78]. Although this architecture effectively improves the capacity and utilization of the networks compared to the previous time division multiplexing (TDM) optical networks, it still suffers from the lack of flexibility in spectrum assignment.

In order to solve the problem that the traditional WDM optical network with fixed wavelength assignment can no longer provide efficient services for users and cannot adapt to the future needs of high-speed, large-scale traffic volume, and highly scalable networks, Jinno et al. (2009) proposed the concept of Spectrum Sliced Elastic Optical Network (EON), which is characterized by high-capacity, high-flexibility, and scalability, and adapted to various forms of network services [79].

However, as the traffic volume increases further, traditional EONs using only C-band or employing single-mode fibers (SMFs) will struggle to handle the future connection requests with extra-large capacities because of the constraints of nonlinear Shannon limit of SMFs. To overcome this limitation, space division multiplexing (SDM) [80, 81] and band division multiplexing (BDM) [82–84] were introduced as promising solutions for EONs, and these new network architectures are called SDM-EONs and Multi-band (MB) -EONs. In SDM-EONs, nodes are connected by fibers with multiple spatial dimensions, such as fiber bundles (FBs), multicore fibers (MCFs) and few-mode fibers (FMFs) [12]. By introducing multiple spatial dimensions in this way, a significant increase in optical network capacity can be achieved. On the other hand, MB-EONs utilize BDM technology, which exploits the available frequency spectrum from the traditional C band to L-, S-, E-, and O-band ranging between 1260nm and 1625nm with attenuation coefficient (fiber loss) less than 0.4dB/km on the same deployed SMF [82,83]. Therefore, network capacity is multiplied without either the employment of dark fibers or the deployment of new fibers achieving large savings of investment for network upgrading [83].

Moreover, in order to correspond to the foreseeable larger traffic volume in the future, there has been a recent increase in the works discussing spatial channel networks (SCNs)

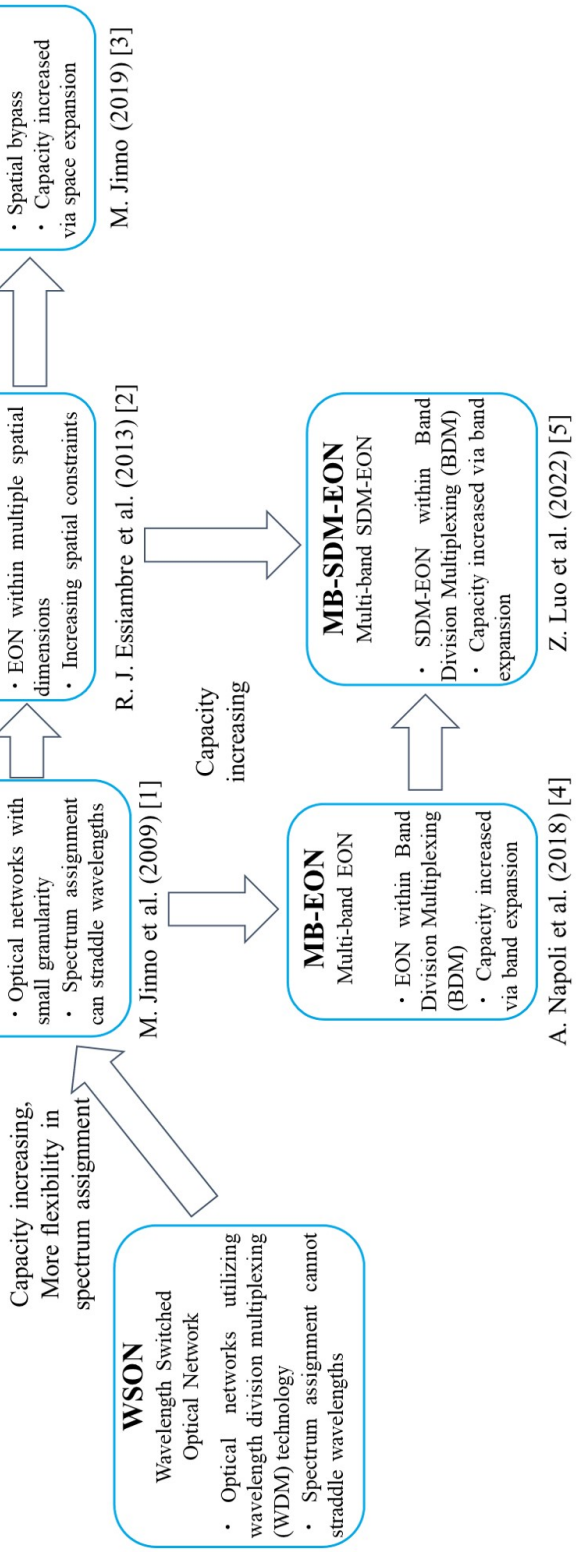

Figure 2.1: Six typical architectures in the development of optical networks.

for the massive SDM era that utilize spatial bypass [85–89], as well as MB-SDM-EONs that combine both BDM and SDM [63, 90].

In this thesis, we focus on resource allocation under two typical next generation architectures, EONs as well as SDM-EONs.

2.1.2 Transmission schemes

In optical networks, there are four types of transmission schemes in which a source specifies a destination to send and receive data: unicast, multicast, broadcast, and anycast. Fig. 2.2 shows a conceptual diagram of the four transmission schemes.

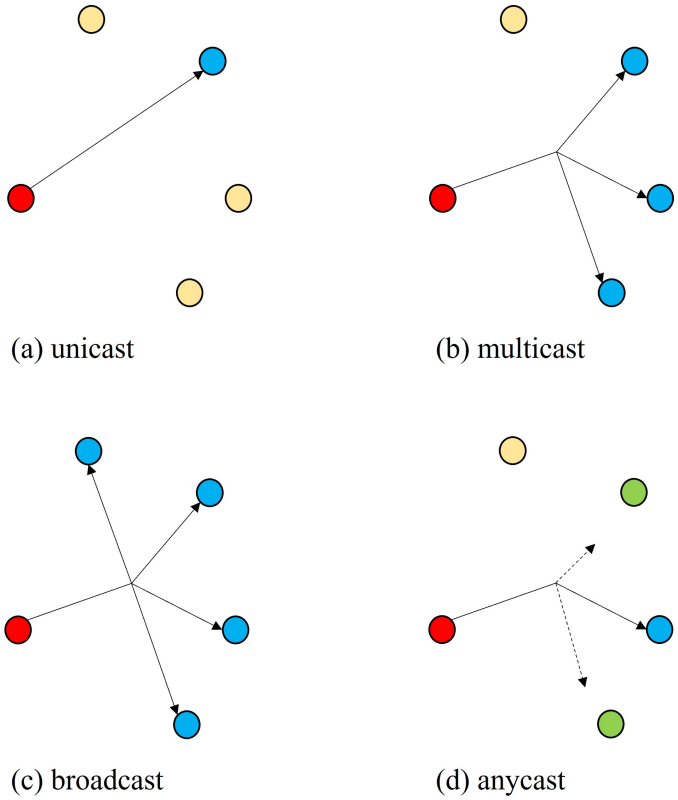

Figure 2.2: Four types of transmission schemes in optical networks.

The red nodes are source hosts (clients), and the yellow, blue, and green nodes are destination hosts (servers). The yellow node represents a destination host that is not the transmission target of the source host, the blue node represents a destination host that is actually transmitting with the source host, and the green node represents a destination host that is the transmission target of the source host but is not transmitting with other nodes. The dotted line in Fig. 2.2 (d) shows the connection between the addresses of the green destination host and the source host.

Unicast is point-to-point transmission between a single source host and destination host (server), as shown in Fig. 2.2 (a). For example, browsing websites and transmitting files are examples of unicast. Multicast is point-to-multipoint transmission between a single source host and multiple destination hosts, as shown in Fig. 2.2 (b). For example, broadcast videoconferencing, such as online teaching, is an example of multicast. Broadcast is point-to-all transmission between a single source host and the entire destination host, as shown in Fig. 2.2 (c). The difference between broadcast and multicast is the range of destination hosts (broadcast is between a source host and all destination hosts on the network). Anycast is point-to-point transmission between a single source and destination host, but an appropriate destination host is selected from among multiple destination hosts, and transmission and reception take place between the selected destination host and the source host, as shown in Fig. 2.2 (d) [91].

In this thesis, we focus on the simplest unicast transmission scheme in order to grasp the characteristics of the model itself. However, the model considered in this paper can be extended to the other three transmission schemes.

2.1.3 Optical fiber transmission

Optical fiber is a very lightweight cable with a diameter almost as thin as a human hair. In the early 1980s, network operators began utilizing optical fibers in telecommunication networks [92].

Compared with other wired physical transmission media, optical fiber transmission supports the current wired transmission system due to its large available bandwidth, low loss etc. The total bandwidth of an optical fiber is about 400 nm while ensuring that the optical loss is less than 0.5 dB/km, and is generally divided into the wavelength bands O, E, S, C, and L [76, 77]. Among them, C-band has a wavelength range of 1530 nm to 1565 nm and covers an available spectrum of about 4 THz. Because of its advantage of low loss, C-band is very conducive to long-distance optical transmission, and is often adopted as the main band for optical fiber transmission [76,77]. In the last few years, the multiplexing of several other bands (e.g., S and L-band) has been discussed in order to correspond to larger traffic volume in the future [63, 82, 83, 90].

2.2 Wavelength switched optical network

2.2.1 Wavelength division multiplexing transmission technology

Wavelength division multiplexing (WDM) technology has revolutionized the landscape of optical communication networks by enabling the simultaneous transmission of multiple data

streams over a single optical fiber. By utilizing distinct wavelengths as independent communication channels, WDM has significantly enhanced the capacity, scalability, and efficiency of modern optical networks. This technology has become a fundamental pillar of long-haul and metropolitan networks, addressing the escalating demand for high-speed and bandwidth-intensive applications [75, 76].

The concept of WDM dates back to the early 1970s when researchers realized the potential of leveraging different wavelengths to increase the capacity of optical fibers. The initial implementation of WDM relied on coarse-grained channels with wide spacing between wavelengths. However, with advancements in fiber optics and laser technology, dense wavelength division multiplexing (DWDM) emerged in the late 1980s, allowing for much narrower wavelength spacing and significantly higher data rates [76].

The adoption of erbium-doped fiber amplifiers (EDFAs) in the early 1990s further fueled the development of WDM technology by enabling efficient amplification of multiple wavelengths simultaneously. This breakthrough eliminated the need for costly and complex optical-electrical-optical (O-E-O) conversions between wavelengths, resulting in more streamlined and cost-effective network architectures. Such an optical network has no O-E-O conversion (i.e., utilizing optical bypass) during transmission and is referred to as an all-optical network [93].

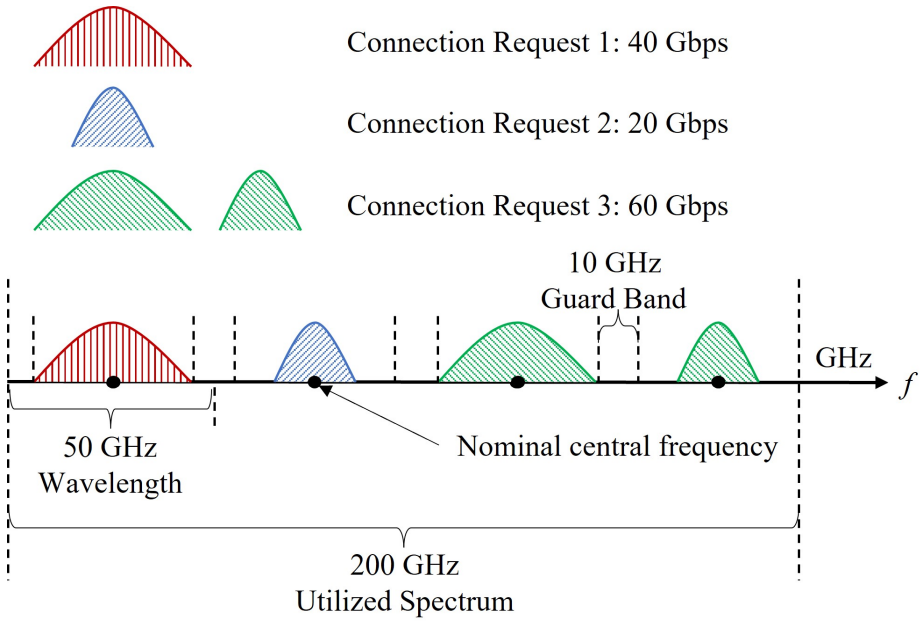

Figure 2.3: Illustration of transmission in fixed 50 GHz grid WSON for connection requests with traffic volume of 20, 40 and 60 Gbps.

A typical WSON uses 50 GHz channel spacing on the C-Band, i.e., the total 4 THz

spectrum on the C-Band is divided into 80 available wavelengths, with each wavelength occupying 50 GHz of spectrum [76–78]. In an optical channel (OCh), the spectrum used to carry data is called the optical carrier (OC). In WSON with this specification, the OCs should be less than 50 GHz because the switching guard band between two OCs needs to occupy a certain spectrum to ensure all-optical switching and routing. Furthermore, in general, the maximum bit rate that can be supported by a single OC is 40 Gbps [78, 94]. In this case, for three connection requests with traffic of 20, 40 and 60 Gbps, the spectrum they use is shown in Fig. 2.3. It can be observed that in WSONs, the minimal unit of spectrum assignment is a whole wavelength, and even when the bandwidth required by a connection request is less than one wavelength, it still occupies the whole wavelength to achieve the transmission.

2.2.2 Routing and wavelength assignment problem

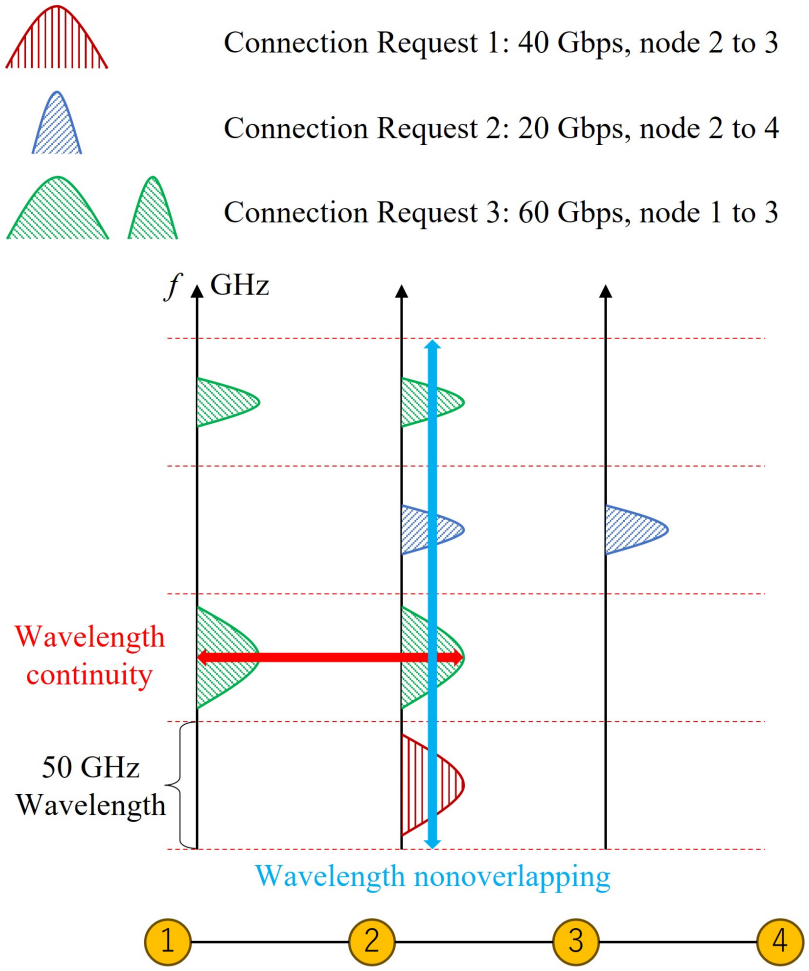

Figure 2.4: Illustration of routing and wavelength assignment problem.

For the design of optical networks, the mathematical optimization problem considering routing, spectrum, and other network resources is called the resource allocation problem for optical networks. Solving the resource allocation problem is significant for reducing network cost and saving energy.

In fixed-grid WDM-based WSONs, the resource allocation problem is referred to as the routing and wavelength assignment (RWA) problem. Specifically, there are two main constraints on the RWA problem, as shown in Fig. 2.4, a wider-spectrum grid, such as the 50 GHz wavelength, is adopted. A light path for one connection request can only be established by occupying the same wavelength on all links it passes through, which is called the wavelength continuity restriction, and a single wavelength can only be employed at most once, which is referred to as the wavelength nonoverlapping restriction. This problem has been proven to be NP-hard and was investigated in many previous works [95, 96].

2.3 Elastic optical network

With the advent of the big data era, video-on-demand and internet video services in the network have led to an explosive growth of data traffic in the network, the use of fixed wavelengths, a single modulation format for the distribution of the traditional wavelength division multiplexing (WDM) optical network (i.e., WSON) is extremely inefficient, has been unable to provide users with efficient services, and can not be adapted to the future of the high-speed, data-rich, and scalable network requirements. In order to improve the efficiency of WSONs, an EON based on coherent optical orthogonal frequency division multiplexing (CO-OFDM) or nyquist wavelength division multiplexing (N-WDM) technology has been proposed (i.e., so-called SLICE architecture proposed via Jinno et al. [79]). EONs adhere to the recommendations of the ITU-T G.694.1 [97]. A total of 4 terahertz of spectrum resources in the C-band can be divided into 320 FSs each with a frequency of 12.5 GHz and a reduced center frequency granularity of 6.25 GHz. Consequently, EONs can create flexible optical channels occupying different numbers of FS with channel spacing being integer multiples of 6.25 GHz, thereby enhancing the utilization of spectrum resources. In other words, flexible optical channels can be established as per requirements to accommodate varying bit rates and efficiently serve connection requests of different traffic volumes.

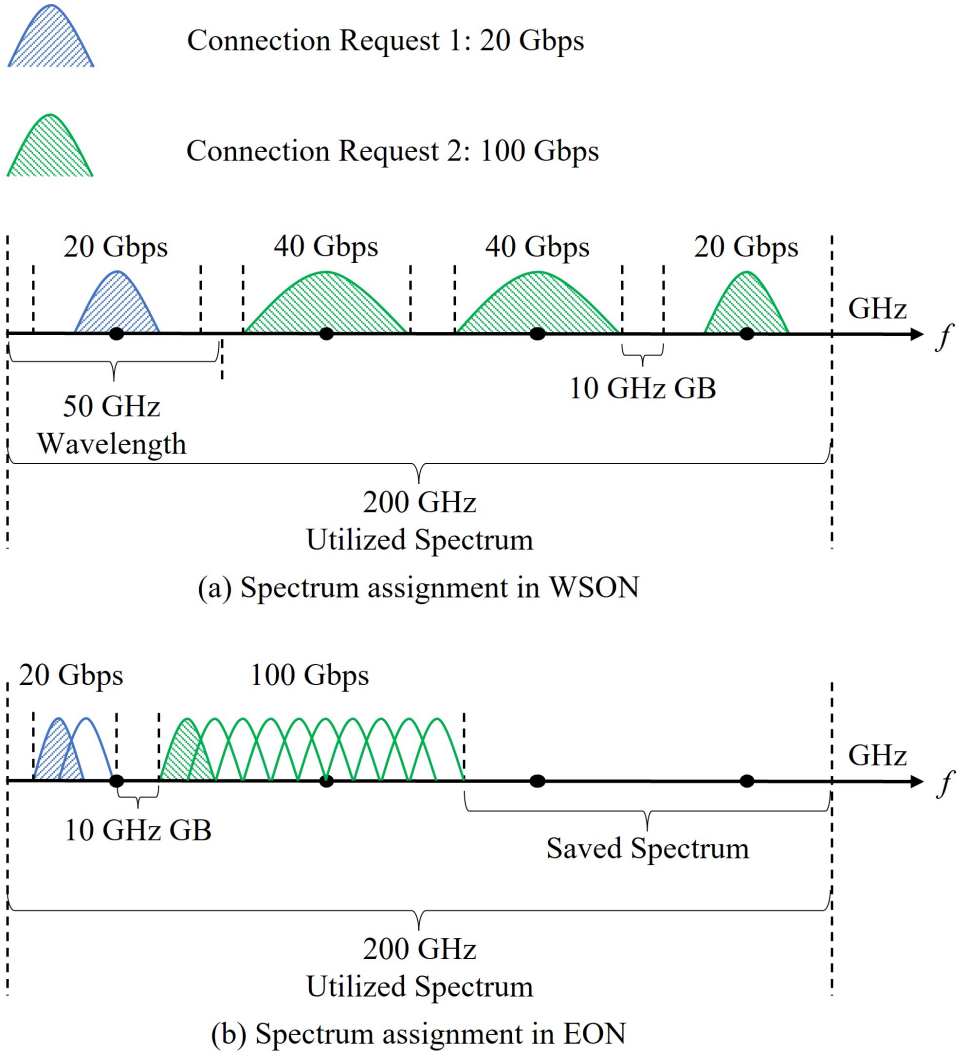

Figure 2.5: Illustration of spectrum assignment between WSONs and EONs.

Fig. 2.5 illustrates the distinction between WSONs and EONs concerning spectrum assignment and the principles behind the ability of EONs to efficiently utilize network bandwidth resources. In the WSON depicted in Fig. 2.5 (a), when the bandwidth of a connection request is smaller than the capacity of a single wavelength, the optical network is still forced to allocate an entire wavelength for that connection request. For instance, if the connection request 1 is only 20 Gbps, the WSON protocol mandates the assignment of a complete wavelength for this relatively small connection request. Similarly, when the bandwidth of a connection request exceeds the capacity of a single wavelength, multiple complete wavelengths must be assigned. For instance, if connection request 2 requires 100 Gbps of bandwidth, even though a single wavelength in WSON has a capacity of 40 Gbps, three complete wavelengths are assigned to connection request 2, and GB is also

needed between the 3 wavelengths, which reduces network efficiency. In contrast, Fig. 2.5 (b) presents one type of EONs, which leverages CO-OFDM technology to generate several subcarriers, allowing 1/2 spectral overlap between adjacent subcarriers. This enables the smallest unit for carrying connection requests to be multiple continuous wavelength division multiplexing subcarriers, which we refer to as FSs. Assuming each FS in the EON shown in Fig. 2.5 (b) has a capacity of 10 Gps, then for connection request 1 and 2 illustrated in Fig. 2.5 (a), connection request 1 only requires 2 FSs instead of an entire wavelength, and connection request 2 only needs 10 FSs instead of 3 complete wavelengths without the need for GBs. However, GBs are still required between different connection requests, such as the GB between connection request 1 and 2. Additionally, employing the grooming strategy to combine small connection requests with same source-destination nodes into larger connection requests for transmission can further save more GBs, thus enhancing network efficiency.

Moreover, WSONs utilize a single modulation format, while EONs support multiple modulation formats, such as binary phase-shift keying (BPSK), quadrature phase-shift keying (QPSK), 8-quadrature amplitude modulation (8QAM), and 16-quadrature amplitude modulation (16QAM). Higher modulation formats represent more information per 1 Hz but may lead to shorter maximum transmission distances. EONs adaptively select the appropriate modulation format based on the distance between source and destination nodes when transmitting information, i.e., DAT.

In summary, EONs present significant advantages over WSONs, allowing for more efficient utilization of network bandwidth resources through FSs and grooming strategies. Furthermore, by supporting multiple modulation formats, EONs can adapt to varying transmission distances, optimizing network performance and efficiency.

2.3.1 Multiplexing technologies in EONs

In EONs, meeting the ever-increasing demands for high data rates and spectral efficiency requires advanced multiplexing technologies. Two prominent technologies that have significantly impacted the design and performance of EONs are CO-OFDM and N-WDM. Both CO-OFDM and N-WDM play crucial roles in enhancing the capacity and efficiency of optical communication systems in EONs.

CO-OFDM is a transformative technology that combines coherent detection with orthogonal frequency division multiplexing (OFDM) [98–102]. The OFDM concept involves dividing the data stream into multiple subcarriers, each with a low symbol rate, and transmitting them simultaneously. Coherent detection, on the other hand, extracts both the amplitude and phase information of received optical signals, enabling robust data transmis-

sion over long distances. By leveraging coherent detection with OFDM, CO-OFDM achieves high spectral efficiency, mitigating impairments caused by fiber dispersion and nonlinearities. This makes CO-OFDM a suitable solution for long-haul transmission and efficient utilization of the optical spectrum in EONs.

N-WDM, based on the Nyquist criterion, is designed to maximize spectral efficiency by spacing channels at half the Nyquist rate [103–106]. This allows for doubling the number of data channels that can be accommodated within the available optical bandwidth without introducing intersymbol interference. N-WDM optimally utilizes the optical spectrum, achieving higher data rates and increased capacity compared to traditional WDM technology. The ability of N-WDM to efficiently utilize optical resources makes it a compelling choice for high-capacity optical networks in EONs.

Both CO-OFDM and N-WDM contribute to the advancement of EONs by offering high data rates, enhanced spectral efficiency, and improved signal performance. The works discussed in the Chapter 3 and 4 of this thesis are mainly under N-WDM based EONs and SDM-EONs.

2.3.2 Distance adaptive transmission

Distance adaptive transmission (DAT) is one of the key features of EONs. With DAT, all available modulation formats dynamically adjust to the transmission distance along the optical path, selecting the most efficient modulation format that does not exceed the maximum transmission distance [5,107]. This adaptive mechanism ensures optimal spectral efficiency and maximizes the utilization of the optical spectrum while maintaining signal integrity across varying transmission distances.

In this thesis, four different modulation formats are considered, which are BPSK, QPSK, 8QAM and 16QAM, respectively. Moreover, we consider these modulation formats with dual polarization (DP), i.e., DP-BPSK, DP-QPSK, DP-8QAM and DP-16QAM, respectively. The transmission distance and modulation levels (in bits per symbol) of these modulation formats are shown in Table 2.1. The data in Table 2.1 for EONs based on CO-OFDM is referenced from Refs. [108–110] and those for EONs based on N-WDM are referenced from Refs. [12,33]. It is worth noting that the transmission distances indicated in the table are in the case where only the optical signal-to-noise ratio (OSNR) of the optical fiber transmission is considered, i.e., without considering the inter-core crosstalk (XT).

From Table 2.1, it can be observed that modulation formats with higher modulation levels can support more bits per symbol (i.e., higher efficiency of transmission), but at the same time have shorter transmission distances. As a result, for connection requests transmitted along lightpaths with different path lengths, EONs can adaptively employ different

Table 2.1: Transmission distance and modulation levels for different modulation formats.

Modulation formats		DP-BPSK	DP-QPSK	DP-8QAM	DP-16QAM
Transmission distance (km)	CO-OFDM	4000	2000	1000	500
	N-WDM	6300	3500	1200	600
Modulation level (bits/s/Hz)		2	4	6	8

modulation formats to provide optimal spectral efficiency.

2.3.3 Super channel in EONs

Super channel (SpCh) is an innovative concept that revolutionizes the way optical data is transmitted for EONs. Instead of using traditional fixed-wavelength channels in WSONs, the SpCh combine multiple adjacent wavelength channels to create a broader and more flexible transmission entity. This aggregation of closely spaced wavelengths allows for the simultaneous transmission of a large amount of data over a wider optical spectrum.

The unique features of SpCh is its flexibility in supporting different bandwidth requirements for connection requests. Thanks to the use of bandwidth-variable optical transceivers (BVTs) and bandwidth-variable wavelength cross-connects (BV-WXCs), SpCh can establish light paths with varying numbers of FSs without the need to switch grid bandwidth intervals. This adaptability enables efficient resource utilization and dynamic allocation of bandwidth to cater to diverse traffic demands [79].

As shown in Figure 2.6, the SpCh is composed of several continuous OCs that are generated by several continuous single-carrier transmitters. Switching GBs exist only between adjacent SpChs, and there are no switching GBs between two adjacent OCs in the same SpCh. Since the SpCh of EON takes only 2 switching GBs at two sides of the SpCh (i.e., 1FS), it has high spectral efficiency compared to the optical channels of WSONs. It is notable that SpChs in EONs are present only at a single spectral dimension (i.e., they do not span spatial dimensions), thus such SpChs are also named spectral SpChs (Spe SpChs). In later section of this chapter, we will also introduce several different types of SpChs in SDM-EONs with multiple spatial dimensions.

The adoption of SpChs in EONs brings significant benefits in terms of increased capacity, enhanced spectral efficiency, and improved network flexibility. It addresses the challenges posed by ever-increasing data demands and supports the efficient transmission of data-intensive applications, making it a fundamental component of next generation optical networks.

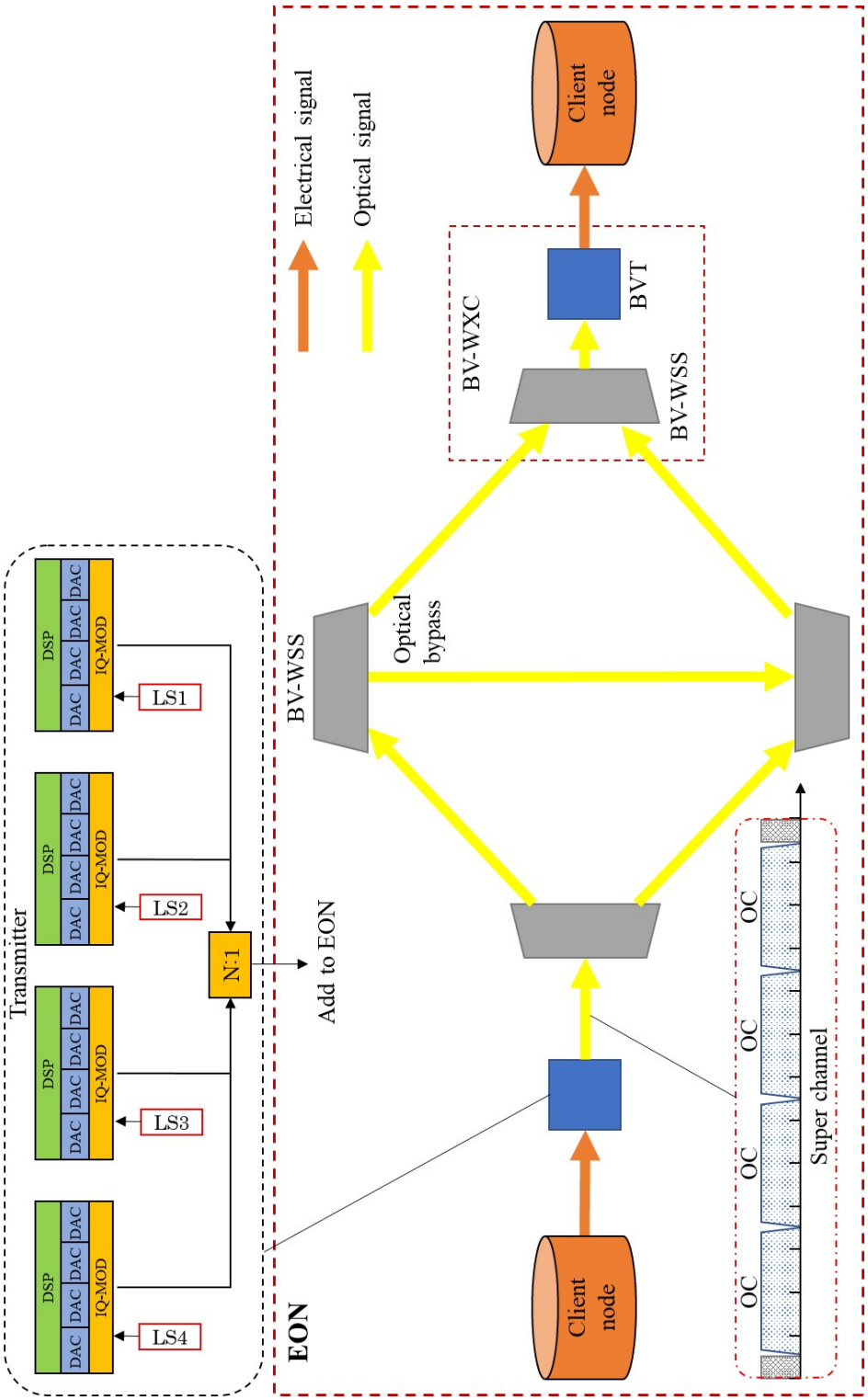

Figure 2.6: Illustration of Spe SpCh and the corresponding transmitter in EON. DSP: digital signal processing, DAC: digital-to-analog converter, IQ-MOD: in-phase and quadrature modulator, LS: laser source, N:1: coupler, BVT: bandwidth-variable transceiver, WSS: wavelength selective switch, WXC: wavelength cross-connect.

2.3.4 Routing, modulation and spectrum assignment problem

As shown in Fig. 2.7, the difference with WSON is that in EONs, narrower-spectrum grids, such as the 12.5 GHz grid, which conforms to the G.694.1 standard recommended by the International Telecommunication Union Telecommunication Standardization Sector (ITU-T) [97], is adopted. Each of the small grids shown in Fig. 2.7 (b) represents the basic unit of the spectrum in EONs, which is called the frequency slot (FS) in this work and the frequency slice in some works [3, 5, 8]. There is a guard band (GB) between any two adjacent connection requests, which prevents data crosstalk between the two connection requests [4, 111]. To more easily visually compare the spectrum resources of WSONs and EONs, the GBs are not shown in this figure. Moreover, light paths for connection requests can be established flexibly by using super channels (SpChs) that are matching the size of connection requests and consisting of different numbers of contiguous FSs without GBs in between. In this context, although EONs have achieved higher spectrum efficiency and more flexible transmission than WSONs, their smaller and more flexible spectrum granularity has also caused the problem of spectrum resource allocation problem to become complicated. For instance, EONs impose more restrictions on the establishment of light paths; that is, the FS allocated to a light path must be contiguous in the spectral domain. This is the well-known routing and spectrum assignment (RSA) problem, which has been proven to be NP-hard by Refs. [2, 112].

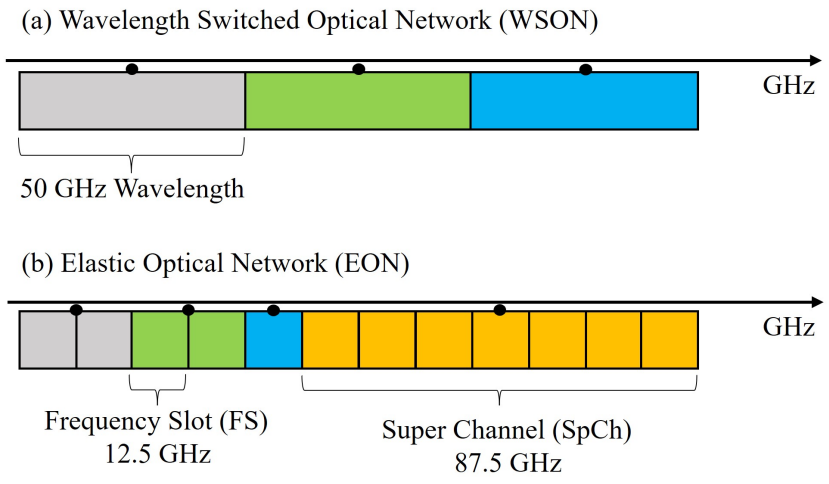

Figure 2.7: Illustration of spectrum usage in WSONs and EONs.

The RSA problem involves finding a single transmission path for a connection request under three basic constraints: FS contiguity, spectrum continuity, and nonoverlapping. FS contiguity is the constraint that the FSs allocated to each connection request must be

contiguous. Spectrum continuity is the constraint that the spectrum of the FSs used in any link must be the same when the light path to serve a connection request uses multiple links. Nonoverlapping is the constraint that an FS on a link cannot be used for two connection requests at the same time.

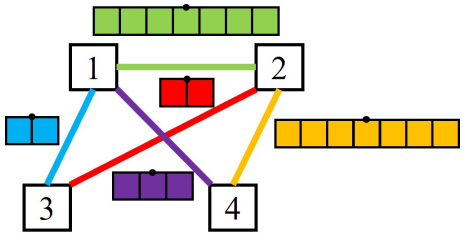

Figure 2.8: Example of connection requests.

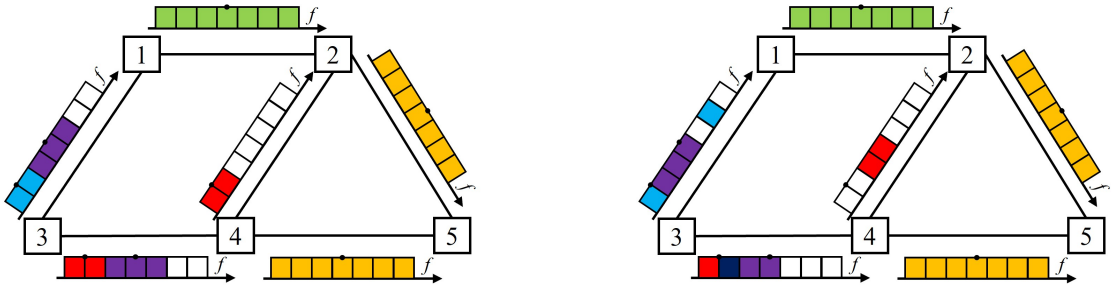

(a) Correct routing and spectrum allocation

(b) Incorrect routing and spectrum allocation

Figure 2.9: Illustration of routing and spectrum assignment problem.

Fig. 2.8 shows the origination and destination nodes and the number of FSs required for each of the five colored connection requests in the illustrative example of the RSA problem in Fig. 2.9. For example, the blue connection request transmits from node 1 to node 3 and requires two FSs. Fig. 2.9 shows an example of the RSA problem. In this case, one grid represents one FS, a colored grid means that the FS is assigned to a connection request of corresponding color, and an uncolored grid means that no connection request is assigned to the FS. Fig. 2.9 (a) shows a correct example of routing and spectrum assignment in an EON with five nodes. All of the connection requests satisfy the three basic constraints described above. Fig. 2.9 (b) shows an incorrect example of an allocation that does not satisfy the basic constraints. In the figure, the connection request in blue does not satisfy FS contiguity because the FS bandwidth is not contiguous. The purple and red connection requests do not satisfy nonoverlapping because they share the second FS of the link between nodes 3 and 4. And the red connection request does not satisfy spectrum continuity because

it uses FSs of different indexes on the two links.

In addition, when considering multiple modulation formats, EONs support using distance adaptive transmission (DAT) to select the modulation formats, i.e., selecting appropriate modulation formats for optical signals depending on the length of the light paths [5,107]. In this context, the RSA problem turns into a more complex routing, modulation format and spectrum assignment (RMSA) problem [16, 28]. In this thesis, our work on the RSA and RMSA problems will be presented in detail in Chapter 3.

2.4 Space division multiplexing elastic optical network

2.4.1 SDM fibers

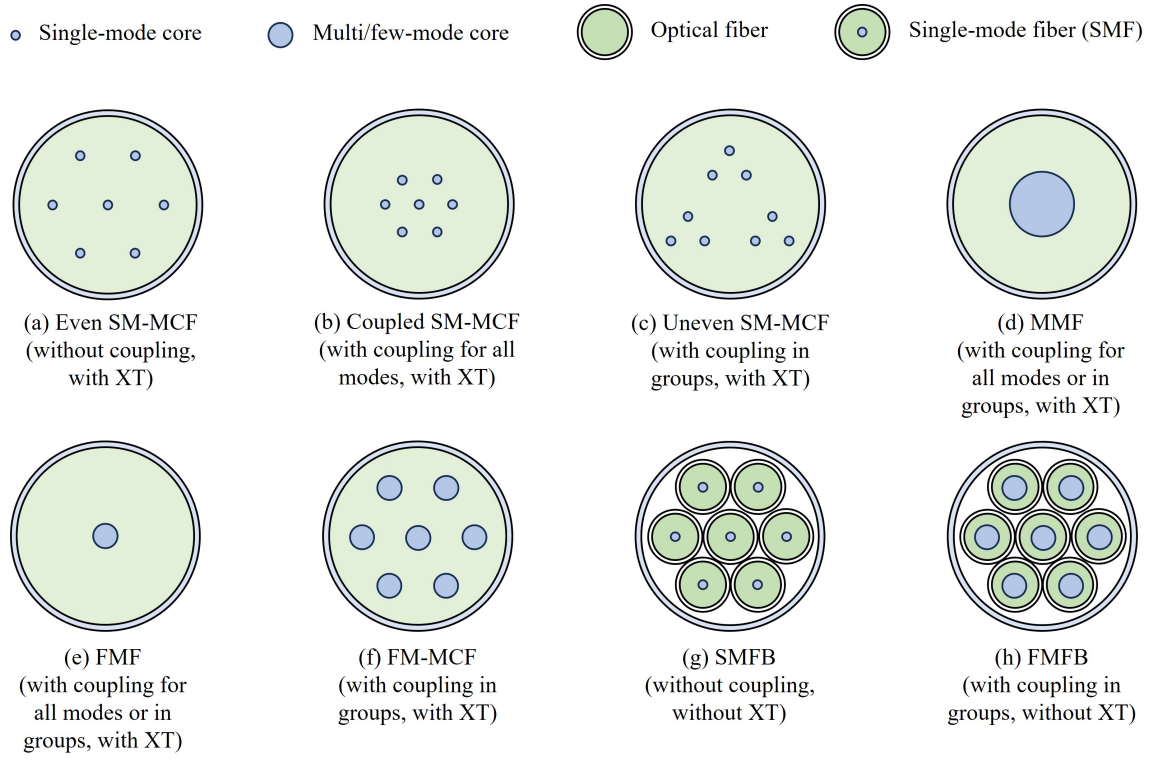

Figure 2.10: Types and properties of SDM fibers.

Space division multiplexing (SDM) is a pioneering approach revolutionizing optical communication by leveraging multiple spatial dimensions to enhance data transmission capacities [80,113]. Within the realm of SDM, various types of optical fibers have been developed to accommodate these spatial dimensions and address the escalating demand for higher data rates and extended transmission distances, as depicted in Fig. 2.10.

One fundamental category is the single-mode multi-core fiber (SM-MCF or MCF) [114–

116]. This innovation entails embedding multiple single-mode cores within a fiber cladding, with each core guiding a distinct mode. The arrangement of cores can adopt diverse structures such as one-ring, dual-ring, linear-array, two-pitched, or hexagonal patterns. Cores can be spaced closely or widely, with even or uneven packing, and they will exhibit varying degrees of coupling, ranging from strong to weak interactions [117–119]. The MCF design optimizes efficient spatial data transmission while offering versatility in core arrangement.

Few-mode fiber (FMF) [120, 121], a subtype of multi-mode fibers (MMF) [122, 123], provides SDM transmission by supporting a relatively low number of transverse modes within a higher index core. FMFs are particularly advantageous for achieving longer transmission distances, as the interference and impairments arising from a limited number of co-propagating modes are easier to manage compared to MMFs with higher mode counts.

Combining the benefits of MCF and FMF, few-mode multi-core fiber (FM-MCF) allows the simultaneous propagation of transverse modes across multiple higher index cores [124, 125]. This configuration mitigates the drawbacks associated with MCF and FMF technologies, resulting in a more balanced performance.

Fiber bundles (FBs) represent the simplest form of SDM, accomplished by aggregating numerous fibers into a bundle. While single-mode fiber bundles (SMFB) are a notable example, supporting a single spatial mode per fiber, there's also the possibility of few-mode fiber bundles (FMFB), where each fiber guides a limited number of modes. SMFB, a commercially available technology, facilitates a seamless transition from existing networks to SDM, owing to its adaptability and compatibility.

Table 2.2: SDM Fibers in previous resource allocation works.

References	SDM fiber
[9, 31–34, 52, 54, 55, 61, 64–67, 67, 72, 73]	SMFB
[9, 24, 30, 31, 35–51, 53, 56–58, 61, 63, 68–71, 73, 126]	MCF
[21, 59–61, 72]	MMF/FMF
[48, 127, 128]	FM-MCF

Table 2.2 presents an overview of prior research exploring resource allocation with various types of SDM fibers. Remarkably, SMFB and MCF, despite the multitude of SDM fiber variants, are the most frequently studied types. This preference can be attributed to several reasons: i) Avoidance of costly multi-input-multi-output digital signal processor (MIMO-DSP) technology, which is crucial in strongly-coupled SDM fibers, as it significantly escalates network costs with the number of modes/cores [87, 129]; ii) Greater flexibility in signal generation, routing, switching, and reception, as strongly-coupled modes/cores necessitate joint processing [12]; iii) Enhanced ease of transitioning from existing optical networks

to SDM-based infrastructures. Consequently, our focus in this thesis is primarily on SMFB and/or MCF. Additionally, the spatial dimension within these fibers, referred to as 'space lane (SL)', plays a pivotal role in our research.

2.4.2 Noise in SDM fibers

In the realm of SDM optical fibers, two critical parameters that significantly influence the performance and quality of transmitted signals are optical signal-to-noise ratio (OSNR) and inter-core crosstalk (XT).

The OSNR is a fundamental metric that measures the quality of an optical signal relative to the noise present in the transmission system. It quantifies the ratio of the optical power of the signal to the power of the noise introduced during transmission and reception. A higher OSNR indicates a stronger signal relative to the noise, leading to improved signal fidelity and better error performance. In SDM fibers, where multiple spatial modes or cores carry different signals simultaneously, maintaining a high OSNR is crucial to ensure reliable data transmission across the various cores or modes. OSNR is a critical factor in determining the achievable data rates and the reach of SDM transmission systems.

Inter-core crosstalk, also known as inter-modal crosstalk or inter-core interference, occurs when optical signals from one core of an SDM fiber interfere with or leak into adjacent cores or modes. This phenomenon can lead to signal degradation, reduced signal-to-noise ratio, and increased bit error rates. XT becomes more pronounced in tightly packed cores or modes and is influenced by factors such as the design of the fiber, the spacing between cores, and the characteristics of the transmitted signals. Managing and minimizing XT is essential to maintaining the integrity of signals carried by different cores or modes and ensuring the overall performance of SDM transmission systems.

In this thesis, we have the following considerations and assumptions about the influence of OSNR and XT on the SDM transmission system. As shown in Figure 2.11, we consider several cases where each link uses the 4-core MCF [130] or the 12-core MCF [131] to connect the networks in our work.

(a) 4-core MCF (b) 12-core MCF

Figure 2.11: The MCFs considered in this thesis.

Based on the ITU-T standard G.694.1, the total number of FSs that each link has (i.e., $|F|$) is set to 320 (i.e., 12.5 GHz per FS at the C-band with a 4 THz bandwidth) [97]. The number of modulation levels $|MF|$ is set to 4. The numbers 1, 2, 3, and 4 indicate the modulation formats double polarization (DP)-BPSK, DP-QPSK, DP-8QAM, and DP-16QAM, respectively. Each OC is generated by a transceiver which can support 50 Gbps via DP-BPSK under 32 Gbaud symbol rate containing 7 GBaud (approximately 20%) for forward error correction (FEC) overhead [51] and occupying in total 37.5 GHz spectrum (i.e., 3 FSs) [132]. Therefore, the supportable bit rates per OC for the modulation formats DP-BPSK, DP-QPSK, DP-8QAM and DP-16QAM are set to 50, 100, 150 and 200 Gbps, respectively.

Table 2.3: Physical features of the MCFs considered in the simulation experiments.

Fiber type	k	Λ	β	r
4-core MCF [130]	5.0×10^{-4}	3.9×10^{-5}	4.0×10^{6}	5.0×10^{-2}
12-core MCF [131]	1.4×10^{-3}	3.7×10^{-5}	–	–

For the maximum transmission distances (km) of the considered modulation formats above, we consider that they are mainly driven by OSNR and XT. As shown in Table 2.3, these physical features of the two types of MCFs we mentioned above are used to calculate the maximum transmission distances for different modulation formats. The parameters k, Λ, β and r represent the coupling coefficient, core pitch, propagation constant, and bend radius, respectively. It should be noted that the coupling coefficients k are calculated according to Ref. [133]. In the coherent systems, the maximum transmission distances of different modulation formats bounded by OSNR, and can be estimated by the Gaussian Noise model of nonlinear interference [33]. And the XT of a connection request in MCFs after D km can be calculated by Eq. (2.1).

$$XT(D) = \frac{C - C \cdot exp\{-2(C+1)uD\}}{1 + C \cdot exp\{-2(C+1)uD\}}, \quad where \quad u = \frac{2k^2 r}{\beta \Lambda} \tag{2.1}$$

In Eq. (2.1), C represents the number of adjacent cores of the core transmitting the current connection request. We assume that the thresholds of XT (XT_m^{thre}) for modulation formats DP-BPSK, DP-QPSK, DP-8QAM, and DP-16QAM are -14, -18.5, -21, and -25 dB, respectively [42], and that the XT oscillation requires a -2 dB margin (XT_{marg}) [20]. Therefore, for a given modulation format m, the maximum transmission distance bounded by XT (D_m^{XT}) can be calculated by Eq. (2.2).

$$D_m^{XT} = max\{D | XT(D) \leq XT_m^{thre} + XT^{marg}\} \tag{2.2}$$

Table 2.4: Maximum transmission distances bounded by OSNR and XT in 4-core MCFs and 12-core MCFs under different modulation formats m.

Limitation factor	Maximum transmission distance (km)			
	DP-BPSK	DP-QPSK	DP-8QAM	DP-16QAM
D_m^{OSNR} [33]	6300	3500	1200	600
D_m^{XT} in 4-core MCFs	38945	13872	7808	3111
D_m^{XT} in 12-core MCFs	4712	1678	944	376

Table 2.5: Maximum transmission distance of each modulation format and maximum traffic volume supported of each OC fixed at 32 Gbaud for 4-core and 12-core MCFs.

Modulation format	DP-BPSK	DP-QPSK	DP-8QAM	DP-16QAM
Transmission distance (4-core) (km)	6300	3500	1200	600
Transmission distance (12-core) (km)	4712	1678	944	376
Traffic volume per OC (Gbps)	50	100	150	200

For connection requests in 4-core and 12-core MCFs with different modulation formats, we can calculate the maximum transmission distances bounded by OSNR (D_m^{OSNR}) [33] and XT (D_m^{XT}), respectively, as shown in Table 2.4. And the maximum transmission distance is the small one of D_m^{OSNR} and D_m^{XT}.

Therefor, the maximum transmission distances (km) of these modulation formats considered and the maximum traffic volume (Gbps) that an OC can carry under each modulation format are shown in Table 2.5.

2.4.3 Super channels in SDM-EONs

Three types of SpChs with different spatial switching granularities have been proposed in SDM-EONs, and they are the spectral super channel (Spe SpCh), the spatial super channel (Spa SpCh), and the spectral and spatial super channel (Spe & Spa SpCh), as shown in Fig. 2.12, 2.13, 2.14, respectively [12]. Here, we assume that the spatial dimension of an SDM-EON is 4 (i.e., a 4-core MCF or 4-fiber SMFB). Then, the SpChs with spatial switching granularities i, which are equal to 1, 2 and 4, correspond to Spe SpCh, Spe & Spa SpCh and Spa SpCh, respectively.

- As shown in Fig. 2.12, a Spe SpCh is composed of several continuous OCs that are generated by several continuous single-carrier transmitters. Switching GBs exist only

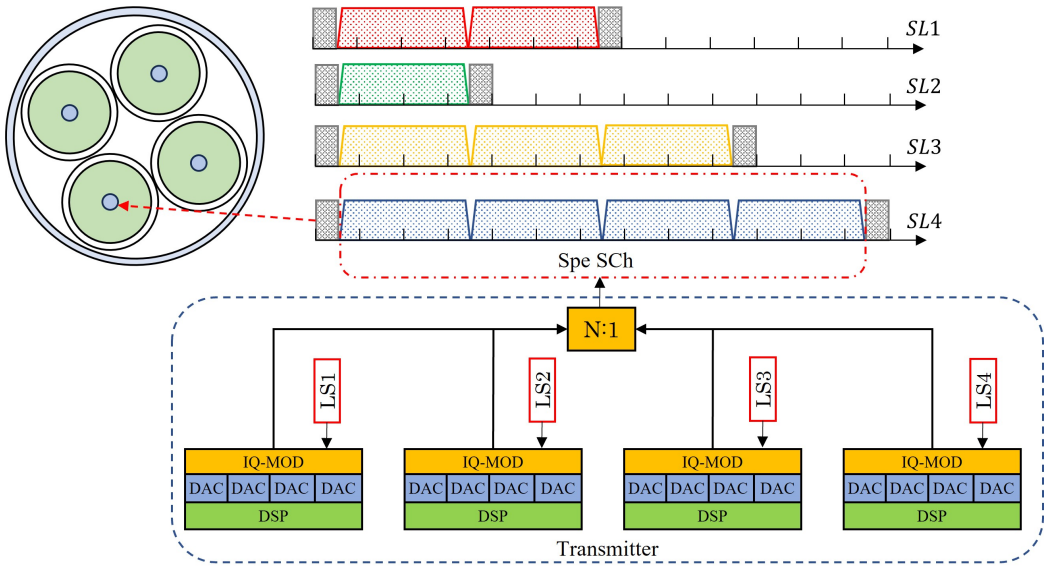

Figure 2.12: Illustration of spectral super channel (Spe SpCh) and spectral super transceiver (i = 1). DSP: digital signal processor, DAC: digital-to-analog converter, IQ-MOD: in-phase and quadrature modulator, LS: laser source, N:1: coupler, FIFO: SDM fan-in/fan-out component.

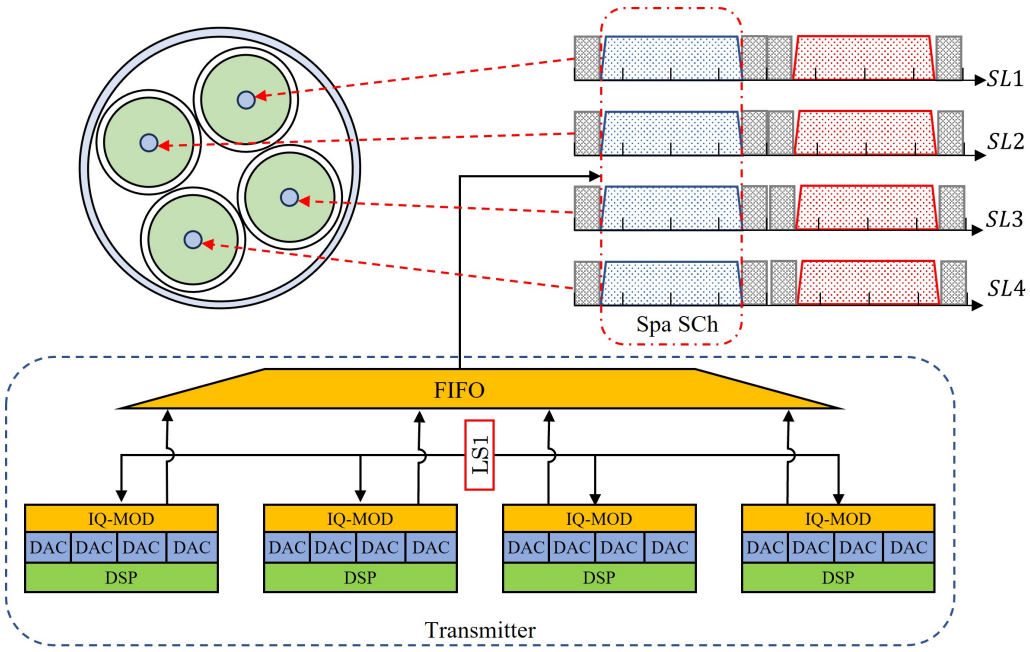

Figure 2.13: Illustration of spectral super channel (Spa SpCh) and spectral super transceiver (i = 4). DSP: digital signal processor, DAC: digital-to-analog converter, IQ-MOD: in-phase and quadrature modulator, LS: laser source, N:1: coupler, FIFO: SDM fan-in/fan-out component.

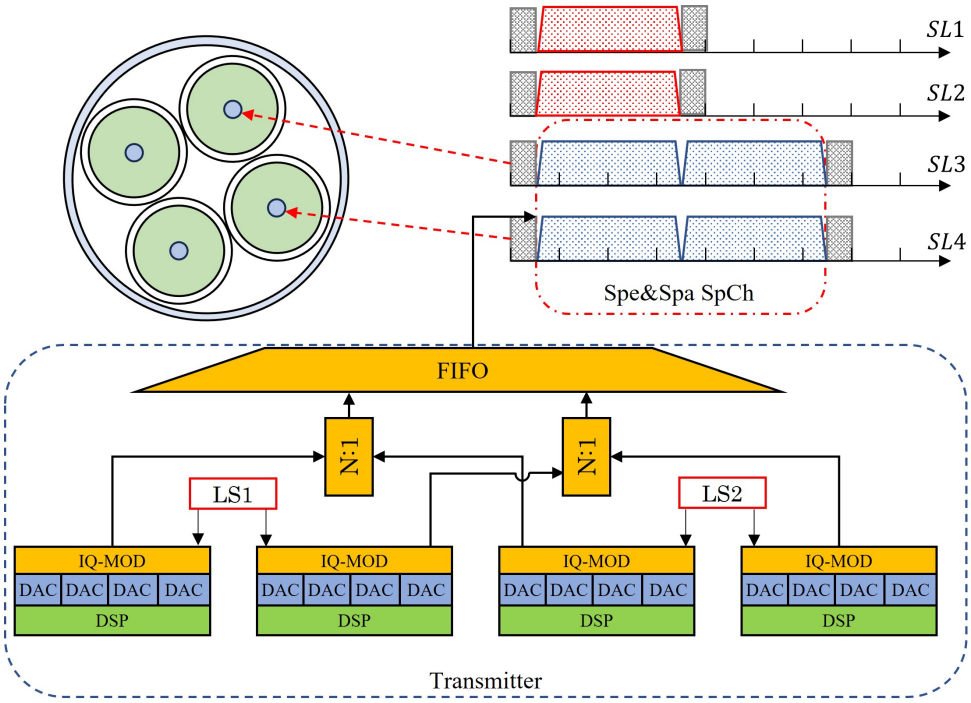

(a) Spectral & Spatial SpCh and Spectral & Spatial super transmitter (i = 2, regular)

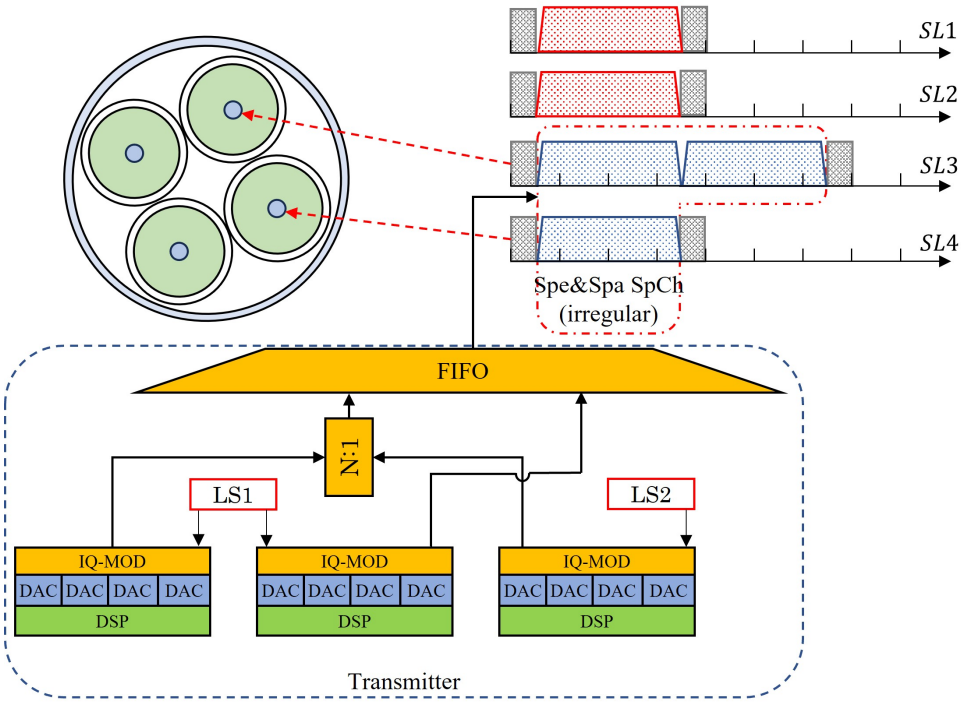

(b) Spectral & Spatial SpCh and Spectral & Spatial super transmitter (i = 2, irregular)

Figure 2.14: Illustration of spectral & spatial super channel (Spe&Spa SpCh) and spectral & spatial super transceiver in regular and irregular case (i = 2). DSP: digital signal processor, DAC: digital-to-analog converter, IQ-MOD: in-phase and quadrature modulator, LS: laser source, N:1: coupler, FIFO: SDM fan-in/fan-out component.

between adjacent SpChs, and there are no switching GBs between two adjacent OCs in the same SpCh. Since a Spe SpCh takes only 2 switching GBs at two sides of the SpCh (i.e., 1FS), it has the highest spectral efficiency. However, a Spe SpCh containing 4 OCs, as in the example in the figure, uses four independent laser sources; hence, it is the most costly.

- Fig. 2.13 illustrates an Spa SpCh containing 4 OCs, and it is generated by a 4×1 joint transmitter and uses a common laser source in different spatial dimensions. Thus, it has the lowest cost, although it has the lowest spectral efficiency.

- A Spe & Spa SpCh containing 4 OCs is shown in Fig. 2.14(a), and it is generated by a 2×2 fractional joint transmitter. OCs allocated on the same spectrum can share a common laser at the transmitter. It is obvious that the Spe & Spa SpCh is a hybrid SpCh that provides intermediate cost and spectral efficiency. Fig. 2.14(b) shows an irregular Spe & Spa SpCh containing 3 OCs, which is not considered in this work.

2.4.4 ROADMs and switching paradigms in SDM-EONs

Space lane change (SLC) is a nonnegligible transmission technique in SDM-EONs. Specifically, with the adoption of SLC technology, connection requests can disregard spatial continuity restrictions and use different spatial dimensions on different links of a light path. As shown in Fig. 2.15(b), the red connection request space lane changed from SL4 to SL2 to make room for the newly added connection request. SLC makes resource allocation more flexible, which further improves spectrum efficiency, especially in dynamic problems. As a negative effect, although SLC can further increase the routing flexibility at the same spatial switching granularity to enable higher spectral efficiency, it consumes higher equipment costs due to its deployment of WSSs with higher port counts. In static scenarios, the savings in spectrum resources that SLC can bring are negligible compared to its equipment cost [9, 25]. Therefore, in this thesis, which focuses on static scenarios, we discuss the non-SLC case.

There are three switching paradigms in SDM-EONs, independent switching (In-Sw), fractional joint switching (FrJ-Sw) and joint switching (J-Sw), corresponding to the Spe SpCh, Spa SpCh and Spe & Spa SpCh, respectively. In-Sw and FrJ-Sw can each be subdivided into two types based on whether they support SLC [25].

Fig. 2.16 shows the architectures of the reconfigurable optical add-drop multiplexers (ROADMs) corresponding to the various switching paradigms with and without SLC. The ROADMs in the figure are all at the 2-degree (i.e., SDM in and SDM out) intermediate nodes in a network that has 4 spatial dimensions on each link.

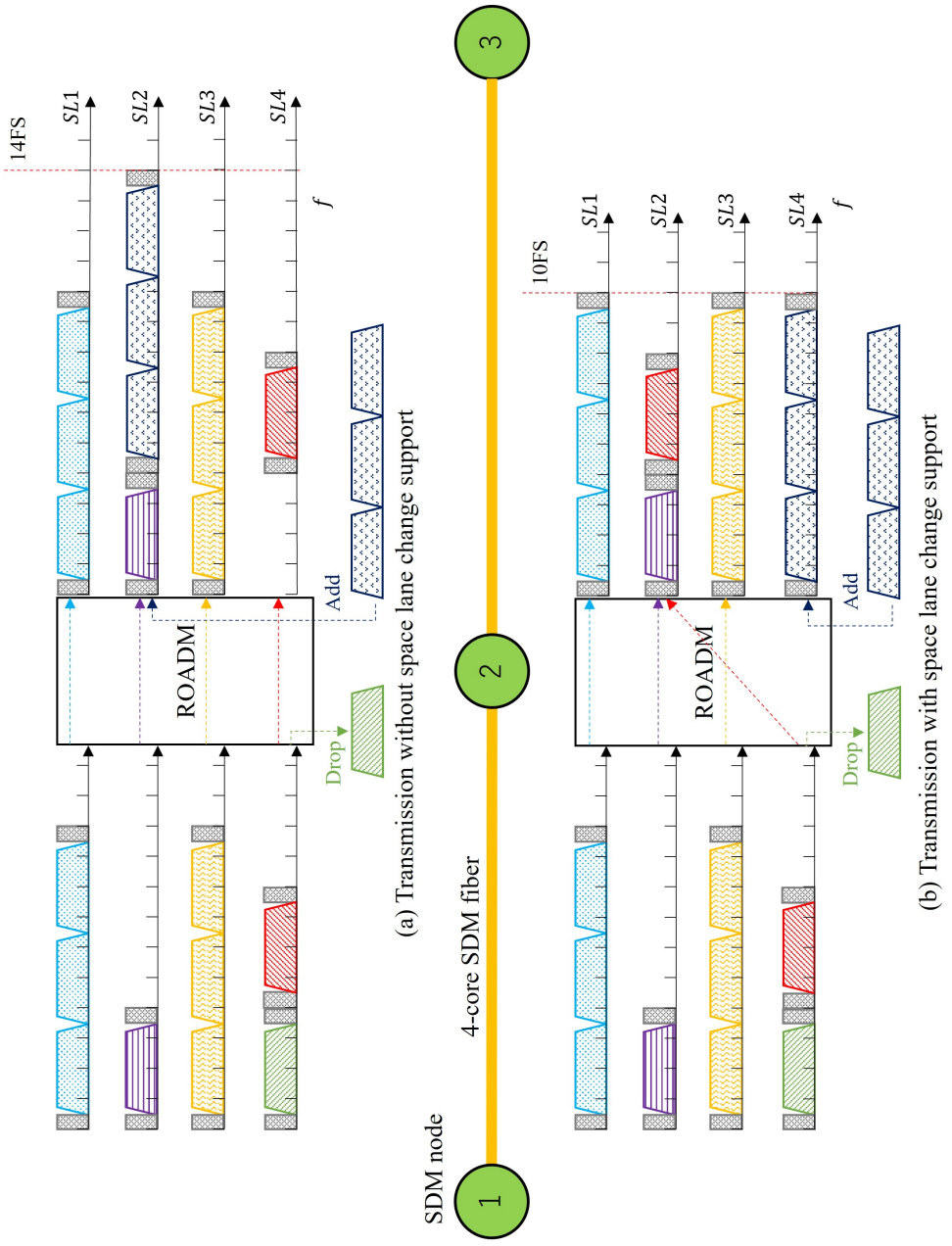

Figure 2.15: Examples of transmission without and with SLC support.

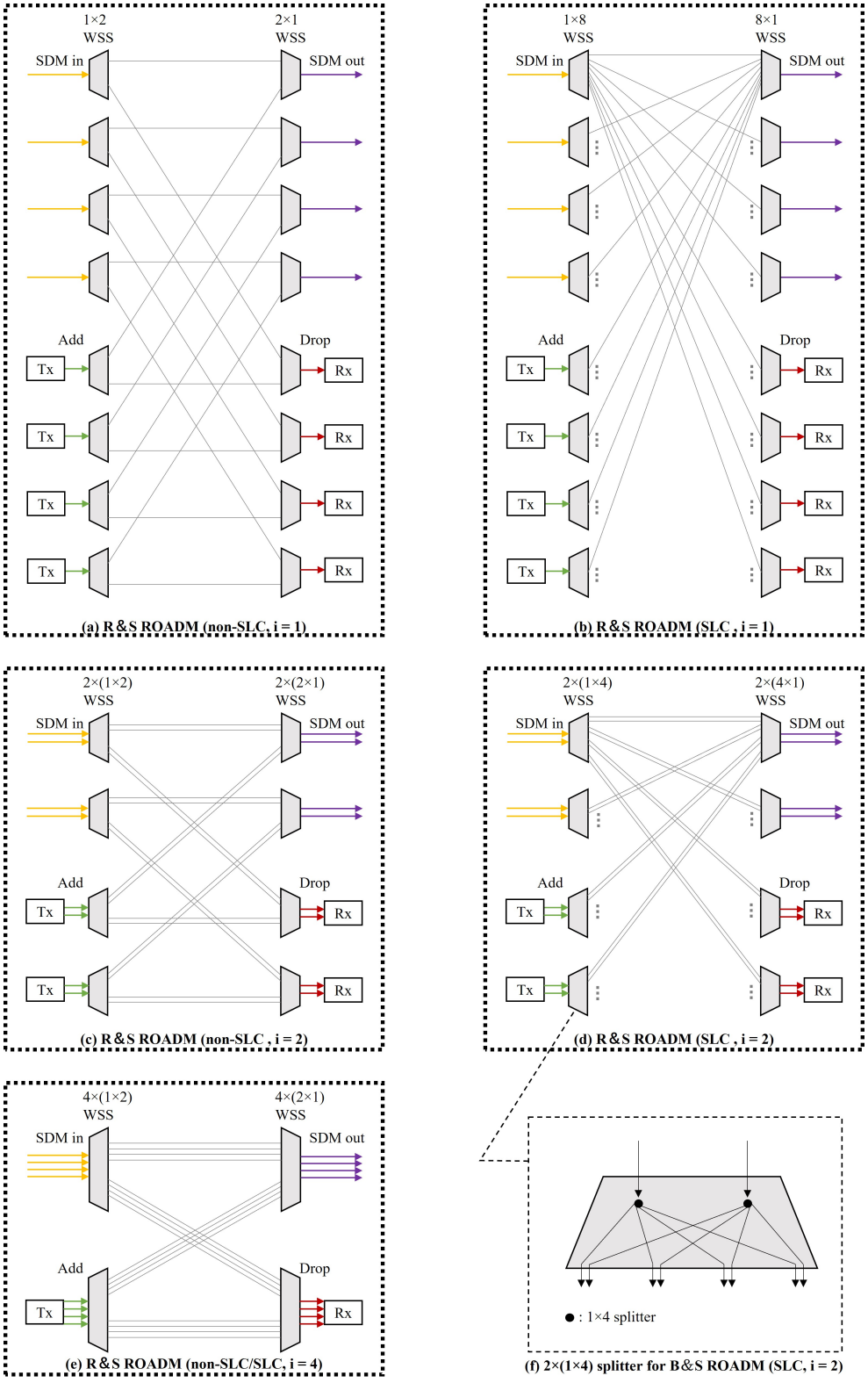

Figure 2.16: Illustration of ROADM architectures for various switching paradigms at spatial switching granularities i, which are equal to 1, 2 and 4, without and with SLC. R&S ROADM: route-and-select reconfigurable optical add-drop multiplexer; B&S ROADM: broadcast-and-select reconfigurable optical add-drop multiplexer; Tx: transmitter; Rx: receiver.

- Fig. 2.16(a) and (b) illustrate the architectures of the route-and-select (R&S) ROADMs corresponding to In-Sw without and with SLC, respectively. In this instance, the spatial switching granularity i is equal to 1. It is observed that the ROADM structure supporting SLC has a higher port count per WSS, resulting in higher costs.

- Fig. 2.16(c) and (d) illustrate the architectures of the R&S ROADMs corresponding to FrJ-Sw without and with SLC, respectively. In this instance, the spatial switching granularity i is equal to 2.

- Fig. 2.16(e) shows the architecture of the R&S ROADM corresponding to J-Sw with and without SLC. In this instance, the spatial switching granularity i is equal to 4. Since there is no spatial dimension group that can be changed when the connection requests pass through the ROADMs, the structures of the ROADMs are the same for the SLC and non-SLC cases when the switching paradigm is J-Sw. In addition, it should be noted that if all WSSs on the LHSs of Fig. 2.16(a) to (e) are replaced by splitters with the corresponding dimensions (e.g., Fig. 2.16(f) for Fig. 2.16(d)), the R&S ROADMs in the figures will change to broadcast-and-select (B&S) ROADMs.

2.4.5 Routing, modulation, space and spectrum assignment problem

Similar to the RWA problem in WSONs to the RSA/RMSA problem in EONs, new network features introduced by new network architectures will lead to evolving optimization problems in optical networks. In SDM-EONs, because of the introduction of multiple spatial dimensions, light-path selection needs to consider the assignment of space lanes (SLs), which makes the resource allocation problem more complex. As shown in Fig. 2.17, there are various scenarios for resource allocation in SDM-EONs because of the increased spatial dimensions. Such a resource allocation problem is the routing, space and spectrum assignment (RSSA) problem [12]. The names and meanings of RSSA problems may vary slightly depending on the different factors considered. For instance, if the fiber type of the network is MCF, the RSSA problem is also known as the routing, core and spectrum assignment (RCSA) problem.

Moreover, similar to the RSA problem, the RSSA problem is complexed into a routing, modulation format, space, and spectrum assignment (RMSSA) problem when multiple modulation formats are considered. The RSSA problem has been discussed and proven as NP-hard in many previous works [12, 27, 33, 48, 52, 134]. Thus, it is easy to realize that the RMSSA problem, which has a much higher complexity, is also obviously NP-hard. In this thesis, our work on the RMSSA problem will be presented in detail in Chapter 4.

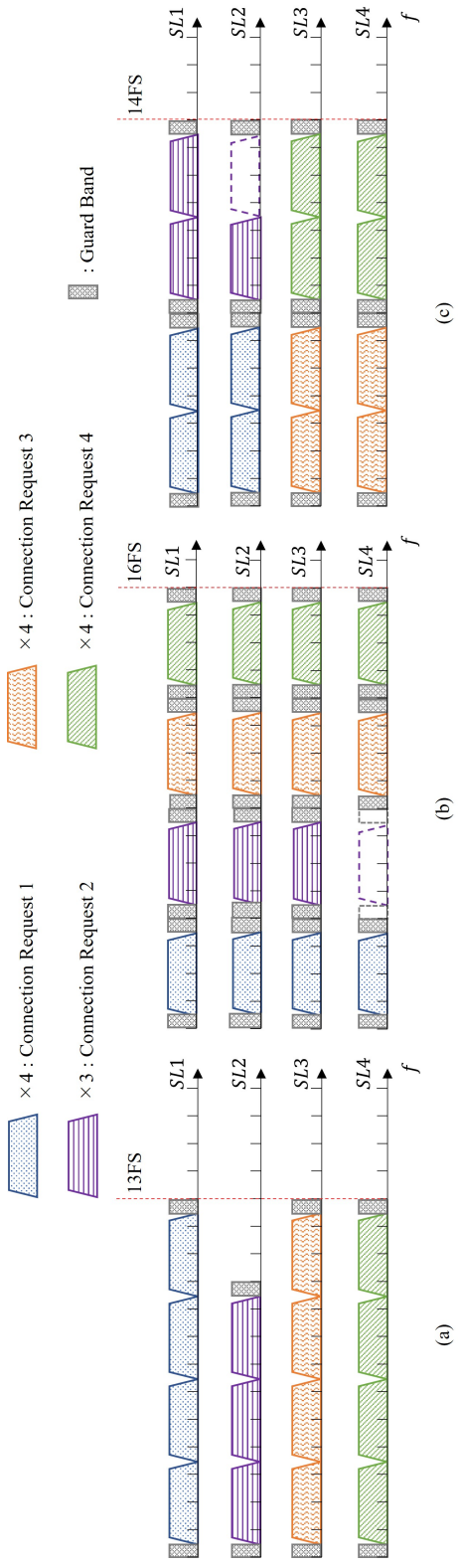

Figure 2.17: Illustration of various scenarios for resource allocation in SDM-EONs.

Chapter 3

ILP models and improved methods for the RSA/RMSA problem in EONs

Up to now, there has been a lot of work related to the RSA/RMSA problem for EON in static scenarios, as we discussed in Subsections 1.2.1 and 2.3.4. For static scenarios, mathematical models, such as the ILP model, are generally employed. These modeling and formulating as ILP can be classified into various types depending on the differences in viewpoints. As we mentioned in subsection 1.2.1, although there is a lot of work using a variety of ILP models to solve the static RSA/RMSA problem, the analysis of the respective characteristics of the various models is not yet clear. In this chapter, in order to better understand the characteristics of each type of models and to improve them for use in newer generations of optical networks, such as SDM-EONs, we systematically classify and summarize the models from previous works on the static RSA/RMSA problem for EONs, improve their computational performance according to the characteristics of each type of models, and compare the differences between them.

This chapter is organized into the following three sections. In Section 3.1, we classify mathematical optimization models for RSA/RMSA problems in previous works, and formulate the four types of mathematical models, path/slot, path/channel, node/slot, and node/channel, as ILP problems. In Section 3.2, we analyze the four models to understand the characteristics of each model, and improve the computation method to compensate for the weaknesses of each model. In Section 3.3, we verify the effectiveness of the improvement through computer experiments, and perform a comparative simulation experiment between the models used the improved calculation methods.

3.1 Optimization models for static RSA/RMSA problem

In this section, we address four optimization models (i.e., path/slot, path/channel, node/slot and node/channel model) with multiple modulations in turn. They are formulated as ILP in different ways. The descriptions of the notations common to these models are shown as follows.

Parameters:

E: the set of links in network topology.

F: the set of FSs index on each link.

MF: the set of available modulation levels.

R: the set of connection requests.

T_r: the traffic volume [Gbps] of connection request r.

P_r: the set of candidate paths for serving connection request r.

t_{OC}: the traffic volume [Gbps] that a single OC using the modulation format with the lowest spectral efficiency can support. How much traffic volume can be supported depends on the symbol-rate of the transceiver.

m_p: the level of modulation format that allows the length of the candidate path $p \in P_r$ according to DAT.

W_{FS}: the bandwidths [GHz] occupied by a FS.

W_{OC}: the bandwidths [GHz] occupied by a single OC.

W_{GB}: the bandwidths [GHz] occupied by a switching GB.

n_r^p: the number of FSs required for transmitting connection request r by using candidate path $p \in P_r$.

n_r^m: the number of FSs required for transmitting connection request r by using modulation level $m \in MF$.

M: a value that is large enough.

Variable:

$F_{max} \in \mathbb{Z}_+$: a nonnegative integer variable that indicates the maximum index of required FSs in the network topology.

For comparison purposes, we set the objective functions of the four models to be the same. That is minimizing the maximum index of required FSs in the network topology (i.e., $F_{\max}$), as shown in Eq. (3.1).

$$\text{minimize} \quad F_{\max} \tag{3.1}$$

In path/slot and path/channel models, n_r^p can be calculated by Eq. (3.2). We can assign modulation levels from small to large for different modulation formats from low to high spectral efficiencies. For instance, if we use the four modulation formats BPSK, QPSK, 8QAM, and 16QAM, which have spectral efficiencies of 1, 2, 3, and 4 [b/s/Hz], then we can assign modulation levels 1, 2, 3, and 4 to BPSK, QPSK, 8QAM, and 16QAM, respectively. In Eq. (3.2), the level of modulation format for candidate path p (i.e., m_p) can be determined by DAT. In other words, among all modulation formats that can serve the length of candidate path p, the modulation format with the highest spectral efficiency is selected, and the level corresponding to that modulation format is the value of m_p. Similarly, m indicates the level of modulation format in the set of available modulation levels MF, and n_r^m can be calculated by Eq. (3.3) in node/slot and node/channel models. In this paper, we assume that the spectrum grid (i.e., W_{FS}) is 12.5 GHz based on the ITU-T standard G.694.1, the transceiver transmits/receives an OC with 37.5 GHz (i.e., W_{OC}) bandwidth at a fixed 32 Gbaud baud rate, and the bandwidth of the switching GB (i.e., W_{GB}) is 12.5 GHz (6.25 GHz on each side of a SpCh).

$$n_r^p = \lceil \frac{\lceil \frac{T_r}{m_p \cdot t_{oc}} \rceil \cdot W_{OC} + W_{GB}}{W_{FS}} \rceil \tag{3.2}$$

$$n_r^m = \lceil \frac{\lceil \frac{T_r}{m \cdot t_{oc}} \rceil \cdot W_{OC} + W_{GB}}{W_{FS}} \rceil \tag{3.3}$$

The following subsections explain in order of additional parameters, variables, and respective constraints of each model.

3.1.1 Path/slot model

In the path/slot model, transmission paths are selected from the prepared candidate paths, and the model allocates FSs by using variables corresponding to themselves. We use the model proposed in [2]. However, the number of formulations for the nonoverlapping constraints of this model in [2] is larger. To simplify the model, we use the formulations of nonoverlapping constraints from [9], by which the number of nonoverlapping constraints can be reduced by $|R|^2 \cdot |P_r|^2$. This model uses the following additional parameters and variables.

Variables (additional)

$f_r \in \mathbb{Z}_+$: a nonnegative integer variable that indicates the index of the first FS used by the connection request r.

$o_{rr'} \in \{0, 1\}$: a binary variable that is equal to 1 if the index of starting FS used by

connection request r is smaller than that used by r', and 0 otherwise.

$x_r^p \in \{0,1\}$: a binary variable that is equal to 1 if candidate path p is used to transmit connection request r, and 0 otherwise.

Constraints

$$\sum_{p \in P_r} x_r^p = 1, \quad \forall r \in R \tag{3.4}$$

$$o_{rr'} + o_{r'r} = 1, \quad \forall r, r' \in R : r \neq r' \tag{3.5}$$

$$\begin{aligned} &f_r + n_r^p \leq f_{r'} + M\left[3 - \left(x_r^p + x_{r'}^{p'} + o_{rr'}\right)\right], \\ &\forall r, r' \in R, p \in P_r, p' \in P_{r'} : r \neq r', p \cap p' \neq \emptyset \end{aligned} \tag{3.6}$$

$$F_{\max} \geq f_r + n_r^p x_r^p - 1, \quad \forall r \in R, \quad p \in P_r \tag{3.7}$$

Eq. (3.4) indicates that only one path p can be selected for any connection request r from the set of candidate paths. Eqs. (3.5) and (3.6) together suggest spectrum non-overlapping constraints between different connection requests. Among them, Eq. (3.5) indicates the prioritization of connection requests, and expresses that there is always a prioritization for any two different connection requests. Eq. (3.6) indicates that the required FSs for different connection requests that have a common link in the path cannot overlap each other. Eq. (3.7) describes how to calculate the maximum index of the required FSs (i.e., $F_{\max}$). The right hand side of the Eq. (3.7) represents the index of the terminal FS used by the connection request r. For all connection requests in the whole network, the maximum index of required FSs $F_{\max}$ is larger than the terminal FS index used by any connection request.

$$\begin{cases} \text{minimize} \quad F_{max} \\ s.t. \\ (a)\ \sum_{p \in P_r} x_r^p = 1, \quad \forall r \in R \\ (b)\ o_{rr'} + o_{r'r} = 1, \quad \forall r, r' \in R : r \neq r' \\ (c)\ f_r + n_r^p \leq f_{r'} + M\left[3 - \left(x_r^p + x_{r'}^{p'} + o_{rr'}\right)\right], \\ \qquad \forall r, r' \in R, p \in P_r, p' \in P_{r'} : r \neq r', p \cap p' \neq \emptyset \\ (d)\ F_{\max} \geq f_r + n_r^p x_r^p - 1, \quad \forall r \in R, \quad p \in P_r \end{cases} \tag{3.8}$$

According to the objective function and constraints above, the path/slot model can be expressed as minimizing Eq. (3.1) under constraints Eqs. (3.4) to (3.7), i.e., Eq. (3.8).

3.1.2 Path/channel model

The path/channel model is a model that transmission paths are selected from the prepared candidate paths and that allocates FSs by using variables corresponding to the prepared candidate channels which consist of multiple adjacent FSs. We use the Channel-Based formulation proposed in Chapter 3 of Ref. [5]. This model uses the following additional parameter and variables.

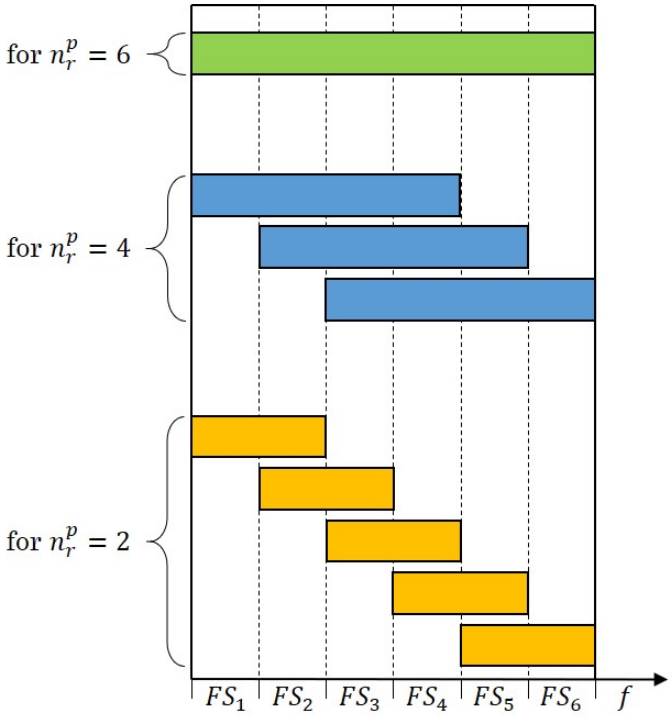

Figure 3.1: Examples of channels construction for connection requests requiring different number of FSs.

Parameters (additional)

C_r^p: the set of candidate channels that fit the number of required FSs for transmitting connection request r by path p.

f_r^{pc}: the index of the first FS in channel c of the connection request r transmitted by path p.

δ_r^{pcf}: a binary constant that is equal to 1 if channel c containing FS f is assigned to connection request r on path p, 0 otherwise.

C_r^p is a pre-computed set obtained by n_r^p. We illustrate it in Fig. 3.1 (assume that the maximum index of FSs on links is 6, shown as $FS_1, FS_2, \cdots, FS_6$). For a connection request requiring 2 FSs (i.e., $n_r^p = 2$), the set of channels $\{(FS_1, FS_2), (FS_2, FS_3), (FS_3, FS_4),$

$(FS_4, FS_5), (FS_5, FS_6)\}$ can be created, which is shown in yellow and has five channels with two FSs. Similarly, for a connection request requiring 4 and 6 FSs (i.e., $n_r^p = 4$ and $n_r^p = 6$), we can create the set of channels shown in blue and green, respectively. The channels construction method above can cover all situations where the connection request uses FSs.

$$C_r^p = \{[FS_i, FS_{i+1}, \ldots, FS_{i+n_r^p-1}] \mid i = 1, \ldots, |C_r^p|\} \tag{3.9}$$

$$|C_r^p| = |F| - n_r^p + 1 \tag{3.10}$$

Eq. (3.9) shows how the channels sets are generated. Each connection request r corresponds to one set of candidate channels C_r^p on each of its candidate paths. For any connection request, offset 1 FS each time to create a channel of size n_r^p, and traverse all FSs in the link to obtain the set of candidate channels for connection request r. Using the method, we can obtain the Eq. (3.10) for calculating the number of channels in the candidate channel set.

Variable (additional)

$x_r^{pc} \in \{0, 1\}$: a binary variable that is equal to 1 if channel c is used to serve connection request r on path p, and 0 otherwise.

Constraints

$$\sum_{p \in P_r} \sum_{c \in C_r^p} x_r^{pc} = 1, \quad \forall r \in R \tag{3.11}$$

$$\sum_{r \in R} \sum_{\substack{p \in P_r \\ e \subseteq p}} \sum_{c \in C_r^p} \delta_r^{pcf} x_r^{pc} \leq 1, \quad \forall e \in E, f \in F \tag{3.12}$$

$$\sum_{p \in P_r} \sum_{c \in C_r^p} (f_r^{pc} + n_r^p)\, x_r^{pc} - 1 \leq F_{\max}, \quad \forall r \in R \tag{3.13}$$

Eq. (3.11) states that for any connection request r, only one path p can be selected from the candidate path set P_r and only one channel c can be selected from the candidate channel set C_r^p on the path p. Eq. (3.12) expresses the spectrum non-overlapping constraint between different connection requests. It means that the number of connection requests using any FS on any link is always one or less. Eq. (3.13) describes how to calculate the maximum index of the required FSs (i.e., $F_{\max}$). It is easy to understand that the left hand side of Eq. (3.13) represents the index of the terminal FS used by the connection request r.

$$\begin{cases} \text{minimize} \quad F_{max} \\ s.t. \\ (a)\ \sum_{p\in P_r}\sum_{c\in C_r^p} x_r^{pc} = 1, \quad \forall r \in R \\ (b)\ \sum_{r\in R}\sum_{\substack{p\in P_r \\ e\subseteq p}}\sum_{c\in C_r^p} \delta_r^{pcf} x_r^{pc} \le 1, \quad \forall e \in E, f \in F \\ (c)\ \sum_{p\in P_r}\sum_{c\in C_r^p} (f_r^{pc} + n_r^p)\, x_r^{pc} - 1 \le F_{\max}, \quad \forall r \in R \end{cases} \tag{3.14}$$

According to the objective function and constraints above, the path/channel model can be expressed as minimizing Eq. (3.1) under constraints Eqs. (3.11) to (3.13), i.e., Eq. (3.14).

3.1.3 Node/slot model

The node-type constructs transmission paths for given connection requests by using variables corresponding to links. The node/slot model is a node-type model that allocates FSs by using variables corresponding to themselves. We use the node-link formulation proposed in Chapter 3 of [5]. To simplify the model, we use the formulations of nonoverlapping constraints from [9], by which the number of nonoverlapping constraints can be reduced by $2|R|^2$. This model uses the following additional parameters and variables.

Parameters (additional)

V: the set of nodes in network topology.
σ_v^+: the set of links leaving from node v.
σ_v^-: the set of links entering node v.
s_r: the origin node for connection request r.
d_r: the destination node for connection request r.
l^e: the length of link e.
a^m: the maximum transmission distance allowed by modulation level m.

Variables (additional)

$h_r \in \mathbb{R}_+$: a nonnegative continuous variable that represents the length of the path used by connection request r.

$u_r^m \in \{0,1\}$: a binary variable that is equal to 1 if connection request r uses the modulation level m, and 0 otherwise.

$x_r^e \in \{0,1\}$: a binary variable that is equal to 1 if connection request r uses link e, and 0 otherwise.

We also employ the variables f_r, $o_{rr'}$ described at subsection 3.1.1.

Constraints (additional)

$$\sum_{e\in\sigma_v^+} x_r^e - \sum_{e\in\sigma_v^-} x_r^e = \begin{cases} 1 & \text{if } v = s_r \\ -1 & \text{if } v = d_r \\ 0 & \text{otherwise} \end{cases} \quad \forall v \in V, r \in R \tag{3.15}$$

$$h_r \geq \sum_{e\in E} l^e x_r^e, \quad \forall r \in R \tag{3.16}$$

$$\sum_{m\in MF} a^m u_r^m \geq h_r, \quad \forall r \in R \tag{3.17}$$

$$\sum_{m\in MF} u_r^m = 1, \quad \forall r \in R \tag{3.18}$$

$$\begin{gathered} f_r + \textstyle\sum_{m\in MF} n_r^m u_r^m \leq f_{r'} + M\left[3 - \left(x_r^e + x_{r'}^e + o_{rr'}\right)\right] \\ \forall r, r' \in R, e \in E : r \neq r' \end{gathered} \tag{3.19}$$

$$F_{\max} \geq f_r + n_r^m u_r^m - 1, \quad \forall r \in R, m \in MF \tag{3.20}$$

Using the flow conservation law, Eq. (3.15) indicates that at each node in the network, one connection request can use only one path [5, 12, 14]. More specifically, in Eq. (3.15), σ_v^+ and σ_v^+ denote the set of links leaving and entering node v, respectively; and $\sum_{e\in\sigma_v^+} x_r^e$ and $\sum_{e\in\sigma_v^-} x_r^e$ denote the value of links leaving and entering node v, respectively. Thus, if x_r^e represents a path for connection request r, LHS of Eq. (3.15) equals to 1 for the origin node s_r and -1 for the destination node d_r. And, LHS of Eq. (3.15) equals to 0 for inter nodes in the path and other nodes without through the path. Note that Eq. (3.15) allows any cycles adding the path. If the cycles exist in the solution, we can delete them form the solution without being to infeasible. In the models where the routing is node-type, the path length is not a constant because the candidate path set is not created in advance. Therefore, it is unclear which modulation method can be used, and the number of FSs required for connection requests cannot be calculated in advance. Eqs. (3.16) to (3.18) represent the binary variable u_r^m for determining modulation level by DAT. Among them, Eq. (3.16) expresses the variable h_r which represents the length of path, Eqs. (3.17) and (3.18) together state that only one modulation level which allows the length of path can be selected for any connection request. Eq. (3.5) in subsection 3.1.1 and Eq. (3.19) together represent spectrum non-overlapping constraints between different connection requests, similar to the path/slot model in subsection 3.1.1. Eq. (3.20) expresses the calculation method of the maximum index $F_{\max}$ of the required FSs.

$$
\begin{cases}
\text{minimize} \quad F_{max} \\
s.t. \\
(a)\ \sum_{e\in\sigma_v^+} x_r^e - \sum_{e\in\sigma_v^-} x_r^e = \begin{cases} 1 & \text{if } v = s_r \\ -1 & \text{if } v = d_r \\ 0 & \text{otherwise} \end{cases} \quad \forall v \in V, r \in R \\
(b)\ h_r \geq \sum_{e\in E} l^e x_r^e, \quad \forall r \in R \\
(c)\ \sum_{m\in MF} a^m u_r^m \geq h_r, \quad \forall r \in R \\
(d)\ \sum_{m\in MF} u_r^m = 1, \quad \forall r \in R \\
(e)\ f_r + \sum_{m\in MF} n_r^m u_r^m \leq f_{r'} + M\left[3 - \left(x_r^e + x_{r'}^e + o_{rr'}\right)\right] \\
\qquad \forall r, r' \in R, e \in E : r \neq r' \\
(f)\ o_{rr'} + o_{r'r} = 1, \quad \forall r, r' \in R : r \neq r' \\
(g)\ F_{\max} \geq f_r + n_r^m u_r^m - 1, \quad \forall r \in R, m \in MF
\end{cases}
\tag{3.21}
$$

According to the objective function and constraints above, the node/slot model can be expressed as minimizing Eq. (3.1) under constraints Eq. (3.5) and Eqs. (3.15) to (3.20), i.e., Eq. (3.21).

3.1.4 Node/channel model

The node/channel model is a node-type model that allocates FSs by using variables corresponding to the prepared candidate channels which consist of multiple adjacent FSs. To the best of our knowledge, there are few works that use the formulation of the node/channel model and consider the modulation formats simultaneously. Therefore, we formulate the following node/channel model based on the 'NL-SA' formulation in [8] and the 'Node-Link' formulation in chapter 3 of [5].

Parameters (additional)

C_r: the set of candidate channels consisting of all possible required numbers of FSs for connection request r.

C_r^m: the set of candidate channels that fit the number of required FSs for transmitting connection r by modulation format m, $C_r^m \subseteq C_r$.

f_r^{mc}: the index of the first FS in channel c of the connection request r transmitted by modulation format m.

γ_r^{cf}: a binary constant that is equal to 1 if channel c in the set of channel for connection

request r contains FS f, 0 otherwise.

$$C_r^m = \{[FS_i, FS_{i+1}, \ldots, FS_{i+n_r^m-1}] \mid i = 1, \ldots, |C_r^m|\} \tag{3.22}$$

$$|C_r^m| = |F| - n_r^m + 1 \tag{3.23}$$

C_r and C_r^m are pre-computed sets obtained by n_r^m. Similar to the path/channel model in subsection 3.1.2, Eq. (3.22) shows how the channels sets are generated. The number of channels in the candidate channel set can be calculated by Eq. (3.23).

We also employ the Parameters V, σ_v^+, σ_v^-, MF, s_r, d_r, l^e, and a^m described at subsection 3.1.3.

Variables (additional)

$x_r^{ec} \in \{0, 1\}$: a binary variable that is equal to 1 if channel c is used to serve connection request r on link e, and 0 otherwise.

$y_r^c \in \{0, 1\}$: a binary variable that is equal to 1 if connection request r uses channel c, and 0 otherwise.

We also employ the variables u_r^m, h_r described at subsection 3.1.3.

Constraints (additional)

$$\sum_{e \in \sigma_v^+} x_r^{ec} - \sum_{e \in \sigma_v^-} x_r^{ec} = \begin{cases} +y_r^c & \text{if } v = s_r \\ -y_r^c & \text{if } v = d_r \\ 0 & \text{otherwise} \end{cases} \quad \forall v \in V, r \in R, c \in C_r \tag{3.24}$$

$$\sum_{c \in C_r^m} y_r^c = u_r^m, \quad \forall r \in R, m \in MF \tag{3.25}$$

$$h_r \geq \sum_{e \in E} \sum_{c \in C_r} l^e x_r^{ec}, \quad \forall r \in R \tag{3.26}$$

$$\sum_{r \in R} \sum_{m \in MF} \sum_{c \in C_r^m} x_r^{ec} \gamma_r^{cf} \leq 1, \quad \forall e \in E, f \in F \tag{3.27}$$

$$\sum_{m \in MF} \sum_{c \in C_r^m} (f_r^{mc} + n_r^m)\, x_r^{ec} - 1 \leq F_{max}, \quad \forall r \in R, e \in E \tag{3.28}$$

Eqs. (3.24) and (3.25) using flow conservation law indicates that at each node in the network, one connection request can use only one channel on only one path. And Eq. (3.25) shows the relationship between channels and modulation formats. Similar to the node/slot

model in subsection 3.1.3, Eqs. (3.17), (3.18) in subsection 3.1.3 and Eq. (3.26) represent the binary variable u_r^m for determining modulation format by DAT. Among them, Eq. (3.26) expresses the variable h_r which represents the length of path, Eqs. (3.17) and (3.18) together state that only one modulation format which allows the length of path can be selected for any connection request. Eq. (3.27) expresses the spectrum non-overlapping constraint between different connection requests, similar to the path/channel model in subsection 3.1.2. Eq. (3.28) describes how to calculate the maximum index of the required FSs (i.e., $F_{\max}$), similar to the path/channel model in subsection 3.1.2.

$$
\begin{cases}
\text{minimize} \quad F_{max} \\
s.t. \\
(a)\ \sum_{e\in\sigma_v^+} x_r^{ec} - \sum_{e\in\sigma_v^-} x_r^{ec} = \begin{cases} +y_r^c & \text{if } v = s_r \\ -y_r^c & \text{if } v = d_r \\ 0 & \text{otherwise} \end{cases} \\
\qquad \forall v \in V, r \in R, c \in C_r \\
(b)\ \sum_{c\in C_r^m} y_r^c = u_r^m, \quad \forall r \in R, m \in MF \\
(c)\ h_r \geq \sum_{e\in E} \sum_{c\in C_r} l^e x_r^{ec}, \quad \forall r \in R \\
(d)\ \sum_{r\in R} \sum_{m\in MF} \sum_{c\in C_r^m} x_r^{ec} \gamma_r^{cf} \leq 1, \quad \forall e \in E, f \in F \\
(e)\ \sum_{m\in MF} a^m u_r^m \geq h_r, \quad \forall r \in R \\
(f)\ \sum_{m\in MF} u_r^m = 1, \quad \forall r \in R \\
(g)\ \sum_{m\in MF} \sum_{c\in C_r^m} (f_r^{mc} + n_r^m)\, x_r^{ec} - 1 \leq F_{max}, \quad \forall r \in R, e \in E
\end{cases}
\tag{3.29}
$$

According to the objective function and constraints above, the node/channel model can be expressed as minimizing Eq. (3.1) under constraints Eq. (3.17), (3.18) and Eqs. (3.24) to (3.28), i.e., Eq. (3.29).

3.1.5 Classification of models in previous works

Through an extensive review of previous works on the static RSA/RMSA problem, we classify and summarize the ILP models as illustrated in Table 3.1.

For instance, Christodoulopoulos et al. [2] formulated a model for the RSA problem considering modulation formats (i.e., the RMSA problem), which matches the characteristics of the path/slot model we illustrated, and presented a decomposition method of the model, which breaks the RMSA problem into its two substituent subproblems.

Velasco et al. [3] first proposed a channel-based ILP model for the RSA problem with no modulation format considered, which matches the characteristics of the path/channel model we illustrated, and compared it with the slot-based model. The model in Walkowiak

Table 3.1: Classification of mathematical optimization models for RSA/RMSA problems in previous works.

	Path	Node
Slot	Christodoulopoulos et al. [2, 4], Wang et al. [13], Walkowiak [5], Wang et al. [29], Miyagawa et al. [10], Yang et al. [9], Wu et al. [16]	Cai et al. [7], Walkowiak [5]
Channel	Velasco et al. [3], Velasco et al. [8], Walkowiak et al. [11], Tornatore et al. [14], Goścień et al. [17], Walkowiak [5], Klinkowski et al. [5], Wu et al. [16]	Velasco et al. [8], Tornatore et al. [14] Klinkowski et al. [12]

et al. [11] also conforms to the path/channel model we introduced, but it differs slightly from the model in Velasco et al. [3] because it is presented in the context of the RSA problem considering modulation formats.

Cai et al. [7] first proposed a model of node-type for the RSA problem with no modulation format considered, which conforms to the node/slot model we introduced.

Velasco et al. [8] formulated a node-link model which used pre-computed slots for the RSA problem with no modulation format considered, which is similar to the node/channel model we illustrated.

3.2 Improved methods for models

To speed up the solution time of these ILP models, several studies have discussed improving computational methods to reduce the size of the variables and constraints of their models or to provide better bounds for these models.

To provide better lower bounds, Christodoulopoulos et al. [2] and Miyagawa et al. [10] formulated a path-type relaxation model in the RSA problem with modulation formats considered. Velasco et al. [3] proposed two relaxed formulations for path-type and node-type models in the RSA problem without modulation formats considered. In our work, we formulated both path-type and node-type relaxation models in the RSA problem with modulation formats considered in Subsection 3.2.2. Furthermore, for the channel model, to the best of our knowledge, no general existing study has proposed a method to reduce the number of channels in advance, as in Subsection 3.2.3.

3.2.1 Characteristics and weaknesses of each model

In order to improve the solving time by using an optimization software, we first observe the characteristics and the weaknesses of each model.

Table 3.2 shows the number of variables and constraints of the formulation of the four models, path/slot, path/channel, node/slot, and node/channel described in Section 3.1. From here, K is the number of candidate paths. For better comparison, we fixed the parameters K, $|V|$, $|E|$, $|MF|$, which are usually smaller than $|R|$ and $|F|$. As shown in Table 3.3, the constraints and the number of variables of each model can be roughly observed by $|R|$ and $|F|$. The following can be observed from Table 3.2 and Table 3.3.

Table 3.2: Number of variables and constraints per model.

Models	Variables	Constraints
path/slot	$\mathrm{O}\big(\lvert R\rvert^2+K\cdot\lvert R\rvert\big)$	$\mathrm{O}\big(K^2\cdot\lvert R\rvert^2\big)$
path/channel	$\mathrm{O}(K\cdot\lvert R\rvert\cdot\lvert C\rvert)$	$\mathrm{O}(\lvert E\rvert\cdot\lvert F\rvert+\lvert R\rvert)$
node/slot	$\mathrm{O}\big(\lvert R\rvert^2+\lvert R\rvert\cdot\lvert MF\rvert+\lvert R\rvert\cdot\lvert E\rvert\big)$	$\mathrm{O}\big(\lvert V\rvert\cdot\lvert R\rvert+\lvert R\rvert\cdot\lvert MF\rvert+\lvert R\rvert^2\cdot\lvert E\rvert\big)$
node/channel	$\mathrm{O}(\lvert R\rvert\cdot\lvert MF\rvert+\lvert R\rvert\cdot\lvert E\rvert\cdot\lvert C\rvert)$	$\mathrm{O}(\lvert V\rvert\cdot\lvert R\rvert\cdot\lvert C\rvert+\lvert R\rvert\cdot\lvert MF\rvert+\lvert E\rvert\cdot\lvert F\rvert+\lvert R\rvert\cdot\lvert E\rvert)$

Table 3.3: Number of variables and constraints per model derived by $|R|$ and $|F|$.

Models	Variables	Constraints
path/slot	$\mathrm{O}\big(\lvert R\rvert^2\big)$	$\mathrm{O}\big(\lvert R\rvert^2\big)$
path/channel	$\mathrm{O}(\lvert R\rvert\cdot\lvert F\rvert)$	$\mathrm{O}(\lvert F\rvert+\lvert R\rvert)$
node/slot	$\mathrm{O}\big(\lvert R\rvert^2\big)$	$\mathrm{O}\big(\lvert R\rvert^2\big)$
node/channel	$\mathrm{O}(\lvert R\rvert\cdot\lvert F\rvert)$	$\mathrm{O}(\lvert R\rvert\cdot\lvert F\rvert)$

(1) Since the number of variables and constraints in the two models of slot-type (path/slot and node/slot models) involves the square of the number of connection requests $|R|^2$, the number of connection requests $|R|$ has a large impact on the path/slot and node/slot models.

(2) Due to the number of constraints, path/slot model is susceptible from changes in the number of candidate paths K. However, since K is usually much smaller than $|R|$ and $|F|$, we can disregard its effect.

(3) From the number of constraints in path/channel model, we can observe that the model is affected by the number of links $|E|$ in network topology, the number of FSs $|F|$ on each link, and the number of connection requests $|R|$. Considering that $|E|$ tends to be much smaller than $|R|$ and $|F|$, we ignore its effect. And from the number of variables, it is also affected by the number of channels $|C|$ in the channel set. Since $|C|$ is positively

correlated with $|F|$, $|F|$ has an effect on the number of variables in the path/channel model.

(4) The node/slot model is not only affected by changes in the number of connection requests $|R|$, but also by the number of nodes $|V|$ and links $|E|$ in the network topology. In addition, it is also affected by the number of modulation levels $|MF|$. Likewise, we can ignore the effects of $|V|$, $|E|$ and $|MF|$ in the comparison.

(5) Node/channel model is influenced by all the parameters mentioned above.

(6) The numbers of variables and constraints of the path/slot and node/slot models are related to the square of the number of connection requests (i.e., $|R|^2$), while they of the path/channel and node/channel models are not only related to $|R|$ but are also affected by the number of FSs in each link $|F|$.

Based on the above observations, we will explore whether the calculation time of each model can be reduced. The number of nodes $|V|$ and the number of links $|E|$ are related to the size and structure of the network topology and cannot be improved in the resource allocation problem. In addition, since the number of connection requests $|R|$ is related to user needs and should not be reduced arbitrarily, we will work on improving the calculation method from other parameters. For example, it is expected that it is effective to reduce the calculation time of the model by first relaxing the part where there are too many constraints in the model and discarding unnecessary channels from channel sets.

3.2.2 Improved lower bound for models

Since there is a large number of constraints on spectrum allocation, if we relax some constraints, the relaxed model will become much easier to be solved. Then we solve the relaxed model and its solution will be a lower bound of the original model. In this way, we can reduce the computation time of solving the original models by some optimization softwares.

Therefore, we consider the following path-type and node-type relaxation models [2,3,10]. Firstly, we solve the relaxation problems. And then, we use the objective function values of the relaxed problems (path-type relaxation and node-type relaxation) as the initial lower bounds of original problems. These can effectively reduce the computation time of solving each ILP model.

The objective function of our RSA problems is to minimize the maximum index of FSs used in the network. The value of F_{use} will be given to the original path-type models as an initial lower bound. The meaning of the parameters and variables is the same as the parameters and variables in the path/slot model in Section 3.1. The lower bound F_{use} for path-type is obtained by the following ILP.

$$\begin{cases} \text{minimize} \quad F_{use} \\ s.t. \\ (a)\ \sum_{p \in P_r} x_r^p = 1, \quad \forall r \in R \\ (b)\ F_{use} \geq \sum_{r \in R} \sum_{\substack{p \in P_r \\ e \subseteq p}} x_r^p n_r^p - 1, \quad \forall e \in E \end{cases} \tag{3.30}$$

The constraint (a) is same as Eq. (3.4) described in subsection 3.1.1.

In order to find F_{use} by using formulation of node-type, we introduce a binary variable b_r^{me} that is equal to 1 if connection request r uses modulation m and link e, and 0 otherwise. And the meaning of the parameters and variables other than b_r^{me} is the same as that in node/slot model in Section 3.1. The lower bound F_{use} for node-type is obtained by the following ILP.

$$\begin{cases} \text{minimize} \quad F_{use} \\ s.t. \\ (a)\ \sum_{e \in \sigma_v^+} x_r^e - \sum_{e \in \sigma_v^-} x_r^e = \begin{cases} 1 & \text{if } v = s_r \\ -1 & \text{if } v = d_r \\ 0 & \text{otherwise} \end{cases} \\ \qquad \forall v \in V, r \in R \\ (b)\ h_r \geq \sum_{e \in E} l^e x_r^e, \quad \forall r \in R \\ (c)\ \sum_{m \in MF} a^m u_r^m \geq h_r, \quad \forall r \in R \\ (d)\ \sum_{m \in MF} u_r^m = 1, \quad \forall r \in R \\ (e)\ \sum_{r \in R} \sum_{m \in MF} b_r^{me} n_r^m - 1 \leq F_{use}, \quad \forall e \in E \\ (f)\ b_r^{me} \leq \frac{1}{2}\left(u_r^m + x_r^e\right), \quad \forall r \in R, m \in MF, e \in E \\ (g)\ b_r^{me} \geq u_r^m + x_r^e - 1, \quad \forall r \in R, m \in MF, e \in E \end{cases} \tag{3.31}$$

The constraints (a) to (d) are same as Eqs. (3.15) to (3.18) described in subsection 3.1.3.

3.2.3 Improved channels generation methods

In the channels construction methods, shown in Subsection 3.1.2 and 3.1.4, the size of the channels set C_r^p or C_r^m is determined by the number of FSs required for each connection request and the total number of FSs given on each link. We assume that 4 THz (C-band) is considered and that the spectrum grid (i.e., wavelength of an FS) is 12.5 GHz according to the ITU-T standard G.694.1 [97]. Therefore, there are 320 FSs on each link. In the case where the number of connection requests and the number of FSs required are not so large, the maximum index of FSs required on each link of the network may be much smaller

than 320. Therefore, if 320 is set as the maximum index of FSs in the preprocessing of creating channels, a large number of unnecessary channels will be created, which will waste computer memory and increase the computation time of the channel-type model. In this regard, if the upper bound of FSs required can be obtained before solving the channel-type model, the unnecessary channels can be effectively reduced by using the value of the upper bound in the preprocessing of creating channels.

Our improved channel generation method for the path/channel model can be described as the following 3 steps.

Step 1:

Obtain the paths for the connection requests by solving the path-type relaxation problem which is described as Eq. (3.30) in Subsection 3.2.2.

Step 2:

Solve the path-type spectrum allocation problem where the paths obtained in Step 1 is used, to obtain an upper bound of F_{max}. The path-type spectrum allocation problem can be described as Eqs. (3.1), (3.5), (3.6) and (3.7) in Section 3.1.

Step 3:

Generate the channels by using the channel generation method where the upper bound of F_{max} obtained in Step 2 is used. The channel generation method is described in Subsection 3.1.2.

Table 3.4: Maximum transmission distance of each modulation format and traffic volume supported of each OC at fixed 32 Gbaud.

Modulation format	DP-BPSK	DP-QPSK	DP-8QAM	DP-16QAM
Maximum transmission distance (km)	6300	3500	1200	600
Traffic volume per OC (Gbps)	50	100	150	200

Node/channel model does not have candidate sets of paths before it is solved, so the lengths of the paths which may be used by connection requests are unknown. Furthermore, if the length of the path is unknown, then we do not know which modulation format will be used. So we create channel sets for each modulation format under consideration. But if we consider all the cases where each modulation format is used, the number of channels will increase in proportion to the number of modulation formats. In practice, the number of FSs required may be the same for several different modulation formats in cases where the traffic volumes of connection requests are not very large. For example, we assume that a single OC comprises 3FSs generated by a transceiver and consider four modulation formats: DP-BPSK, DP-QPSK, DP-8QAM, and DP-16QAM. The volume of traffic that can

be transmitted simultaneously by one OC with each modulation format and the maximum distance that each modulation format can transmit, as in [33], are presented in Table 3.4. Then a connection request with 50 Gbps can be transmitted by an OC (3FSs) no matter what modulation format is used. In this case, if we create channel sets for all modulation formats, three of the channel sets will actually be wasted. Here, the modulation formats corresponding to the channel sets where waste occurs are called unnecessary modulation formats for connection requests (i.e., DP-QPSK, DP-8QAM and DP-16QAM in the example).

Similarly, our improved channel generation method for the node/channel model can be described as the following 4 steps.

Step 1:

Obtain the links and modulation levels for the connection requests by solving the node-type relaxation problem which is described as Eq. (3.31) in Subsection 3.2.2.

Step 2:

Solve the node-type spectrum allocation problem where the links and modulation levels obtained in Step 1 is used, to obtain an upper bound of F_{max}. The node-type spectrum allocation problem can be described as Eqs. (3.1), (3.5), (3.19) and (3.20) in Section 3.1.

Step 3:

Filter to obtain the set of useful modulation levels, where each modulation level leads to a different value of x_r^m.

Step 4:

Generate the channels by using the channel generation method where the upper bound of F_{max} obtained in Step 2 and the set of useful modulation levels obtained in Step 3 is used. The channel generation method is described in Subsection 3.1.4.

3.3 Simulation and numerical results

In this section, we first observe the effectiveness of our improved methods by using a 6-node ring network, and then compare the models through simulation experiment in N6S9 network.

Gurobi optimizer v9.0.1 [135] is the solver software used for the optimization of the models in this chapter. Since the RSA/RMSA problem mentioned in Subsection 2.3.4 has been proven to be NP-hard, the ILP models of the RSA/RMSA problem may not be solved completely (i.e., they may not find the optimal solution) in a reasonable time for some traffic data sets. Therefore, we set the upper limit of computation time for the solver to solve one instance in 3600 seconds. The simulation experiments were executed under

Microsoft Windows 10 by a computer with Intel 4-core 8 thread 3.7 GHz CPU and 16 GB memory.

3.3.1 Effectiveness of improvement

In this subsection, we will compare the models before and after the improvement in the 6-node ring shown in Fig. 3.2.

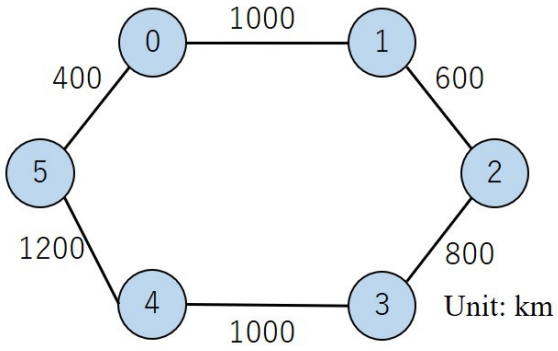

Figure 3.2: 6-node ring network topology

The total number of FSs that each link has (i.e., $|F|$), is set to 320 and the number of modulation levels $|MF|$ is set to 4. The amount of traffic that can be transmitted simultaneously by one OC with each modulation format and the maximum transmission distance that each modulation format can support are shown in Table 3.4.

We consider different number of connection requests – from 20 to 100, 20 per step. And 20 traffic data sets are generated randomly for each number of connection requests. The traffic volume (Gbps) of each connection request is randomly selected from 50, 100, 150, and 200 Gbps, and the origin and destination nodes of each connection request are randomly selected from the nodes in the network topology used. The candidate paths between each node pair are found in advance by the k-shortest path (KSP) algorithm [**?**]. Since it is a ring, there are two types of paths: when $K = 1$, only the shortest path is considered, and when $K = 2$, the path is chosen from all two candidate paths.

Table 3.5 shows the experimental results before and after the improvement of the path/slot model. In the table, "$K = 1$" and "$K = 2$" mean that the number of candidate paths is 1 and 2, respectively. "Done" indicates the ratio solved within the time limit of 3600 seconds in 20 experiments for each number of connection requests. "FS index" is the obtained value output within the time limit, and if the model can be solved within the time limit, it is the value of objective at optimal solution. "Gap" is the ratio of the difference between the obtained upper and lower bound for the objective function. So the

Table 3.5: Results before and after the improvement of path/slot model.

	$\|R\|$	K=1		K=2	
		original	improved	original	improved
Done (%)	20	100.00	100.00	100.00	100.00
	40	90.00	100.00	0.00	95.00
	60	5.00	100.00	0.00	75.00
	80	0.00	100.00	0.00	35.00
	100	0.00	100.00	0.00	20.00
FS index	20	31.00	31.00	23.60	23.60
	40	55.60	55.60	43.80	43.75
	60	75.85	75.85	61.75	60.75
	80	100.55	100.55	87.45	80.10
	100	121.90	121.90	112.45	101.1
Gap (%)	20	0.00	0.00	0.00	0.00
	40	2.27	0.00	53.95	0.12
	60	35.87	0.00	75.40	0.49
	80	57.18	0.00	84.66	2.55
	100	62.44	0.00	86.31	3.65
Runtime (s)	20	0.16	0.02	26.39	14.38
	40	429.78	0.02	3600.00	183.52
	60	3473.83	0.04	3600.00	1000.44
	80	3600.00	0.05	3600.00	2546.36
	100	3600.00	0.08	3600.00	2962.44

larger this value is, the more the solver is in the middle of its computation, and the less complete the process of solving the model is. "Runtime" indicates the computation time to solve the model. And the values of "FS index", "Gap", and "Runtime" are the average of the results obtained from 20 experiments.

From the results in Table 3.5, we can see that the performance of the path/slot model has been enhanced after the improvement. For instance, from the computation time "Runtime", we can see that the computation time of the improved model is clearly shorter than that before the improvement. In addition, the results in Table 3.5 also show that the path/slot model has a slow convergence of the lower bound. For instance, in the case that the number of candidate paths is 1 (i.e., $K = 1$), the completion rate of solving the model "Done" and the provisional FS index output within the time limit "FS index" show that the path/slot model before the improvement almost never be solved completely in time limit when the number of connection requests exceeds 60. But the provisional value obtained is the same as the value of the objective at optimal solution obtained from the improved model. This

is due to the very slow convergence of the lower bound of the path/slot model before the improvement. In other words, the improved model overcame the weakness of the slow convergence of the lower bound to a certain extent.

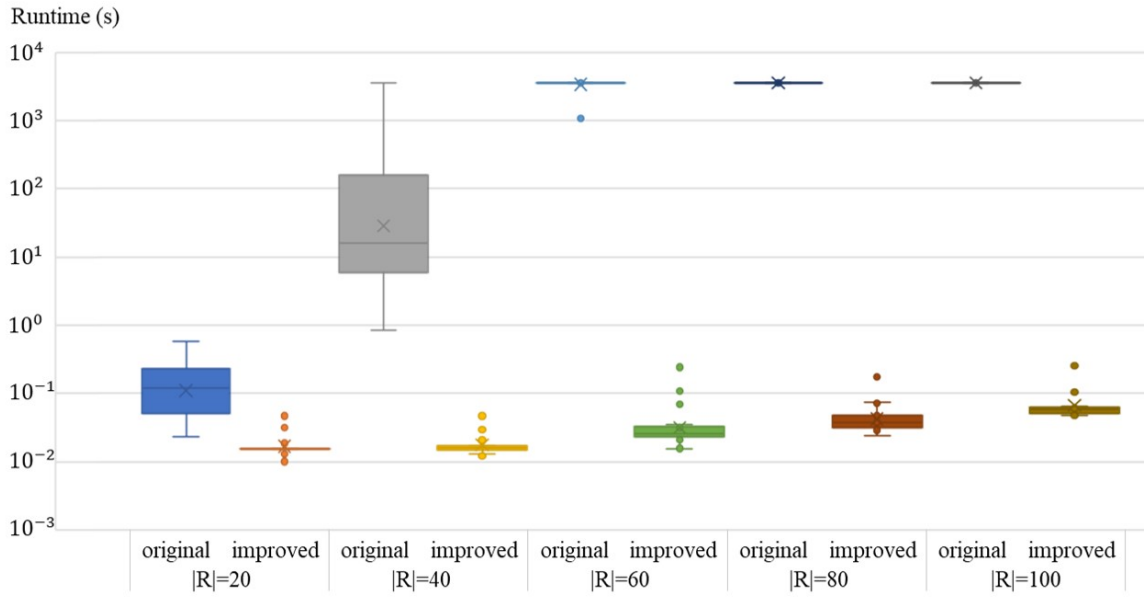

Figure 3.3: "Runtime" (before and after improvement) for all 20 traffic data sets at K=1 in path/slot model

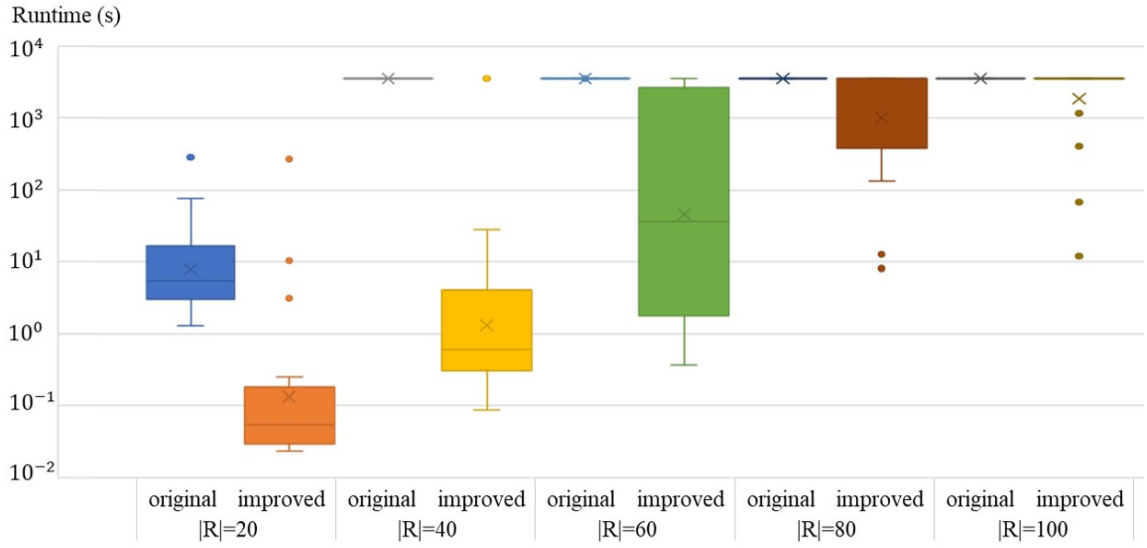

Figure 3.4: "Runtime" (before and after improvement) for all 20 traffic data sets at K=2 in path/slot model

Furthermore, Fig. 3.3 and Fig. 3.4 show the "Runtime" (before and after improvement) for all 20 traffic data sets at "K=1" and "K=2", respectively. We can observe that our

improved method has very positive performance, especially in the case of $K = 1$. However, the number of variables and constraints in path/slot is related to $K^2 \cdot |R|^2$, and since we are not improving the model itself, the effectiveness of our improved method decreases slightly when the number of connection requests increases to 60 and above, in the case of $K = 2$.

Table 3.6: Results before and after the improvement of path/channel model.

	$\|R\|$	K=1		K=2	
		original	improved	original	improved
Done (%)	20	100.00	100.00	100.00	100.00
	40	100.00	100.00	100.00	100.00
	60	100.00	100.00	95.00	100.00
	80	100.00	100.00	95.00	100.00
	100	100.00	100.00	90.00	100.00
FS index	20	31.00	31.00	23.60	23.60
	40	55.60	55.60	43.70	43.70
	60	75.85	75.85	60.45	60.45
	80	100.55	100.55	78.05	78.05
	100	121.90	121.90	97.35	97.35
Gap (%)	20	0.00	0.00	0.00	0.00
	40	0.00	0.00	0.00	0.00
	60	0.00	0.00	0.09	0.00
	80	0.00	0.00	0.07	0.00
	100	0.00	0.00	0.17	0.00
Runtime (s)	20	0.27	0.05	1.56	0.09
	40	1.69	0.12	8.50	0.54
	60	8.70	0.26	211.08	3.38
	80	11.22	0.48	280.41	12.30
	100	21.39	0.78	559.65	19.11

Table 3.6, Fig. 3.5 and Fig. 3.6 respectively show the results before and after the improvement of path/channel model and the details in "Runtime" of the 20 traffic data sets. We can observe that by improving the channels generation algorithm, path/channel model has also been well improved.

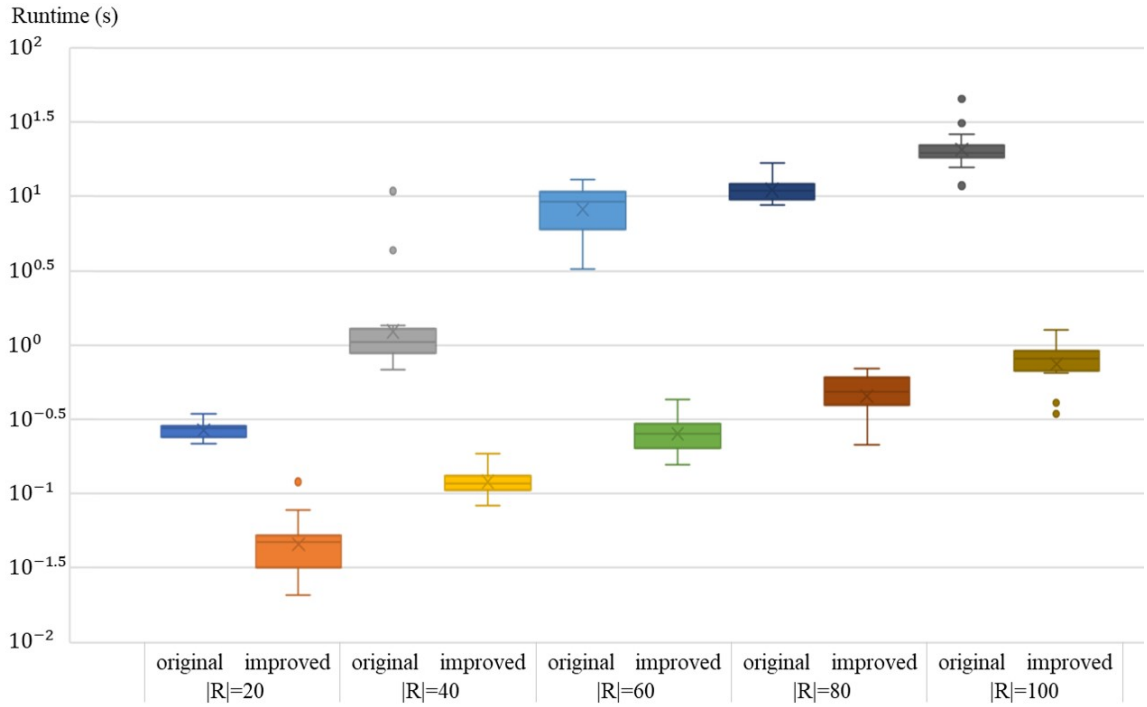

Figure 3.5: "Runtime" (before and after improvement) for all 20 traffic data sets at K=1 in path/channel model

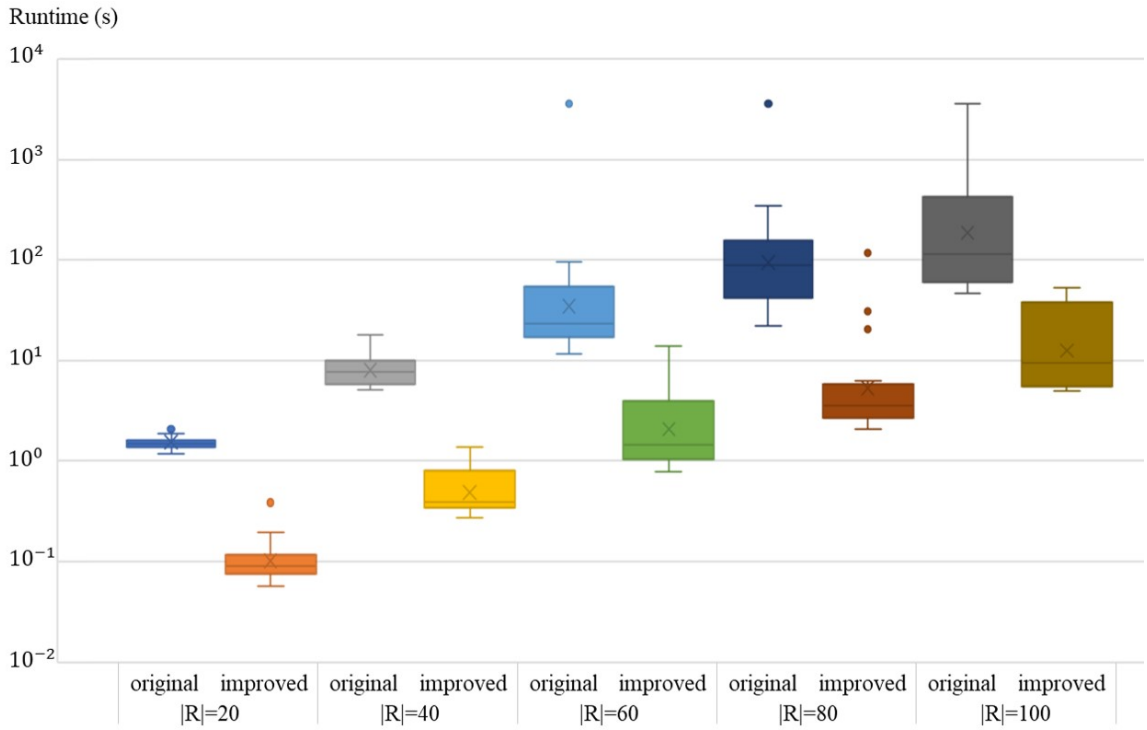

Figure 3.6: "Runtime" (before and after improvement) for all 20 traffic data sets at K=2 in path/channel model

Table 3.7: Results before and after the improvement of two node models.

	$\|R\|$	node/slot		node/channel	
		original	improved	original	improved
Done (%)	20	85.00	100.00	100.00	100.00
	40	0.00	95.00	—	100.00
	60	0.00	70.00	—	—
	80	0.00	35.00	—	—
	100	0.00	40.00	—	—
FS index	20	23.60	23.60	23.60	23.60
	40	43.80	43.75	—	43.70
	60	62.35	60.85	—	—
	80	86.95	79.80	—	—
	100	112.60	100.40	—	—
Gap (%)	20	1.52	0.00	0.00	0.00
	40	62.37	0.12	—	0.00
	60	79.27	0.60	—	—
	80	85.45	2.17	—	—
	100	88.98	3.04	—	—
Runtime (s)	20	804.94	44.92	553.63	73.59
	40	3600.00	230.67	—	1017.32
	60	3600.00	1473.16	—	—
	80	3600.00	2711.99	—	—
	100	3600.00	2440.28	—	—

The results before and after the improvement of the node/slot and node/channel model are given in Table 3.7. And Fig. 3.7 shows the details in "Runtime" of all 20 traffic data sets in the node/slot model. Similar to the path/slot model, the effectiveness of the improved method decreases slightly as the number of connection requests increases. Since it is difficult for the node/channel model to obtain a feasible solution within the time limit after the number of connection requests reaches a certain number, we have not counted the results of all 20 sets of traffic data sets of the model. The hyphen sign in Table 3.7 means that no feasible solution was found within the time limit. We can see that the performance of the node/slot and node/channel models has been improved after the improvement. It is worth mentioning that when the number of connection requests $|R|$ is more than 60, the node/channel model before and after the improvement did not find a feasible solution within the time limit, which indicates that the performance of the node/channel model is relatively low.

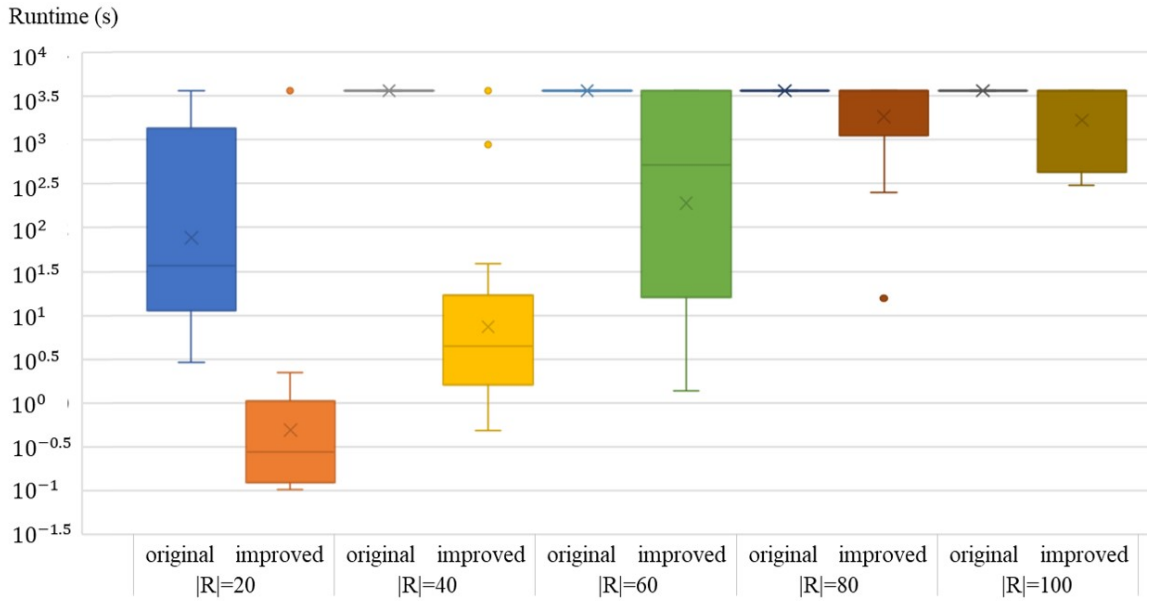

Figure 3.7: "Runtime" (before and after improvement) for all 20 traffic data sets in node/slot model

3.3.2 Comparative simulation

In this subsection, we perform a comparative simulation experiment to compare the models by using the improved calculation methods in Subsection 3.3.1 on the N6S9 and NSF networks [20] shown in Figs. 3.8 and 3.9. The simulation environment and the connection requests used in the N6S9 network topology are the same as those in Subsection 3.3.1. Similar to the traffic data sets generation approach in Subsection 3.3.1, in the simulation of the NSF network topology, we also consider different numbers of connection requests – from 20 to 100, 20 per step. Ten traffic data sets are generated randomly for each number of connection requests. The traffic volume (Gbps) of each connection request is randomly selected from 50, 100, 150, and 200 Gbps, and the origin and destination nodes of each connection request are randomly selected from the nodes in the network topology used.

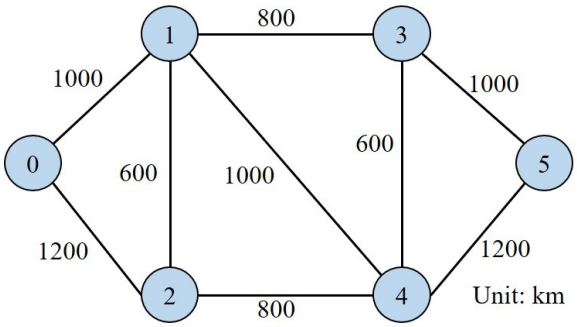

Figure 3.8: N6S9 network topology

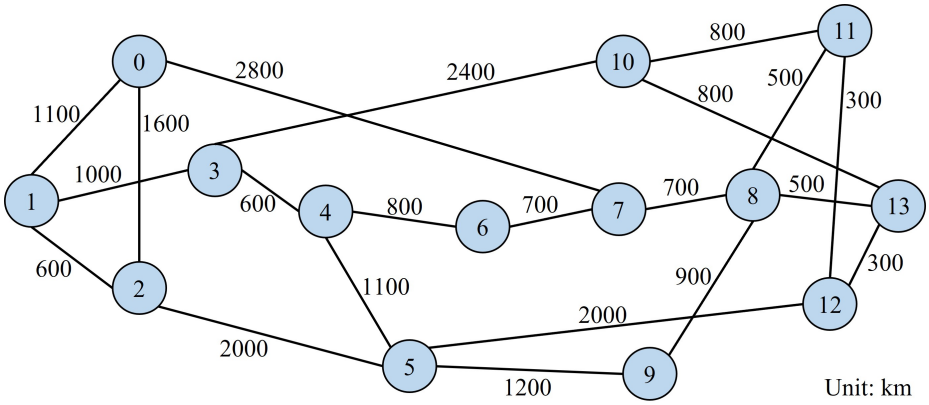

Figure 3.9: NSF network topology

Tables 3.8 and 3.9 show the results of our simulation on the N6S9 network and NSF network, respectively. The results in the table show the differences between path-type and node-type models and between slot-type and channel-type models.

We do not show the computational time for finding the initial bounds in our results for the following two reasons.

a) In our work, the main focus is on comparing the performances of the models. Since the initial bounds we provided to the four ILP models are the same, these bounds do not influence the comparison of the model computational times.

b) Actually, we performed 10 sets of pre-experiments for the path/slot model with K = 3, R = 100, and the average computation time for finding the initial bounds was 0.16s, which is much less than the average solution time of 2358.09s for the model in that case.

(1) Differences between path-type and node-type models

The differences between path-type and node-type models are mainly in computation time and the quality of the model solution.

Concerning the results of comparing the computation time “Runtime”, similar observa-

tions can be drawn from both N6S9 and NSF network topologies. That is, the two node-type models (i.e., node/slot and node/channel models) are slower than the two path-type models (i.e., path/slot and path/channel models). And the path-type models are quite fast in computation time, especially when the number of candidate paths K is small. The reason for the difference in computation time may be that the path-type and node-type models handle different numbers of paths. Specifically, for a path-type model, when $K = 1$, the path is already determined and only the spectrum allocation is to be determined. So its computation time should be the fastest. However, as K increases, the spectrum allocation also changes with respect to which path is chosen, thus expanding the search area. On the other hand, the node-type model has to determine the spectrum allocation and search for all possible paths between two nodes in the network regardless of the candidate paths, so the search area is quite large, which leads to a long calculation time.

For the quality of the model solution (i.e., the value of "FS index"), since all paths are considered in node-type model, an optimal solution can be obtained when the model is completely solved. However, the path-type models may not provide an optimal solution when not enough number of paths for the candidate is given. From the obtained value "FS index" output within the time limit, both network topologies indicate similar results. That is, in the results for $K = 1$ and $K = 2$ on both networks, and even in some results for $K = 3$ on the NSF network (e.g., $|R| = 20$ and $|R| = 40$), the two path-type models did not perform as well as the node-type models. This is because the candidate paths of the path-type models are limited when $K = 1$ and $K = 2$. When the number of candidate paths K is increased (e.g., $K = 3$, $K = 4$ and $K = 5$ on N6S9 network), the computation time of the path-type models became longer, but the solution became better. In other words, there is a trade-off between the solution quality of path-type model and the computation time.

(2) Differences between slot-type and channel-type models

The difference between slot-type and channel-type models is mainly in the computation time.

Firstly, when the number of connection requests is more than 60 on the N6S9 and 40 on the NSF network, the path/slot, path/channel, and node/slot models found feasible solutions, while the node/channel model did not even find a feasible solution within the time limit. This may be due to the large increase in the number of channels in the node/channel model. It is not possible to compare the two models in the node-type. Therefore, we only compare the path/slot model and the path/channel model in the path-type to analyze the difference between the slot-type and channel-type models.

The results for the path/slot and path/channel models on both network topologies show the high performance of the path/channel model. For instance, in the cases where

the number of candidate paths K was 2, 3, 4 and 5 on the N6S9 network and K was 2 and 3 on the NSF network, as the number of connection requests increased, the computation time of the path/slot model and the number of times the model was not solved significantly increased, while the path/channel model showed no particular increase in computation time and gap. This is probably due to the fact that the slot-type model has quite a lot of constraints on the prioritization of FSs assigned to connection requests. According to the observations in Section 3.2, the number of these constraints is related to the square of the number of connection requests, so as the number of connection requests increases, the number of constraints in the slot-type model increases exponentially, and the computation time of the slot-type model also increases significantly. On the other hand, the channel-type model satisfies the FSs contiguity constraints before solving the model, and creates a candidate set of channels with the required number of FSs for each connection request in advance. Therefore, in a channel-type model, there is no need to determine the prioritization of FSs assigned to connection requests, so there are no constraints on this, which reduces the computation time of the model.

Table 3.8: Results of comparative experiment on N6S9 network.

	$\|R\|$	path/slot					path/channel					node/slot	node/channel
		K=1	K=2	K=3	K=4	K=5	K=1	K=2	K=3	K=4	K=5		
Done (%)	20	100.00	100.00	100.00	100.00	100.00	100.00	100.00	100.00	100.00	100.00	100.00	100.00
	40	100.00	100.00	100.00	100.00	100.00	100.00	100.00	100.00	100.00	100.00	100.00	100.00
	60	100.00	95.00	95.00	75.00	75.00	100.00	100.00	100.00	100.00	100.00	70.00	—
	80	100.00	80.00	80.00	70.00	70.00	100.00	100.00	100.00	100.00	100.00	60.00	—
	100	100.00	60.00	40.00	40.00	35.00	100.00	100.00	100.00	100.00	100.00	25.00	—
FS index	20	23.55	15.05	14.75	14.75	14.75	23.55	15.05	14.75	14.75	14.75	14.75	14.75
	40	47.95	28.05	27.50	27.50	27.50	47.95	28.05	27.50	27.50	27.50	27.50	27.50
	60	67.30	37.95	37.55	37.70	37.70	67.30	37.70	37.50	37.45	37.45	37.90	—
	80	86.00	50.75	50.45	50.65	50.70	86.00	50.55	50.25	50.25	50.25	51.05	—
	100	98.40	60.05	60.30	60.40	60.85	98.40	59.50	59.40	59.40	59.40	60.75	—
Gap (%)	20	0.00	0.00	0.00	0.00	0.00	0.00	0.00	0.00	0.00	0.00	0.00	0.00
	40	0.00	0.00	0.00	0.00	0.00	0.00	0.00	0.00	0.00	0.00	0.00	0.00
	60	0.00	0.66	0.13	0.62	0.69	0.00	0.00	0.00	0.00	0.00	1.18	—
	80	0.00	0.41	0.41	0.79	0.90	0.00	0.00	0.00	0.00	0.00	1.49	—
	100	0.00	0.92	1.50	1.67	2.36	0.00	0.00	0.00	0.00	0.00	2.25	—
Runtime (s)	20	0.01	0.02	0.07	0.13	0.19	0.03	0.05	0.07	0.12	0.09	1.69	9.42
	40	0.01	0.38	14.73	4.69	71.53	0.09	0.19	0.23	0.29	0.43	199.37	441.41
	60	0.02	911.46	296.96	944.95	1270.59	0.15	0.67	0.83	1.29	1.72	1271.57	—
	80	0.03	951.66	863.60	1198.64	1276.59	0.27	1.75	1.78	2.31	4.69	1857.49	—
	100	0.03	1556.70	2358.09	2442.63	2457.69	0.35	2.15	4.18	6.10	7.78	2978.29	—

Table 3.9: Results of comparative experiment on NSF network.

	$\|R\|$	path/slot			path/channel			node/slot	node/channel
		K=1	K=2	K=3	K=1	K=2	K=3		
Done (%)	20	100.00	100.00	100.00	100.00	100.00	100.00	100.00	100.00
	40	100.00	100.00	100.00	100.00	100.00	100.00	90.00	—
	60	100.00	90.00	50.00	100.00	100.00	100.00	40.00	—
	80	100.00	80.00	30.00	100.00	100.00	100.00	30.00	—
	100	100.00	80.00	10.00	100.00	100.00	80.00	0.00	—
FS index	20	24.70	16.70	15.10	24.70	16.70	15.10	14.30	14.30
	40	41.50	27.70	26.20	41.50	27.70	26.20	25.80	—
	60	58.70	39.20	37.10	58.70	39.10	36.60	37.00	—
	80	67.00	45.50	44.50	67.00	45.30	43.10	44.60	—
	100	87.90	56.80	57.30	87.90	55.80	54.50	58.40	—
Gap (%)	20	0.00	0.00	0.00	0.00	0.00	0.00	0.00	0.00
	40	0.00	0.00	0.00	0.00	0.00	0.00	0.48	—
	60	0.00	0.29	1.33	0.00	0.00	0.00	3.23	—
	80	0.00	0.42	3.12	0.00	0.00	0.00	3.56	—
	100	0.00	1.85	5.38	0.00	0.00	0.39	8.07	—
Runtime (s)	20	0.08	0.12	0.07	0.11	0.19	0.10	4.57	189.01
	40	0.06	0.76	3.08	0.20	0.54	1.04	833.77	—
	60	0.08	364.15	1836.74	0.34	2.65	9.47	2918.29	—
	80	0.12	741.18	2537.93	0.47	23.75	32.76	3326.55	—
	100	0.28	3084.25	3279.35	0.79	85.12	909.45	3600.00	—

Chapter 4

Solving the RMSSA problem in SDM-EONs via a node-type ILP model

In SDM-EONs, because of the introduction of multiple spatial dimensions, light-path selection needs to consider the assignment of space lanes (SLs), which makes the resource allocation problem more complex. Such a resource allocation problem is the routing, space and spectrum assignment (RSSA) problem [12]. Similarly, the RSSA problem is complexed into a routing, modulation format, space, and spectrum assignment (RMSSA) problem when multiple modulation formats are considered. As we stated in Subsection 1.2.2, in the design phase of optical networks, the resource allocation problem in static scenarios needs to be solved to ensure a more rational network design. In order to ensure the optimal solution, mathematical models such as ILP models are often used to solve the resource allocation problems in static scenarios. Node-type ILP models are important for the resource allocation problems in static scenarios due to its global optimal solutions. To the best of our knowledge, there has not been any study that addresses the RMSSA problem involving multiple modulation formats by modeling a node-based ILP in the static scenario of SDM-EONs. In our work, considering the limitations of the role of SLC in static scenarios, a novel non-SLC node-type ILP model considering all three types of SpChs is proposed, and several computational methods to speed up the model are discussed.

This chapter is organized into the following three sections. In Section 4.1, we depict our non-SLC node-type ILP model for solving the RMSSA problem with the objective of minimizing the maximum FS index. In Section 4.2, we develop four algorithms based on the model, three of which are used to solve the model exactly for small-scale instances and the other one is a heuristic algorithm for large-scale instances. In Section 4.3, we compare the three exact algorithms for solving our model and verify the effectiveness of the three algorithms via lower bounds of our model and results of the heuristic algorithm.

In addition, we compare our model with the previous k-path-type one in Refs. [9, 16] via simulation experiments.

4.1 Problem formulation

In this section, we construct a node-type ILP model for the static non-SLC RMSSA problem (referred to as the non-SLC node-type ILP model) with arbitrary spatial switching granularity.

4.1.1 Non-SLC node-type ILP model

Parameters

i: the spatial switching granularity.

G_i: the set of spatial dimension g determined by the spatial granularity i.

V: the set of network topology nodes.

E: the set of network topology links.

σ_v^+: the set of links leaving from node $v \in V$.

σ_v^-: the set of links entering node $v \in V$.

l^e: the length of link $e \in E$.

MF: the set of available modulation levels.

a^m: the largest connection distance that can be reached in modulation level $m \in MF$.

R: the set of connection requests.

W_{FS}: the bandwidth of one FS.

W_{GB}: the bandwidth of one GB.

W_{OC}: the bandwidth of one OC.

s_r: the source node of connection request $r \in R$.

d_r: the destination node of connection request $r \in R$.

t_{OC}: the traffic volume [Gbps] that can be transmitted by a single OC using the least spectrally efficient modulation format.

T_r: the traffic volume [Gbps] of connection request $r \in R$.

n_r^{mi}: the number of FSs necessary to connection request $r \in R$ using modulation level $m \in MF$ at spatial granularity i.

M: a value that is large enough.

Notably, the set of available modulation levels is constructed by assigning the modulation levels from small to large according to the order of low to high spectral efficiency. Specifically, to construct a set of available modulation levels MF, we can assign modu-

lation levels 1, 2, 3, and 4 in MF corresponding to the modulation formats DP-BPSK, DP-QPSK, DP-8QAM, and DP-16QAM with spectral efficiencies of 2, 4, 6, and 8 [b/s/Hz], respectively [5].

Thus, in the node-type ILP model, the number of FSs n_r^{mi} can be calculated by Eq. (4.1). In this chapter, we assume that the spectrum grid (i.e., W_{FS}) is 12.5 GHz based on the ITU-T standard G.694.1, the transceiver transmits/receives an OC with 37.5 GHz (i.e., W_{OC}) bandwidth at a fixed 32 Gbaud baud rate, and the bandwidth of the switching GB on each side of an SpCh (i.e., W_{GB}) is 6.25 GHz.

$$n_r^{mi} = \left\lceil \frac{\left\lceil \left\lceil \frac{T_r}{m \cdot t_{oc}} \right\rceil / i \right\rceil \cdot W_{OC} + 2W_{GB}}{W_{FS}} \right\rceil \tag{4.1}$$

Variables

$x_r^{eg} \in \{0, 1\}$: a binary variable is set equal to 1 if connection request r uses spatial dimension group g on link e and 0 otherwise.

$u_r^m \in \{0, 1\}$: a binary variable that is set equal to 1 if connection request r uses the modulation level m and 0 otherwise.

$o_{rr'} \in \{0, 1\}$: a binary variable that is set equal to 1 if the index of starting FS used by r is smaller than that used by r' and 0 otherwise.

$h_r \in \mathbb{R}_+$: a nonnegative continuous variable that represents the length of the path used by connection request r.

$f_r \in \mathbb{Z}_+$: a nonnegative integer variable that indicates the index of the first FS used by the connection request r.

$F_{max} \in \mathbb{Z}_+$: a nonnegative integer variable that indicates the maximum index of required FSs in the network topology.

Objective function

$$\text{Minimize} \quad F_{max} \tag{4.2}$$

The objective function of the model is to minimize the maximum index of the required FSs F_{max} in the network topology, as shown in Eq. (4.2).

Constraints

Constraint for light path uniqueness and spatial continuity:

$$\sum_{e\in\sigma_v^+} x_r^{eg} - \sum_{e\in\sigma_v^-} x_r^{eg} = \begin{cases} 1 & \text{if } v = s_r \\ -1 & \text{if } v = d_r \\ 0 & \text{otherwise} \end{cases} \quad \forall v \in V, r \in R, g \in G_i \tag{4.3}$$

$$\sum_{e\in\sigma_v^-} \sum_{g\in G_i} x_r^{eg} \leq 1, \quad \forall v \in V, r \in R \tag{4.4}$$

$$\sum_{e\in\sigma_v^+} \sum_{g\in G_i} x_r^{eg} \leq 1, \quad \forall v \in V, r \in R \tag{4.5}$$

Eqs. (4.3) to (4.5) ensure that only one path and one spatial dimension group are used for each connection request, i.e., ensure light path uniqueness and spatial continuity (i.e., non-SLC) constraints. Specifically, Eq. (4.3) uses the law of flow conservation. If the light path transmitting the connection request r uses the spatial dimension group g on link e, then the left-hand side of Eq. (4.3) will equal 1 at the source node s_r and -1 at the destination node d_r, and it will equal 0 at inter nodes on the light path and at nodes not on the light path. Eqs. (4.4) and (4.5) enable that there is no cycle in the light path. Specifically, a connection request r can enter and exit a node at most once, regardless of the spatial dimension g.

Constraint for DAT:

$$h_r \geq \sum_{e\in E} \sum_{g\in G_i} l^e x_r^{eg}, \quad \forall r \in R \tag{4.6}$$

$$\sum_{m\in MF} a^m u_r^m \geq h_r, \quad \forall r \in R \tag{4.7}$$

$$\sum_{m\in MF} u_r^m = 1, \quad \forall r \in R \tag{4.8}$$

Eqs. (4.6) to (4.8) represent that only one modulation level, which is determined by the length of the path, can be selected for any connection request. Specifically, the path lengths h_r under different decision variables x_r^{eg} are obtained by Eq. (4.6). Then the appropriate $m \in MF$ can be selected by Eq. (4.7). Eq. (4.8) ensures that only the same m will be used for a connection request.

Constraint for spectrum continuity and spectrum nonoverlapping:

$$o_{rr'} + o_{r'r} = 1, \quad \forall r, r' \in R : r \neq r' \tag{4.9}$$

$$f_r + \sum_{m \in MF} n_r^{mi} u_r^m \leq f_{r'} + M(3 - x_r^{eg} - x_{r'}^{eg} - o_{rr'}) \quad \forall r, r' \in R, e \in E, g \in G_i : r \neq r' \tag{4.10}$$

$$f_r + \sum_{m \in MF} n_r^{mi} u_r^m - 1 \leq F_{max}, \quad \forall r \in R \tag{4.11}$$

Eqs. (4.9) and (4.10) prevent the overlapping of the spectrum used by different connection requests. Specifically, Eq. (4.9) captures the relationship between the starting FS of r and r'. If r and r' use the same link e and spatial dimension g and f_r less than $f_{r'}$ which means the starting FS of r is before r', the RHS of Eq. (4.10) is equal to $f_{r'}$. To ensure that Eq. (4.10) holds, the RHS of Eq. (4.10) needs to be greater than f_r plus the number of FSs required for r which on the LHS of the Eq. (4.10). On the contrary, if r and r' do not use the same link e and spatial dimension g simultaneously, or if the starting FS of r' is before r, the RHS of the equation is large enough for Eq. (4.10) to hold. Eq. (4.11) expresses the calculation method of F_{max}.

$$\begin{cases} \text{minimize} \quad F_{max} \\ s.t. \\ (a)\ \sum_{e \in \sigma_v^+} x_r^{eg} - \sum_{e \in \sigma_v^-} x_r^{eg} = \begin{cases} 1 & \text{if } v = s_r \\ -1 & \text{if } v = d_r \\ 0 & \text{otherwise} \end{cases} \\ \qquad \forall v \in V, r \in R, g \in G_i \\ (b)\ \sum_{e \in \sigma_v^-} \sum_{g \in G_i} x_r^{eg} \leq 1, \quad \forall v \in V, r \in R \\ (c)\ \sum_{e \in \sigma_v^+} \sum_{g \in G_i} x_r^{eg} \leq 1, \quad \forall v \in V, r \in R \\ (d)\ h_r \geq \sum_{e \in E} \sum_{g \in G_i} l^e x_r^{eg}, \quad \forall r \in R \\ (e)\ \sum_{m \in MF} a^m u_r^m \geq h_r, \quad \forall r \in R \\ (f)\ \sum_{m \in MF} u_r^m = 1, \quad \forall r \in R \\ (g)\ o_{rr'} + o_{r'r} = 1, \quad \forall r, r' \in R : r \neq r' \\ (h)\ f_r + \sum_{m \in MF} n_r^{mi} u_r^m \leq f_{r'} + M(3 - x_r^{eg} - x_{r'}^{eg} - o_{rr'}) \\ \qquad \forall r, r' \in R, e \in E, g \in G_i : r \neq r' \\ (i)\ f_r + \sum_{m \in MF} n_r^{mi} u_r^m - 1 \leq F_{max}, \quad \forall r \in R \end{cases} \tag{4.12}$$

According to the objective function and constraints above, the node/channel model can be expressed as Eq. (4.12).

4.1.2 Analysis for scales of the proposed ILP model

In this subsection, we summarize our proposed non-SLC node-type ILP model (hereafter referred to as node-type model) and compare it with the previous k-path-type ILP model

in Ref. [16]. The major differences are stated as follows.

Table 4.1: Number of variables and constraints per model.

Models	Variables	Constraints
k-path-type	$O(k \cdot \|R\| \cdot \|E\| \cdot \|G_i\| \cdot \|F\|)$	$O(k \cdot \|R\| \cdot \|E\| \cdot \|F\|)$
node-type	$O(\|R\| \cdot \|E\| \cdot \|G_i\| + \|R\|^2)$	$O(\|R\|^2 \cdot \|E\| \cdot \|G_i\|)$

Table 4.1 shows the order of magnitude of the variables and constraints for the node-type and path-type model. Where the same notations as in Subsection 4.1.1 are used, and k indicates the number of alternate routes in the k-path-type model.

- The number of variables and constraint expressions in the node-type model is related to the square of the number of connection requests, so the number of connection requests significantly impacts the node-type model.
- The node-type model is not only affected by the number of connection requests but also by the number of links in the network topology and changes in the number of spatial dimensions.
- The path-type model is sensitive to changes in the number of candidate paths k. In addition, the path-type model is influenced by the number of links in the network topology, the total number of FS on each link, and the number of connection requests.

Since the number of variables and constraints of the model are proportional to $|R|^2$, $|E|$ and $|G_i|$, the model will become increasingly difficult to solve as the number of connection requests, spatial dimensions and scale of the network topology increase. Hence, for large-scale instances, such as dealing with a large number of connection requests in a network topology with a large number of nodes, links and spatial dimensions, the model may be difficult to solve with ILP solvers. Actually, in our pre-experiments that included a small 6-node network, the model was difficult to solve directly when there were more than 100 connection requests in the network, which obviously needs to be improved.

4.2 Algorithms for solving the node-type ILP model

In this section, we address three model decomposition algorithms named direct model decomposition (DMD), All-SLC model decomposition (ASLC-MD), and Semi-SLC model decomposition (SSLC-MD) algorithms for enabling the ILP solvers to solve the model more efficiently, and also propose a heuristic algorithm named first-fit greedy (FF-G) algorithm to corresponding large-scale instances that are difficult to solve via ILP solvers.

4.2.1 Direct model decomposition (DMD) algorithm

Node-type models are difficult to solve exactly with ILP solvers since the default initial bounds provided by ILP solvers are often of low quality. Providing superior initial bounds by decomposing the model for solving in multiple stages is a method that can effectively speed up the solving of the model. Such the method has been used in several previous related works Ref. [2, 3, 10] which focused on the RSA/RMSA problem of EONs.

For the RMSSA problem of SDM-EONs, the increase in spatial dimensions makes the model decomposition methods more diverse. In particular, since the constraints related to spectrum assignment (SA) have a huge number, it is necessary to keep the number of constraints included in this part as small as possible when decomposing the model. However, if the part related to routing assignment (RA) contains too many constraints, it may lead to too slow solving of the relaxation model in this part, thus affecting the overall solving process. We discussed the three decomposition methods "RA + modulation format, space and spectrum assignment (MSSA)", "routing and modulation format assignment (RMA) + space and spectrum assignment (SSA)", and "routing, modulation format and space assignment (RMSA) + SA" in our pre-experiments and found that the RMSA+SA decomposition method can be used effectively. Therefore our decomposition method uses the RMSA+SA approach that makes the part related to SA as light as possible.

Parameters (additional)

m_r^{out}: the selected modulation level for serving connection request r obtained by solving the RMSA model.

Variables (additional)

$b_r^{meg} \in \{0, 1\}$: A binary variable that is equal to 1 if connection request r uses modulation level m and spatial dimension group g on link e and 0 otherwise.

$F_{max}^{lb} \in \mathbb{Z}_+$: A nonnegative integer variable that indicates the maximum index of required FSs in the RMSA model.

$F_{max}^{ub} \in \mathbb{Z}_+$ A nonnegative integer variable that indicates the maximum index of required FSs in the SA model.

We decompose the original RMSSA model in SDM-EONs (i.e., the non-SLC node-type model in Subsection 4.1.1 that solves the RMSSA problem) into the routing, modulation format and space assignment (RMSA) model (the object is Equation (4.13) to satisfy Eqs. (4.3)–(4.8) and (4.14)–(4.16)) and the spectrum assignment (SA) model (the object is Eq. (4.17) to satisfy Eqs. (4.9) and (4.18)–(4.21)). Here, F_{max}^{lb} and F_{max}^{ub} are non-negative

integer variables that represent the maximum index of the required FSs in the RMSA and SA models, respectively, and their values obtained by solving these two decomposition models (i.e., the RMSA and SA models) can be used as the lower and upper bound values for the original RMSSA model separately. The notation b_r^{meg} indicates a binary variable that is equal to 1 if connection request r uses modulation level m and spatial dimension group g on link e and 0 otherwise. m_r^{out} denotes the selected modulation level for serving connection request r obtained by solving the RMSA model.

RMSA model

The RMSA model relaxed all the constraints on the spectrum such as spectrum continuity constraint and spectrum nonoverlapping constraint to find a better lower bound.
Objective Function:

$$\text{Minimize} \quad F_{max}^{lb} \tag{4.13}$$

Subject to:

$$\sum_{e\in\sigma_v^+} x_r^{eg} - \sum_{e\in\sigma_v^-} x_r^{eg} = \begin{cases} 1 & \text{if } v = s_r \\ -1 & \text{if } v = d_r \\ 0 & \text{otherwise} \end{cases} \quad \forall v \in V, r \in R, g \in G_i \tag{4.3}$$

$$\sum_{e\in\sigma_v^-} \sum_{g\in G_i} x_r^{eg} \leq 1, \quad \forall v \in V, r \in R \tag{4.4}$$

$$\sum_{e\in\sigma_v^+} \sum_{g\in G_i} x_r^{eg} \leq 1, \quad \forall v \in V, r \in R \tag{4.5}$$

$$h_r \geq \sum_{e\in E} \sum_{g\in G_i} l^e x_r^{eg}, \quad \forall r \in R \tag{4.6}$$

$$\sum_{m\in MF} a^m u_r^m \geq h_r, \quad \forall r \in R \tag{4.7}$$

$$\sum_{m\in MF} u_r^m = 1, \quad \forall r \in R \tag{4.8}$$

$$b_r^{meg} \leq \frac{1}{2} \cdot (u_r^m + x_r^{eg}), \quad \forall r \in R, m \in MF, e \in E, g \in G_i \tag{4.14}$$

$$b_r^{meg} \geq u_r^m + x_r^{eg} - 1, \quad \forall r \in R, m \in MF, e \in E, g \in G_i \tag{4.15}$$

$$\sum_{r\in R}\sum_{m\in MF} b_r^{meg} n_r^{mi} - 1 \leq F_{max}^{lb}, \quad \forall e \in E, g \in G_i \tag{4.16}$$

SA model

Objective Function:

$$\text{Minimize} \quad F_{max}^{ub} \tag{4.17}$$

Subject to:

$$o_{rr'} + o_{r'r} = 1, \quad \forall r, r' \in R : r \neq r' \tag{4.9}$$

$$F_{max}^{ub} \geq F_{max}^{lb} \tag{4.18}$$

$$F_{max}^{ub} \geq f_r + n_r^{m_r^{out}} - 1, \quad \forall r \in R \tag{4.19}$$

$$\begin{gathered} f_r + n_r^{m_r^{out}i} \leq f_{r'} + M \cdot (1 - o_{rr'}) \\ \forall r, r' \in R, e \in E, g \in G_i : r \neq r' \end{gathered} \tag{4.20}$$

$$m_r^{out} = \{m \in MF : r \in R, e \in E, g \in G_i | b_r^{meg} = 1\} \tag{4.21}$$

As shown in Figure 4.1, by solving the RMSA model first, we can take the obtained destination function value as the initial lower bound for the original model. After that, we substitute the solutions obtained in the RMSA model as known parameters into the SA model and solve it. Finally, the value of the objective function obtained by solving the SA model is used as the initial upper bound for the original model, and the solutions of the RMSA and SA models are substituted into the original model as the initial solutions to solve it.

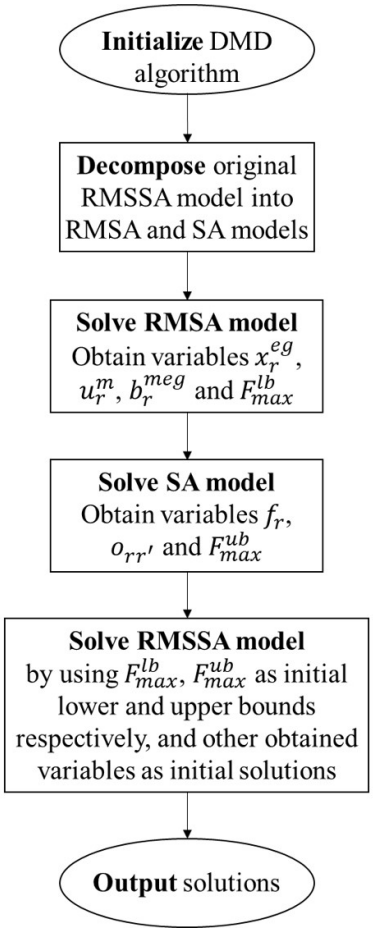

Figure 4.1: Framework of the DMD algorithm.

4.2.2 All-SLC model decomposition (ASLC-MD) algorithm

The model relaxation approach is not only the relaxation of spectral constraints discussed in Subsection 4.2.1. Since the SLC node-based model does not have the constraints related to spatial continuity, it is easier to solve compared to the non-SLC node-based model. And as we have narrated in Subsection 1.2.2, for the RMSSA problem in static scenarios, the savings in spectrum resources that SLC can bring about are minimal [9, 25]. That is, for the RMSSA problem in static scenarios, the solution of the problem considering SLC can be transformed into the solution of the non-SLC problem in the vast majority of cases (i.e., the number of times SLC occurs can be reduced to zero). In this subsection, we introduce this decomposition method with relaxed spatial constraints.

If we relax the restrictions related to the spatial continuity of the non-SLC node-type model in Subsection 4.1.1 (i.e., Equation (4.3), the model will be changed to a node-type model that supports SLC. In this case, the formulation related to routing and space using the law of flow conservation in the SLC node-type model will become Equation (4.22) below.

$$\sum_{e\in\sigma_v^-}\sum_{g\in G_i} x_r^{eg} - \sum_{e\in\sigma_v^+}\sum_{g\in G_i} x_r^{eg} = \begin{cases} 1 & \text{if } v = s_r \\ -1 & \text{if } v = d_r \\ 0 & \text{otherwise} \end{cases} \quad \forall v \in V, r \in R \tag{4.22}$$

Since the number of constraints in the SLC model in Equation (4.22) is reduced in comparison with the non-SLC model in Equation (4.3), the time required to solve the SLC node-type model may be shorter than that required for the non-SLC model.

Objective function

Major objective:

The major objective function aims to minimize the maximum index of the required FSs F_{max} and is the same as the objective function of the non-SLC node-type model in Subsection 4.1.1 (i.e., Eq. (4.2)).

$$\text{Minimize} \quad F_{max} \tag{4.2}$$

Minor objective:

$$\text{Minimize} \quad \sum_{v\in V}\sum_{r\in R} SLC_r^v \tag{4.23}$$

Here, SLC_r^v denotes a binary variable that is equal to 1 if connection request r changes the space lane used in the former link when passing through node v and 0 otherwise. Eq. (4.23) denotes the minimization of the number of SLC counts performed for all connection requests in the entire network. As we mentioned in Subsections 1.2.2 and 2.4.4, from the statements and experimental results in Refs. [9, 25], the effect of the spectrum savings from SLC is negligible in the static scenario. Therefore, we can equate the RMSSA model in Section **??** to the SLC-RMSSA model with Eqs. (4.2), (4.4)–(4.11), and (4.22)–(4.25) if the value of its minor objective function (i.e., Eq. (4.23)) is equal to 0. Here, SLC_r^v denotes a binary variable that is equal to 1 if connection request r changes the space lane used in the former link when passing through node v and 0 otherwise.

Constraints

$$\sum_{e\in\sigma_v^-}\sum_{g\in G_i} x_r^{eg} - \sum_{e\in\sigma_v^+}\sum_{g\in G_i} x_r^{eg} = \begin{cases} 1 & \text{if } v = s_r \\ -1 & \text{if } v = d_r \\ 0 & \text{otherwise} \end{cases} \quad \forall v \in V, r \in R \tag{4.22}$$

$$\sum_{e\in\sigma_v^-}\sum_{g\in G_i} x_r^{eg} \leq 1, \quad \forall v \in V, r \in R \tag{4.4}$$

$$\sum_{e\in\sigma_v^+}\sum_{g\in G_i} x_r^{eg} \leq 1, \quad \forall v \in V, r \in R \tag{4.5}$$

$$h_r \geq \sum_{e\in E}\sum_{g\in G_i} l^e x_r^{eg}, \quad \forall r \in R \tag{4.6}$$

$$\sum_{m\in MF} a^m u_r^m \geq h_r, \quad \forall r \in R \tag{4.7}$$

$$\sum_{m\in MF} u_r^m = 1, \quad \forall r \in R \tag{4.8}$$

$$o_{rr'} + o_{r'r} = 1, \quad \forall r, r' \in R : r \neq r' \tag{4.9}$$

$$f_r + \sum_{m\in MF} n_r^{mi} u_r^m \leq f_{r'} + M(3 - x_r^{eg} - x_{r'}^{eg} - o_{rr'}) \quad \forall r, r' \in R, e \in E, g \in G_i : r \neq r' \tag{4.10}$$

$$f_r + \sum_{m\in MF} n_r^{mi} u_r^m - 1 \leq F_{max}, \quad \forall r \in R \tag{4.11}$$

$$\sum_{e\in\sigma_v^+} x_r^{eg} - \sum_{e\in\sigma_v^-} x_r^{eg} \leq SLC_r^v \quad \forall v \in V, r \in R, g \in G_i : v \neq s_r, v \neq d_r \tag{4.24}$$

$$\sum_{e\in\sigma_v^-} x_r^{eg} - \sum_{e\in\sigma_v^+} x_r^{eg} \leq SLC_r^v \quad \forall v \in V, r \in R, g \in G_i : v \neq s_r, v \neq d_r \tag{4.25}$$

Eqs. (4.24) and (4.25) achieve the count of SLC times. According to the objective function and constraints above, the equivalent original model for ASLC-MD algorithm can be expressed as Eq. (4.26).

$$
\begin{cases}
\text{Major objective:} \\
\quad \text{Minimize} \quad F_{max} \\
\text{Minor objective:} \\
\quad \text{Minimize} \quad \sum_{v\in V}\sum_{r\in R} SLC_r^v \\
s.t. \\
(a)\ \sum_{e\in\sigma_v^-}\sum_{g\in G_i} x_r^{eg} - \sum_{e\in\sigma_v^+}\sum_{g\in G_i} x_r^{eg} = \begin{cases} 1 & \text{if } v = s_r \\ -1 & \text{if } v = d_r \\ 0 & \text{otherwise} \end{cases} \\
\quad \forall v \in V, r \in R \\
(b)\ \sum_{e\in\sigma_v^-}\sum_{g\in G_i} x_r^{eg} \le 1, \quad \forall v \in V, r \in R \\
(c)\ \sum_{e\in\sigma_v^+}\sum_{g\in G_i} x_r^{eg} \le 1, \quad \forall v \in V, r \in R \\
(d)\ h_r \ge \sum_{e\in E}\sum_{g\in G_i} l^e x_r^{eg}, \quad \forall r \in R \\
(e)\ \sum_{m\in MF} a^m u_r^m \ge h_r, \quad \forall r \in R \\
(f)\ \sum_{m\in MF} u_r^m = 1, \quad \forall r \in R \\
(g)\ o_{rr'} + o_{r'r} = 1, \quad \forall r, r' \in R : r \ne r' \\
(h)\ f_r + \sum_{m\in MF} n_r^{mi} u_r^m \le f_{r'} + M(3 - x_r^{eg} - x_{r'}^{eg} - o_{rr'}) \\
\quad \forall r, r' \in R, e \in E, g \in G_i : r \ne r' \\
(i)\ f_r + \sum_{m\in MF} n_r^{mi} u_r^m - 1 \le F_{max}, \quad \forall r \in R
\end{cases}
\tag{4.26}
$$

As shown in Fig.4.2, the ASLC-MD algorithm is actually the process of decomposing and solving the SLC-RMSSA model with major and minor objective functions. First, we address an SLC-RMSSA model with only the major objective, which consists of Eqs. (4.2), (4.4) to (4.11) and (4.22). This model is decomposed into the SLC-RMSA and SA models (the SA model is independent of whether SLC is supported or not since it does not include the selection of spatial dimensions). Similar to the DMD algorithm in Subsection 4.2.1, we solve the SLC-RMSA and SA models in turn and confer the solutions of the SLC-RMSA and SA models as initial solutions to the SLC-RMSSA model with only the major objective. Different from the DMD algorithm, after that, we address an SLC-RMSSA model with only the minor objective, which consists of Eqs. (4.4) to (4.11) and (4.22) to (4.25). The value of F_{max} obtained by solving the SLC-RMSSA model with only the major objective is fixed, and the other variables are assigned to the SLC-RMSSA model with only the minor objective as the initial solution. If the SCL number $\sum_{v\in V}\sum_{r\in R} SLC_r^v$ is equal to 0 upon solving this model, the solutions of the model are output; otherwise, F_{max} will be brought into the DMD algorithm as an initial lower bound to solve the original RMSSA model.

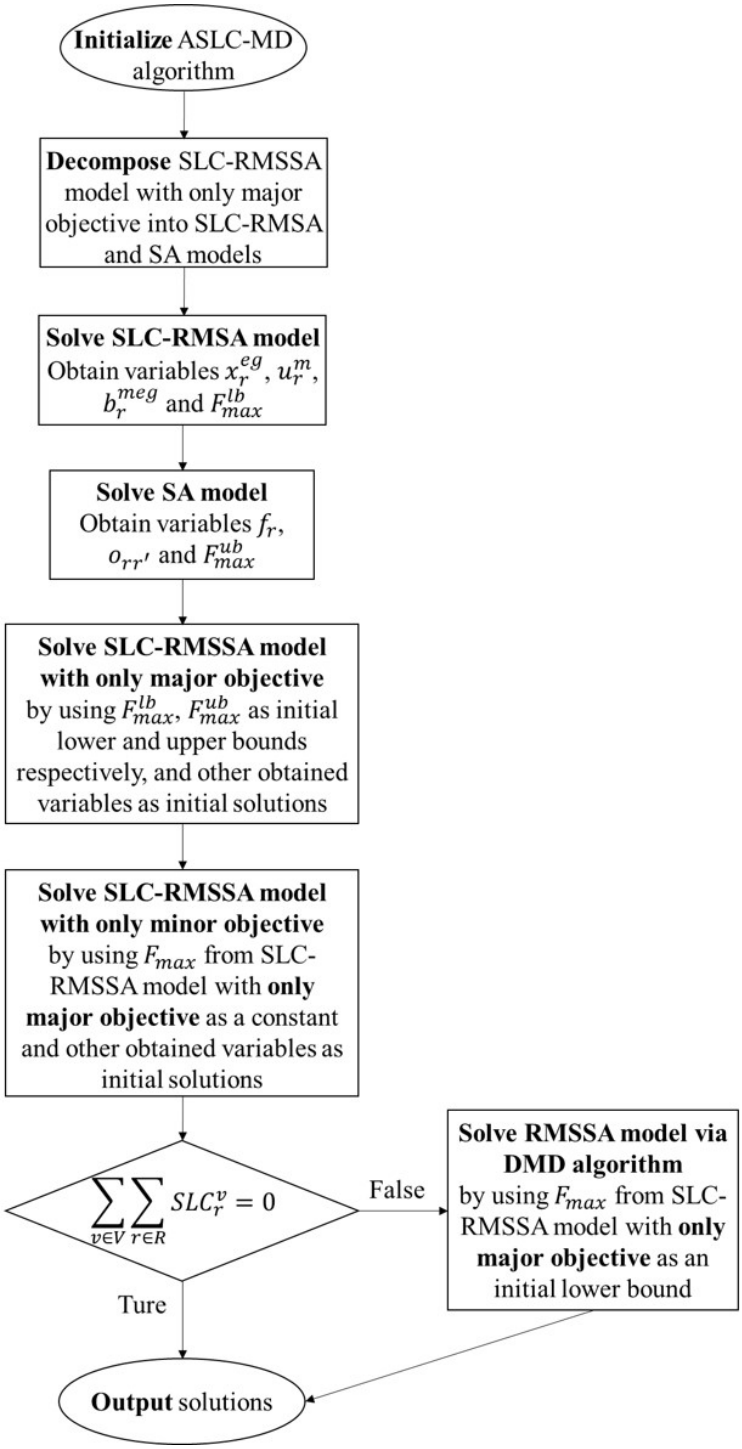

Figure 4.2: Framework of the ASLC-MD algorithm.

4.2.3 Semi-SLC model decomposition (SSLC-MD) algorithm

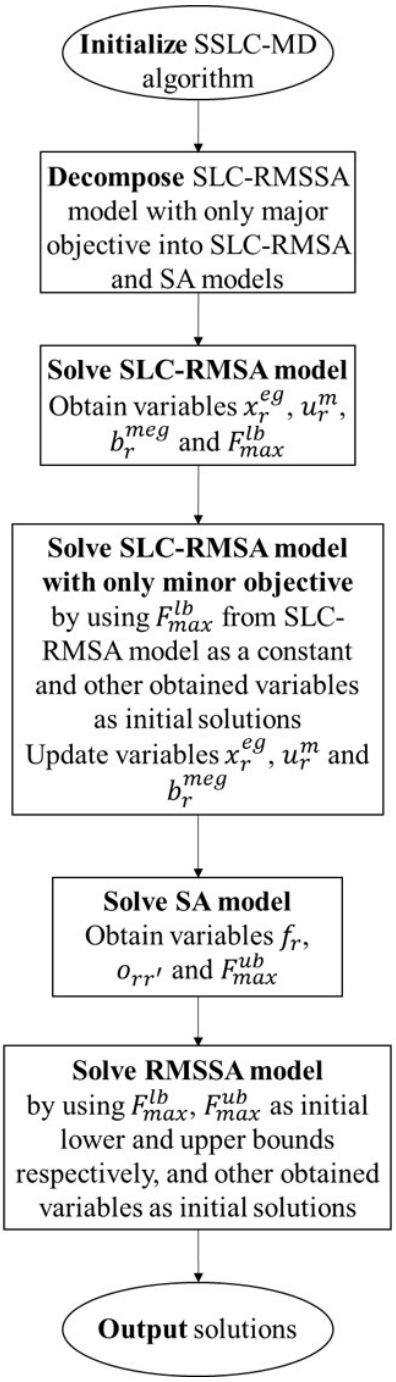

Figure 4.3: Framework of the SSLC-MD algorithm.

The ASLC-MD algorithm minimizes the SLC number after solving the SLC-RMSSA model, and the step that minimizes the SLC number requires much time because of the high complexity of the SLC-RMSSA model. Therefore, we consider a semi-SLC model

decomposition (SSLC-MD) algorithm, which minimizes the SLC number after solving the decomposed SLC-RMSA model to ensure that a light path without SLC is obtained.

The framework of the SSLC-MD algorithm is shown in Figure 4.3. Different from the ASLC-MD algorithm, the SSLC-MD algorithm supports SLC only in the RMSA model, while the RMSSA model is the original non-SLC node-type model. The SSLC-MD algorithm minimizes the SLC number (i.e., solving the SLC-RMSA model with only a minor objective) after solving the SLC-RMSA model (i.e., minimizing the maximum index of the required FSs). Since the FSs are not yet assigned in the SLC-RMSA model, whether SLC is considered does not have an impact on the maximum index of the required FSs (i.e., the SLC number in the SLC-RMSA model with SLC can converge to 0).

4.2.4 First-fit greedy (FF-G) algorithm

Since it is difficult to solve the model in subsection 4.1.1 exactly in a reasonable time for some large-scale instances, in this subsection, we propose a heuristic algorithm named first-fit greedy (FF-G), the details about which can be accessed in our previous work Ref. [29].

Algorithm First-Fit Greedy

Update the available FSs and spatial dimension groups
for $Method$ in $SORTS$ **do**
  Sort the set of connection requests R via $Method$
  for r in R **do**
    Find all physical paths P_r for r
    for p in P_r **do**
      Determine the most efficient modulation format m_r^p for each physical path p via DAT
    end for
    Calculate $n_r^{m_r^p i}$
    Create the candidate spectral blocks set B_r with spatial continuity and FSs contiguity restrictions imposed, and $b_r^{mp} \in B_r$ is composed of $n_r^{m_r^p i}$ FSs
    for b_r^{mp} in B_r **do**
      Assign b_r^{mp} to r on a trial and calculate the maximum index $FS_{max}^{b_r^{mp}}$ of the FSs used in the network after the trial assignment
    end for
    Find the minimum $FS_{max}^{b_r^{mp}}$, realign its corresponding b_r^{mp} to r and update the available FSs and spatial dimension groups
  end for
  Record the maximum FSs index used in the network under the current sorting method of R
end for
Select the allocation scheme for the sorting method, which determines a minimum value of the maximum FSs index used in the network

Here, $SORTS$ is a set of different sorting methods. We discuss 9 sorting methods

according to the different properties of connection requests, which are sorting by traffic volume from small to large and large to small, the average hops of all paths from small to large and large to small, the hops of the shortest path from small to large and large to small, the hops of the longest path from small to large and large to small, and random sorting. We previously search for all possible simple paths (i.e., paths without cycles) between the source and destination nodes of each connection request via the depth-first search (DFS) algorithm, and the set of all possible simple paths for the connection request r is denoted as P_r.

4.2.5 Analysis for scales of the ILP models

The variables and constraints in each model mentioned in Sections 4.1 and 4.2 are shown in Table 4.2. RMSSA and RMSA indicate the original model proposed in Subsection 4.1.1 (i.e., Non-SLC node-type ILP model) and the relaxation model employed by the DMD algorithm in Subsection 4.2.1, respectively. SLC-RMSSA and SLC-RMSA denote the node-type ILP model supporting SLC and the relaxation model supporting SLC, respectively, which are employed in the algorithms ASLC-MD in Subsection 4.2.2 and SSLC-MD in Subsection 4.2.3. SA is the model considering only the spectrum assignment which is used in Subsections 4.2.1–4.2.3.

Table 4.2: Number of variables and constraints per model.

Models	**Variables**	**Constraints**
RMSSA	$O(\|R\|\cdot\|E\|\cdot\|G_i\|+\|R\|^2)$	$O(\|R\|\cdot\|V\|\cdot\|G_i\|+\|R\|^2\cdot\|E\|\cdot\|G_i\|)$
SLC-RMSSA	$O(\|R\|\cdot\|E\|\cdot\|G_i\|+\|R\|^2)$	$O(\|R\|\cdot\|V\|+\|R\|^2\cdot\|E\|\cdot\|G_i\|)$
RMSA	$O(\|R\|\cdot\|MF\|\cdot\|E\|\cdot\|G_i\|)$	$O(\|R\|\cdot\|V\|\cdot\|G_i\|+\|R\|\cdot\|MF\|\cdot\|E\|\cdot\|G_i\|)$
SLC-RMSA	$O(\|R\|\cdot\|MF\|\cdot\|E\|\cdot\|G_i\|)$	$O(\|R\|\cdot\|V\|+\|R\|\cdot\|MF\|\cdot\|E\|\cdot\|G_i\|)$
SA	$O(\|R\|^2)$	$O(\|R\|^2)$

Analyzing the number of variables and constraints for each model, the following can be derived.

(1) The number of connection requests $|R|$ affects RMSSA and SLC-RMSSA significantly because the numbers of variables and constraints in these two models are related to the square of the number of connection requests $|R|^2$.

(2) The numbers of variables and constraints of the models RMSA, SLC-RMSA, and SA used in the decomposition algorithms are not affected by the square of the number of connection requests. Thus, it is expected that the decomposition algorithms effectively reduce the computation time compared to solving the original model directly.

(3) SLC-RMSSA and SLC-RMSA show a reduction in the number of constraints (from $O(|R| \cdot |V| \cdot |G_i|)$ to $O(|R| \cdot |V|)$) compared to RMSSA and RMSA. Due to the effect of $|R|^2$, the impact on the computation time caused by the change may be negligible in SLC-RMSSA and RMSSA. However, in SLC-RMSA and RMSA, when constraints whose number is $O(|R| \cdot |V| \cdot |G_i|)$ (i.e., Equation (4.3) in Subsection 4.1.1, which uses the law of flow conservation) are abundantly present, the change has the potential to reduce the computation time of the model.

4.3 Simulation and numerical results

In this section, we first verify the effectiveness of the three algorithms proposed in Section 4.2 via lower bounds of our model and results of the FF-G algorithm in the N6S9 network and then compare our model with the path-type models proposed via M. Yang et al. [9] and Q. Wu et al. [16] in the NSF network.

4.3.1 Environmental parameters and assumptions

As shown in Fig. 2.11 in Subsection 2.4.2, we consider several cases, where each link uses the 4-core MCF [130] or the 12-core MCF [131] to connect the network in the simulation experiments. As we mentioned in the Subsection 2.4.2, based on the ITU-T standard G.694.1, the total number of FSs that each link has (i.e., $|F|$) is set to 320 (i.e., 12.5 GHz per FS at the C-band with a 4 THz bandwidth) [97]. The number of modulation levels $|MF|$ is set to 4. The numbers 1, 2, 3, and 4 indicate the modulation formats double polarization (DP)-BPSK, DP-QPSK, DP-8QAM, and DP-16QAM, respectively. Each OC is generated by a transceiver, which can support 50 Gbps via DP-BPSK under the 32 Gbaud symbol rate containing 7 GBaud (approximately 20%) for forward error correction (FEC) overhead [51] and occupying in total 37.5 GHz spectrum (i.e., 3 FSs) [132]. Therefore, the supportable bit rates per OC for the modulation formats DP-BPSK, DP-QPSK, DP-8QAM and DP-16QAM are set to 50, 100, 150 and 200 Gbps, respectively. The maximum transmission distances (km) of these modulation formats considered and the maximum traffic volume (Gbps) that an OC can carry under each modulation format are shown in Table 2.5.

The Gurobi optimizer v9.5.2 [136] is the solver software used to solve the models in this chapter. Since the RSA problem is a well-known NP-hard problem that has been proven by [2, 112], it is obviously NP-hard for the RMSSA problem that considers multiple spatial dimensions and modulation formats based on the RSA problem. Thus, for some instances, ILP models cannot be completely solved in a reasonable time (i.e., the obtained solution cannot be verified as optimal). To obtain a feasible solution of the model when solving each

instance, we set an upper limit of 3600 seconds for the computation time of each part of the algorithms (e.g., in the DMD algorithm, the upper limit of computation time for the RMSA, SA, and RMSSA models are all 3600 seconds). The simulation experiments are executed in a Microsoft Windows 10 OS on a computer with an Intel 8-core 16-thread 3.6 GHz CPU and 64 GB memory.

4.3.2 Simulation results of the algorithms

In this subsection, we compare the algorithms for solving the non-SLC node-type model in the N6S9 network shown in Fig. 4.4, which consists of 6 nodes and 18 directed links interconnected by 4-core MCFs [130]. The available spatial switching granularities i are 1, 2, and 4, corresponding to the cases of Ind-Sw, FrJ-Sw, and J-Sw, respectively.

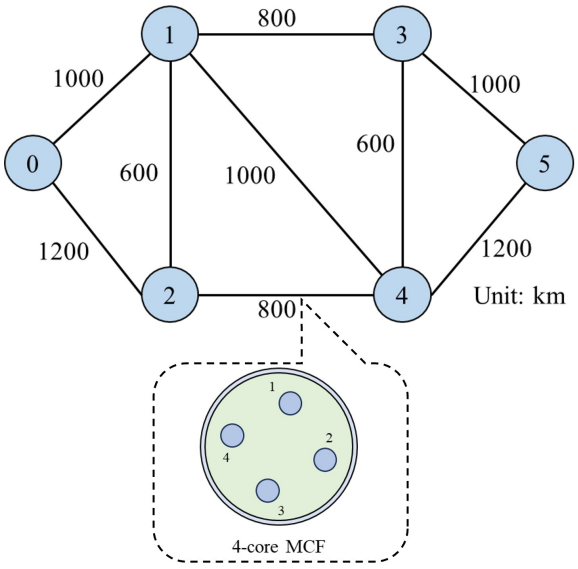

Figure 4.4: 4-core N6S9 network topology.

The traffic volume (Gbps) of each connection request is generated ranging from 100 Gbps to 1 Tbps in accordance with a uniform distribution. The source node and destination node of each connection request are randomly selected from the nodes in the network topology used. We consider different numbers of connection requests—from 50 to 200, 50 per step. Thirty traffic data sets are generated randomly for each number of connection requests.

Since there is not yet any work that involves multiple modulation formats by formulating node-type ILP models to solve the RMSSA problem, we consider lower bounds of the model and results of the following commonly used the FF-G algorithm mentioned in Subsection 4.2.4 for solving the model as the indicators to evaluate the effectiveness of our algorithms.

Table 4.3: Maximum FS index of the non-SLC node-type model solved by the DMD, ASLC-MD, SSLC-MD and FF-G algorithms.

$\|R\|$	i	Algorithms				LB
		DMD	ASLC-MD	SSLC-MD	FF-G	
50	1	30.60 (0)	30.60 (0)	30.60 (0)	31.80 (0)	30.60 (0)
	2	30.55 (0)	30.55 (0)	30.55 (0)	33.33 (0)	30.55 (0)
	4	37.87 (0)	37.87 (0)	37.87 (0)	41.40 (0)	37.87 (0)
100	1	49.76 (5)	50.60 (14)	49.68 (5)	53.53 (0)	49.28 (1)
	2	55.90 (3)	56.25 (8)	55.80 (3)	59.63 (0)	55.55 (1)
	4	69.63 (2)	69.57 (1)	69.60 (2)	75.73 (0)	69.50 (0)
150	1	74.93 (19)	–	74.52 (17)	76.53 (0)	70.90 (4)
	2	80.20 (1)	–	80.57 (2)	86.30 (0)	80.17 (0)
	4	102.50 (9)	102.63 (13)	102.60 (13)	110.63 (0)	102.17 (0)
200	1	95.03 (19)	–	96.43 (21)	99.30 (0)	92.07 (4)
	2	105.67 (7)	–	105.70 (8)	112.80 (0)	105.33 (0)
	4	134.83 (18)	134.67 (14)	134.67 (14)	144.17 (0)	133.60 (0)

Table 4.3 shows the experimental results in the N6S9 network shown in Fig. 4.4, which consists of 6 nodes and 18 directed links interconnected by 4-core MCFs [130], for the maximum FS index of the non-SLC node-type model solved by the DMD, ASLC-MD, SSLC-MD and FF-G algorithms in the cases of spatial switching granularities i equal to 1, 2, and 4. The result is the value of the parameter 'ObjVal' output by Gurobi, which is the global optimal value when the model is completely solved in the time limit and is the local optimal value or current best value if a solution exists when the model is not completely solved in the time limit. 'LB' indicates the lower bound given by the parameter 'Objbound' of Gurobi when solving the RMSA model. The numbers listed in the parentheses indicate the numbers of sets in the 30 traffic data sets for which the optimal solutions are not obtained within the time limit (i.e., the number of times the model is not solved completely). The ASLC-MD algorithm does not obtain feasible solutions in the time limit for instances whose numbers of connection requests are 150 and 200. For the 30 traffic data sets with 150 connection requests, there are 24 sets when i is equal to 1 and 29 sets when i is equal to 2, where no feasible solution is found. For the 30 data sets with 150 connection requests, no feasible solutions are found for all 30 sets when i is equal to 1 and 2. As shown in Table 4.3, the results of the ASLC-MD algorithm are not very satisfactory, and it would be difficult to find feasible solutions in a reasonable time when the number of connection requests becomes larger. By comparing the results of the DMD, SSLC-MD, FF-G algorithms and lower bound, it can be observed that DMD and SSLC-MD can effectively solve the node-type model in the instances that were originally difficult to solve directly, and the qualities

of the solutions obtained by DMD and SSLC-MD in the time limit were approximately the same and much better than the solutions obtained by heuristic FF-G algorithm.

Furthermore, it can be observed that with the number of connection requests being 150 and 200, all of our three algorithms yielded a large number of instances that could not be solved completely within the time limit. As we analyzed in Section 4.2.5, our model is strongly influenced by the number of connection requests. Therefore, when facing large-scale instances with a high number of connection requests, it will be difficult to solve in a reasonable time. In our pre-experiments, we noticed that the maximum number of connection requests that our algorithms can handle in the limited 10,000-second time is about 300. That is, for instances larger than 300 connection requests, we suggest using other efficient heuristic algorithms to solve them.

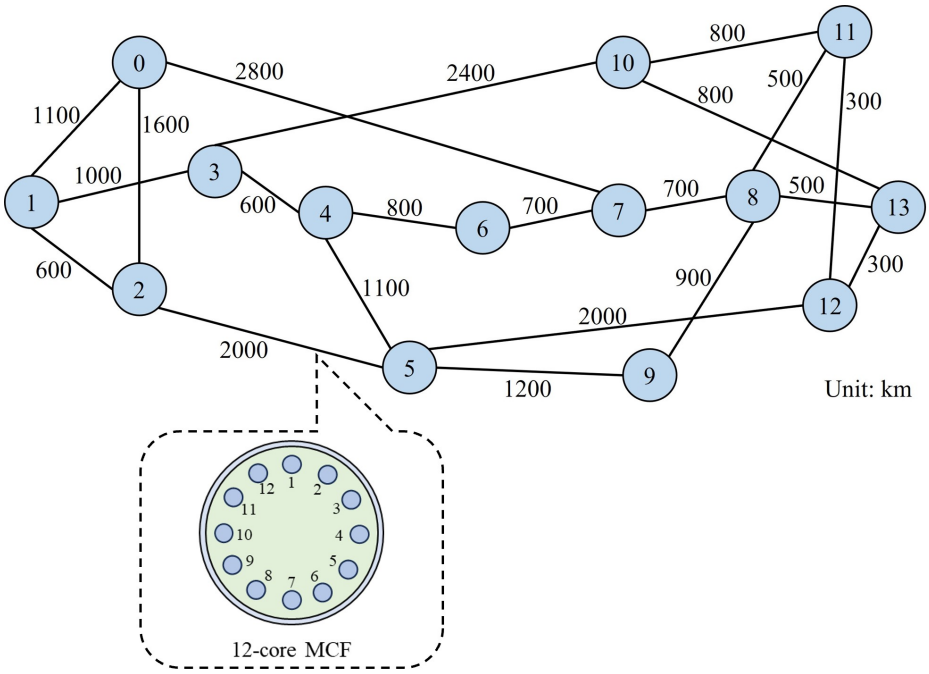

Figure 4.5: 12-core NSF network topology.

For instance, Table 4.4 shows the results of the FF-G algorithm for large-scale instances whose numbers of connection requests are 300 and 600 in the NSF network shown in Fig. 4.5, which consists of 14 nodes and 42 directed links interconnected by 12-core MCFs. 'FS index' indicates the average value of the maximum FS index used in the network for the 30 traffic data sets. 'Lower bound' indicates the lower bound given by the parameter 'Objbound' of Gurobi when solving the RMSA model. In the case where $|R| = 600$ and $i = 1$, the RMSA model did not find a valid lower bound in 3600 seconds of time limit and 64 GB of memory because of the excessive computational complexity. 'Runtime' indicates the

Table 4.4: Results of the FF-G algorithm for large-scale instances.

$\|R\|$	i	FS index	Lower bound	Runtime (s)
300	1	60.77	59.97	1089.07
	2	59.10	49.63	545.16
	3	63.07	54.20	365.65
	4	68.10	58.67	278.78
	6	81.63	68.10	190.82
	12	116.87	96.73	105.48
600	1	100.60	–	2356.19
	2	107.23	90.53	1140.22
	3	117.17	102.57	748.90
	4	128.23	112.17	556.32
	6	152.97	130.58	383.33
	12	222.10	187.83	199.83

average computation time for these indices. It can be observed that the results obtained by our proposed heuristic FF-G algorithm were relatively close to the lower bound in overall. When the spatial switching granularity i was small, the results obtained by the FF-G algorithm were much closer to the lower bound, but as i increased, the difference between the results obtained by the FF-G algorithm and lower bound increased somewhat.

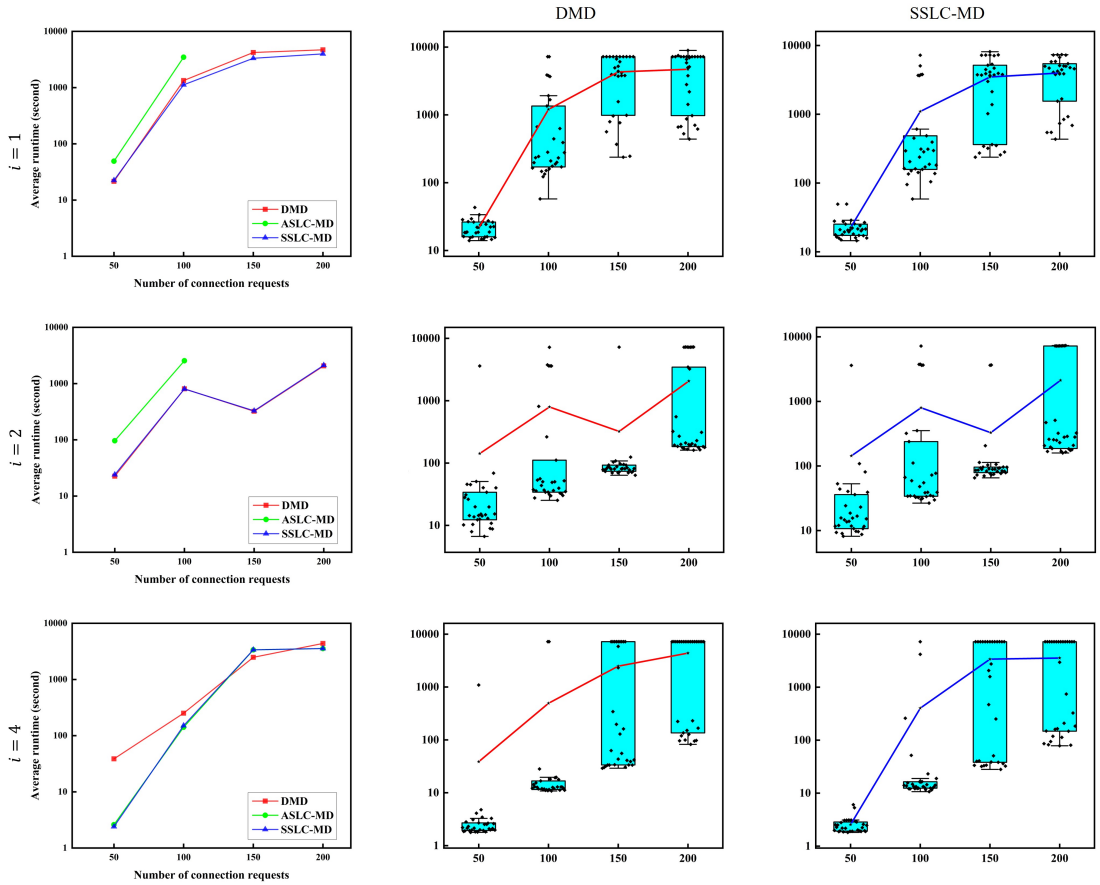

Figure 4.6: Execution time of the non-SLC node-type model solved by the DMD, ASLC-MD and SSLC-MD algorithms.

Fig. 4.6 shows the experimental results regarding the execution time of the non-SLC node-type model solved by the DMD, ASLC-MD and SSLC-MD algorithms in the cases of spatial switching granularities i equal to 1, 2, and 4 in the 4-core N6S9 network shown in Fig. 4.4. The vertical coordinate called 'average runtime' indicates the average execution times of Gurobi when solving the model. The horizontal coordinate indicates the number of connection requests from 50 to 200 with 50 requests per step. Since the computation time of the heuristic FF-G algorithm is more than 10 times faster than those of the DMD, ASLC-MD, and SSLC-MD algorithms, which are used to solve the model, we do not include it in the comparison. The three figures in the left-hand column show the average execution times of the three algorithms used to solve the model for various values of spatial switching granularities i. The performance of the ASLC-MD algorithm was the worst. Moreover, by comparing the other two algorithms, DMD and SSLC-MD, it can be observed that in the case where the switching paradigms of the SLC and non-SLC models are different (i.e., the cases where $i = 1$ and $i = 2$), there is a larger number of spatial dimension groups, and

the performance of SSLC-MD is superior to that of DMD (e.g., the average execution time of SSLC-MD is shorter than that of DMD in the case of $i = 1$; however, in the case of $i = 2$, since the number of spatial dimension groups is reduced, the advantage of SSLC-MD compared to DMD is also reduced). In the case where $i = 4$, the switching paradigms of SLC and non-SLC are the same, and the results of DMD and SSLC-MD are both good and bad. The figures in the middle column and the right-hand column show the box plots of the results of DMD and SSLC-MD for various cases of spatial switching granularities i, respectively, and we can see the dispersion of the results for all 30 traffic data sets through these plots.

To better verify the difference in performance between the DMD and SSLC-MD algorithms with different numbers of spatial dimension groups, we increase the number of cores of MCF to 6 and perform experiments using the same 30 traffic data sets with connection request numbers of 50, 100, and 150. In this case, there are 4 possible values of spatial switching granularities, which are 1, 2, 3, and 6, corresponding to the numbers of spatial dimension groups, which are 6, 3, 2, and 1, respectively. Fig. 4.8 shows the experimental results regarding the execution time of the non-SLC node-type model solved by the DMD and SSLC-MD algorithms in the cases of the 6-core N6S9 network shown in Fig. 4.7. The figures in the middle column and the right hand column show the box plots of the results of DMD and SSLC-MD for various cases of spatial switching granularities i, respectively. It is obvious that when the spatial switching granularity i is small (i.e., when the number of spatial dimension groups is large, such as when $i = 1$), the SSLC-MD algorithm has a shorter average computation time and shows better performance; however, when the spatial switching granularity i increases and the number of spatial dimension groups decreases, the SSLC-MD algorithm is inferior to the DMD algorithm. Therefore, to better solve the node-type model, we should select the appropriate decomposition algorithm according to the number of spatial dimension groups.

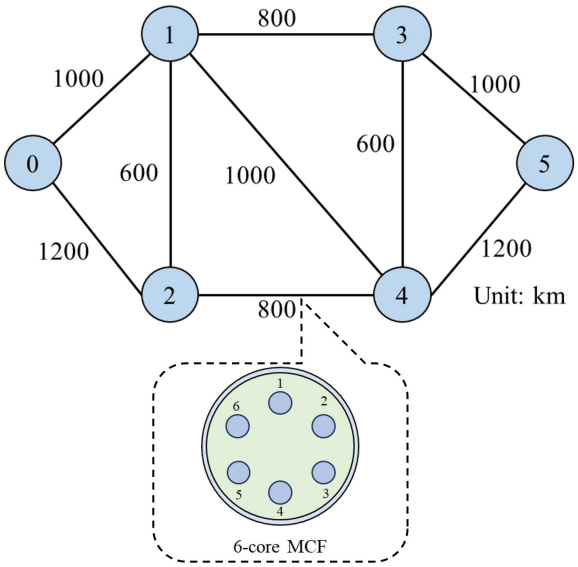

Figure 4.7: 6-core N6S9 network topology.

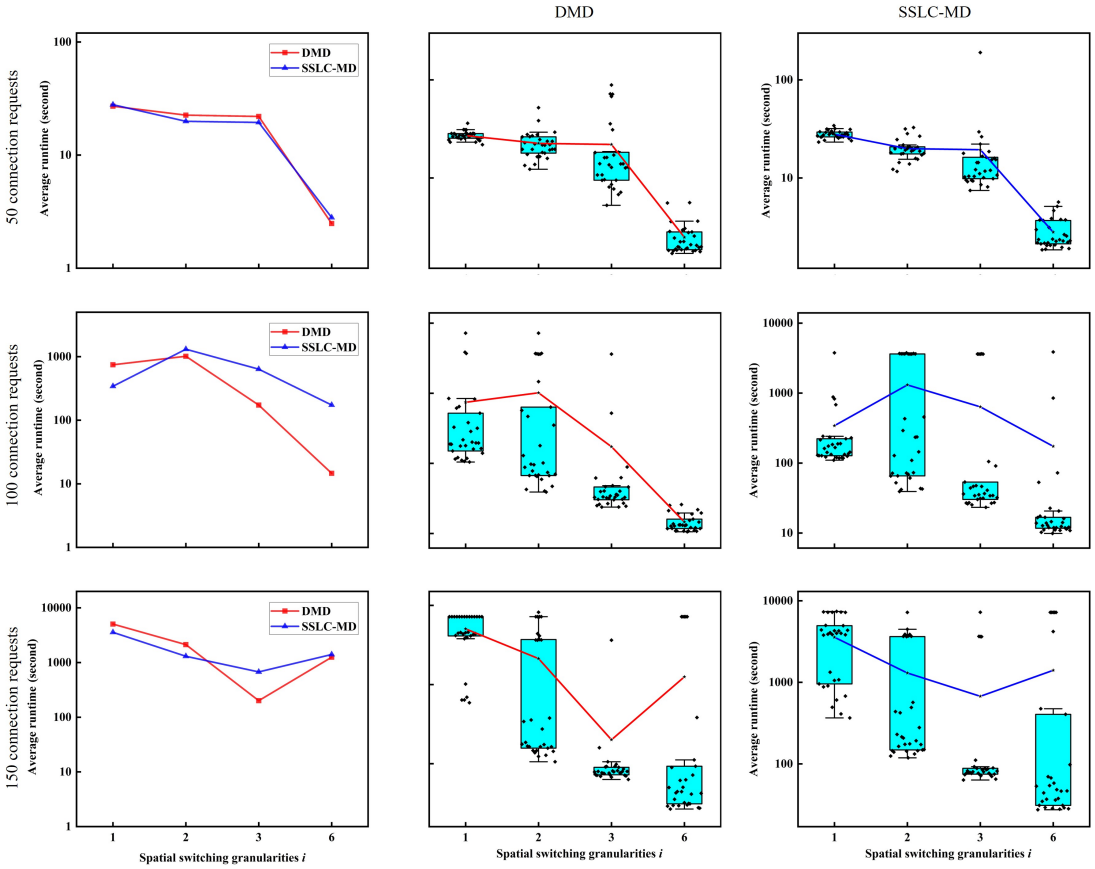

Figure 4.8: Execution time of the non-SLC node-type model solved by DMD and SSLC-MD algorithms in the case of the 6-core N6S9 network.

4.3.3 Comparison of the proposed non-SLC node-type model and the previous k-path-type model

In this subsection, we compare the non-SLC node-type model (hereafter referred to as the node-type model) in this work with the previous k-path-type model in Refs. [9,16] (hereafter referred to as the k-path-type model) in the NSF network shown in Figure 4.9, which consists of 14 nodes and 42 directed links interconnected by 4-core MCFs. For illustrative purposes, we conduct simulation experiments only at Ind-Sw with spatial switching granularity $i = 1$.

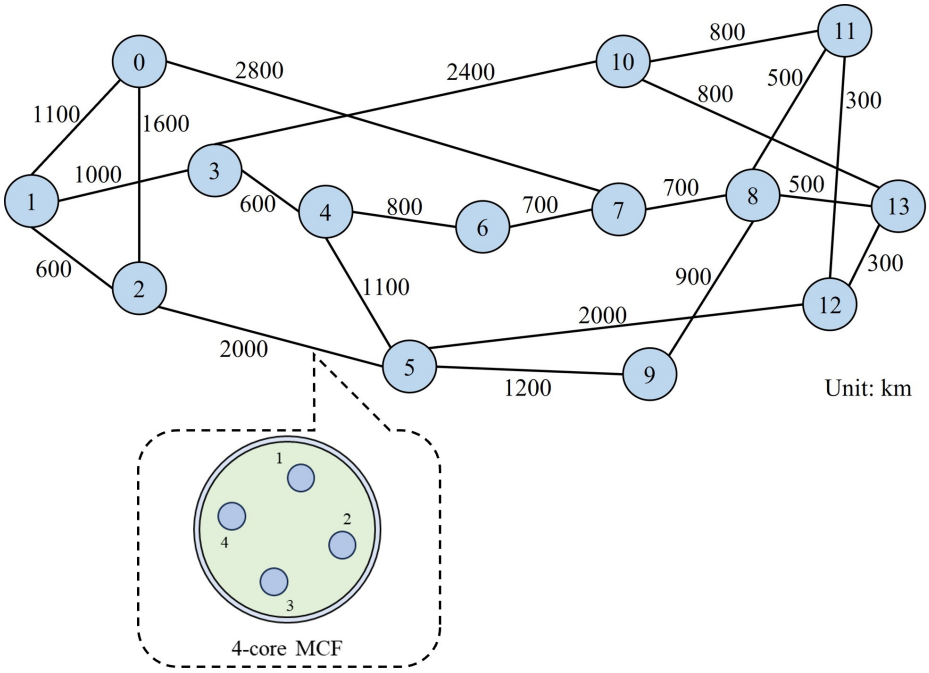

Figure 4.9: 4-core NSF network topology.

The set of candidate paths (k-shortest paths) for the k-path-type model is determined by the same routing algorithm as mentioned in Refs. [9, 16]. We precompute two sets of candidate paths with candidate path numbers K equal to 2, 3, 4 and 5 in the NSF network and provide them to the k-path-type model. Since it takes a longer time to solve the node-type model, the node-type model is solved by using the solutions of the k-path-type model as the initial solutions. The upper limit of computation time for each model is set to 3600s.

Table 4.5 shows the results of the node-type model and the k-path-type model on the NSF network in our simulation. We performed simulation experiments for each of the four types of connection requests in the case where $i = 1$ and the number of connection requests was equal to 100. 'Random nodes', 'Same source nodes', 'Same destination nodes' and 'Not uniform nodes' denote the types of connection requests whose source and destination are randomly generated, source nodes are the same, destination nodes are the same, and source

and destination nodes are not all randomly generated, respectively (we fix the source and destination nodes of 20 of the 100 connection requests as nodes 4 and 9). Thirty traffic data sets are generated for each type of connection requests. The same instances of connection requests are solved for the two models. The numbers listed in the parentheses indicate the numbers of sets in the 30 traffic data sets for which the optimal solutions are not obtained within the time limit (i.e., the number of times the model is not solved completely). The results of 'FS index' are output via the parameter 'ObjVal' of Gurobi and indicate the maximum FS index used in the network. The result is the optimal value when the model is completely solved in the time limit and is the feasible solution if a solution exists when the model is not completely solved in the time limit. The results of 'LB' indicate the lower bounds given by the parameter 'Objbound' of Gurobi. 'Node' and 'K-Path' indicate the node-type and k-path-type models, respectively.

We can observe that the qualities of the solutions of the k-path-type model are not better than those of the node-type one for the various types of connection requests. This is because the sets of candidate paths of the k-path-type model do not completely include all possible paths, which leads to the solutions obtained by the k-path-type model not being the optimal solutions. For instance, when $K = 2$, the set of candidate paths for each connection request contains only two possible paths, so although the computation times for solving the model might be greatly reduced, the qualities of the solutions are more insecure. However, when $K = 3$, the solutions (i.e., FS index) and the lower bound of the k-path-type model are improved compared to those of the case when $K = 2$. We also observe that in the cases of $K = 4$ and $K = 5$, in some instances for the k-path-type model, although the lower bounds become closer to the lower bounds of the node-type model as K increases, the solutions become worse. The reason is that as K increases, the computational time required to solve the k-path-type model becomes much longer, so that more feasible but nonoptimal solutions that fail to solve the model completely appear. Therefore, it is often necessary to determine a reasonable value for the candidate path number K by pre-experimentation when we solve this type of problem with the k-path-type model. In addition, the node-type model is more difficult to solve in a short time than the k-path-type one, but since it considers all possible paths, if the node-type model can be solved completely, the qualities of its solutions are more reliable than those of the k-path-type one. On the other hand, the node-type model can be used to check the qualities of the solutions of k-path-type model for various values of K through operations such as solving the node-type model by using the solutions obtained by k-path-type model as the initial solutions (i.e., if the solutions obtained by the node-type model are better than those of k-path-type one, the solutions of k-path-type one can still be improved).

Table 4.5: Comparison of the maximum FS index used in the network for node-type and k-path-type models.

	Types of Connection Requests	**Node**	**K-Path**			
			$K = 2$	$K = 3$	$K = 4$	$K = 5$
FS index	Random nodes	59.23 (7)	60.13 (3)	59.30 (4)	59.50 (4)	59.50 (4)
	Same source nodes	120.93 (7)	138.67 (0)	121.13 (0)	121.60 (3)	122.67 (7)
	Same destination nodes	120.67 (15)	126.30 (1)	120.77 (2)	122.00 (5)	121.20 (7)
	Not uniform nodes	66.00 (16)	72.30 (8)	68.47 (13)	68.13 (18)	66.57 (7)
LB	Random nodes	59.03 (2)	60.03 (0)	59.17 (0)	59.10 (0)	59.07 (0)
	Same source nodes	120.93 (0)	138.67 (0)	121.13 (0)	120.93 (0)	120.93 (0)
	Same destination nodes	120.50 (0)	126.27 (0)	120.70 (0)	120.50 (0)	120.50 (0)
	Not uniform nodes	65.47 (10)	72.03 (0)	67.83 (0)	66.93 (0)	65.83 (0)

Chapter 5

Conclusion and future work

5.1 Conclusion

This Ph.D. thesis introduced and addressed the static resource allocation problems in several generations of optical networks, from the traditional WSONs to the EONs, and further to the SDM-EONs. The conclusion of this thesis are per chapter summarized as follows:

- In Chapter 1, we explained the research background and significance of this thesis. In addition, we summarized our contributions in the research field of resource allocation for EONs and SDM-EONs.

- In Chapter 2, we introduced the background knowledge and key technologies, as well as assumptions in the three representative generations of optical network architectures, WSONs, EONs, and SDM-EONs, that are relevant to the content of this thesis. In addition, we discussed the relationship between physical devices and the challenges of the optical network resource allocation problems.

- In Chapter 3, we focused on the static RSA/RMSA problem in EONs. In order to better understand the characteristics of each type of models and to improve them for use in newer generations of optical networks, such as SDM-EONs, MB-EONs and SCNs, we divided the models in static RSA/RMSA problem into four types (i.e., path/slot, path/channel, node/slot, node/channel) based on different perspectives for routing and spectrum assignment. After that, we analyzed and summarized the characteristics of each model, and proposed a series of improved methods to enhance the computational performance of each model. Specifically, we found a better lower bound by relaxing the constraints of spectral and improved the computational speed by decomposing the model. Finally, we verified the effectiveness of the improved methods and analyzed the differences between the models through a comparative simulation experiment. Specifically, our improved methods can significantly speed up the solver

or the exact algorithm for solving the models. Moreover, we can observe that the node-type model, which is harder to solve compared to the path-type model, can provide a global optimal solution theoretically, which will be very helpful in the design phase of optical networks. The path/channel model showed overwhelming performance in the simulation. Considering the advantages of the model, the availability of the path/channel model in large backbone networks and more complex EONs (e.g., SDM-EONs) are also worth being looked forward to. Although it is not introduced in this thesis, we discussed the extension of the path/channel model for SDM-EONs in our work Ref. [16], and the extended model demonstrated excellent performance.

- In Chapter 4, we proposed a node-type ILP model without SLC for the static resource allocation problem of SDM-EONs (i.e., the RMSSA problem). Since this model has a large number of constraints and variables and is difficult to solve directly, we proposed three exact algorithms based on model decomposition (i.e., the DMD, ASLC-MD, and SSLC-MD algorithms) to better solve it. Specifically, in DMD, we found a better lower bound by relaxing the constraints of spectral and improved the computational speed by decomposing the model. In ASLC-MD, we transformed the Non-SLC model into an SLC-supported model by relaxing the spatial constraints. After that, we zeroed out the number of SLC counts in the network by setting the minor function to find the solution of the original model. In SSLC-MD, we combined the above two methods to find the lower bound by solving the relaxation model with the SLC-supported model. Through the comparison experiments, we investigated the performance of the DMD and SSLC-MD algorithms, which can solve the node-type model effectively, and found that we should select the appropriate decomposition algorithm according to the number of spatial dimension groups to better solve the node-type model. In addition, we also compared our node-type model with the k-path-type one in the previous works Refs. [9, 16]. The results indicate that our node-type model has an advantage over the previous k-path-type model in terms of solution quality, and our node-type model is a promising approach for checking the qualities of the solutions of the k-path-type models.

5.2 Possible future work

Following the evolution of optical network architectures introduced in this paper, it can be inferred that there are still many pending future works in this research field. As we introduced in Subsection 2.1.1, architectures such as MB-EON based on band-division multiplexing, MB-SDM-EON, and SCN based on large-scale SDM have been proposed in recent

years, taking into account the larger network traffic in the future. These architectures are considered to be promising, cost-effective solutions for future network planning [63, 82–90]. However, as always, the evolution of network architectures always brings both opportunities and challenges, and the concept of network resources such as SpChs in these new network architectures will change essentially again. For instance, spatial channels in SCNs can allocate the bandwidth resources of the entire C-band to a single connection request to achieve Pbps-level optical transmission, and enable spatial bypassing so that wavelength switching at the optical layer is not required. Therefore, it is necessary to establish a reasonable mathematical optimization models for the resource allocation problems in new architectures such as MB-EON, MB-SDM-EON, SCN, etc., and design efficient algorithms to solve them. Moreover, in order to cope with failures in the networks to ensure survivability of transmissions, protection and restoration of transmissions (i.e., guaranteeing efficient transmission of connection requests despite a certain degree of link or optical path failures) should also be considered in the network design [90, 137–141]. These elements are a part of our future work.

In addition, as we state in Section 1.1, it is not practical to build mathematical optimization models and solve them exactly in static scenarios for large-scale instances or in dynamic scenarios. Therefore, in such cases, designing and applying a heuristic algorithm or reinforcement learning approach with high accuracy and robustness also has important implications for the design and application of optical network architectures. These elements are also the focus in our future work.

Appendix

Publications in journals

1. **J. Wang**, S. Chen, Q. Wu, Y. Tan, and M. Shigeno, "Solving the Static Resource-Allocation Problem in SDM-EONs via a Node-Type ILP Model", *Sensors*, 22(24), 9710, Dec. 2022.
2. **J. Wang**, M. Shigeno, and Q. Wu, "ILP models and improved methods for the problem of routing and spectrum allocation", *Optical Switching and Networking*, 45, 100675, Sept. 2022.
3. Q. Wu, **J. Wang**, and M. Shigeno, "A novel channel-based model for the problem of routing, space, and spectrum assignment", *Optical Switching and Networking*, 43, 100636, Feb. 2022.

Publications in conferences

1. Q. Wu, ◯**J. Wang**, S. Chen, and A. Kanai, "Resource allocation problem in multi-band space-division multiplexing elastic optical networks", in *18th International Conference on Computational Intelligence and Security (CIS)*, pp. 225-228, 2023-04, Chengdu, China.
2. ◯Y. Tan, Y. Nakano, **J. Wang**, and M. Shigeno, "Designing of OTN/WDM Networks with Recovery Methods for Multiple Failures", in *27th OptoElectronics and Communications Conference (OECC) and International Conference on Photonics in Switching and Computing (PSC)*, 2022-07, Toyama, Japan.
3. ◯Y. Tan, Q. Wu, Y. Nakano, **J. Wang**, and S. Maiko, "Network Design Models with Partial Protection Schemes against Multiple Failures under Optical-Channel Data Unit Constraints", in *IEEE 6th Optoelectronics Global Conference*, pp. 38-46, 2021-09, Shenzhen, China.
4. ◯**J. Wang**, Q. Wu, and M. Shigeno, "A novel ILP model for the routing and spectrum allocation problem in SDM-EONs–In consideration of space lane change", in *IEICE Technical Report; IEICE Tech. Rep.*, 2020-08, Online.
5. ◯**J. Wang**, H. Xuan, Y. Wang, Y. Yang, and S. Liu, "Optimization Model and Algorithm for Routing and Spectrum Assignment in Elastic Optical Networks", in *14th International Conference on Computational Intelligence and Security (CIS)*, 2018-11, Hangzhou, China.

Bibliography

[1] X. Liu, "Evolution of fiber-optic transmission and networking toward the 5g era," *Iscience*, vol. 22, pp. 489–506, 2019.

[2] K. Christodoulopoulos, I. Tomkos, and E. A. Varvarigos, "Elastic bandwidth allocation in flexible ofdm-based optical networks," *Journal of Lightwave Technology*, vol. 29, no. 9, pp. 1354–1366, 2011.

[3] L. Velasco, M. Klinkowski, M. Ruiz, and J. Comellas, "Modeling the routing and spectrum allocation problem for flexgrid optical networks," *Photonic Network Communications*, vol. 24, pp. 177–186, 2012.

[4] K. Christodoulopoulos, I. Tomkos, and E. A. Varvarigos, "Routing and spectrum allocation in ofdm-based optical networks with elastic bandwidth allocation," in *2010 IEEE Global Telecommunications Conference GLOBECOM 2010*, pp. 1–6, IEEE, 2010.

[5] K. Walkowiak, *Modeling and optimization of cloud-ready and content-oriented networks*, vol. 56. Springer, 2016.

[6] M. Klinkowski and K. Walkowiak, "Routing and spectrum assignment in spectrum sliced elastic optical path network," *IEEE Communications Letters*, vol. 15, no. 8, pp. 884–886, 2011.

[7] A. Cai, G. Shen, L. Peng, and M. Zukerman, "Novel node-arc model and multiiteration heuristics for static routing and spectrum assignment in elastic optical networks," *Journal of Lightwave Technology*, vol. 31, no. 21, pp. 3402–3413, 2013.

[8] L. Velasco, A. Castro, M. Ruiz, and G. Junyent, "Solving routing and spectrum allocation related optimization problems: From off-line to in-operation flexgrid network planning," *Journal of Lightwave Technology*, vol. 32, no. 16, pp. 2780–2795, 2014.

[9] M. Yang, C. Zhang, Q. Wu, W. Zheng, and Y. Zhang, "Comparison of switching policies in terms of switching cost and network performance in static sdm-eons," *Optical Switching and Networking*, p. 100573, 2020.

[10] Y. Miyagawa, Y. Watanabe, M. Shigeno, K. Ishii, A. Takefusa, and A. Yoshise, "Bounds for two static optimization problems on routing and spectrum allocation of anycasting," *Optical switching and networking*, vol. 31, pp. 144–161, 2019.

[11] K. Walkowiak and M. Klinkowski, "Joint anycast and unicast routing for elastic optical networks: Modeling and optimization," in *2013 IEEE International Conference on Communications (ICC)*, pp. 3909–3914, IEEE, 2013.

[12] M. Klinkowski, P. Lechowicz, and K. Walkowiak, "Survey of resource allocation schemes and algorithms in spectrally-spatially flexible optical networking," *Optical Switching and Networking*, vol. 27, pp. 58–78, 2018.

[13] Y. Wang, X. Cao, Q. Hu, and Y. Pan, "Towards elastic and fine-granular bandwidth allocation in spectrum-sliced optical networks," *IEEE/OSA Journal of Optical Communications and Networking*, vol. 4, no. 11, pp. 906–917, 2012.

[14] M. Tornatore, C. Rottondi, R. Goscien, K. Walkowiak, G. Rizzelli, and A. Morea, "On the complexity of routing and spectrum assignment in flexible-grid ring networks," *Journal of Optical Communications and Networking*, vol. 7, no. 2, pp. A256–A267, 2015.

[15] M. Klinkowski, M. Żotkiewicz, K. Walkowiak, M. Pióro, M. Ruiz, and L. Velasco, "Solving large instances of the rsa problem in flexgrid elastic optical networks," *Journal of Optical Communications and Networking*, vol. 8, no. 5, pp. 320–330, 2016.

[16] Q. Wu, J. Wang, and M. Shigeno, "A novel channel-based model for the problem of routing, space, and spectrum assignment," *Optical Switching and Networking*, vol. 43, p. 100636, 2022.

[17] R. Goscień, K. Walkowiak, and M. Klinkowski, "Tabu search algorithm for routing, modulation and spectrum allocation in elastic optical network with anycast and unicast traffic," *Computer Networks: The International Journal of Computer and Telecommunications Networking*, vol. 79, no. C, pp. 148–165, 2015.

[18] L. Gong, X. Zhou, W. Lu, and Z. Zhu, "A two-population based evolutionary approach for optimizing routing, modulation and spectrum assignments (rmsa) in o-ofdm networks," *IEEE Communications letters*, vol. 16, no. 9, pp. 1520–1523, 2012.

[19] K. Walkowiak, P. Lechowicz, M. Klinkowski, and A. Sen, "Ilp modeling of flexgrid sdm optical networks," in *2016 17th International Telecommunications Network Strategy and Planning Symposium (Networks)*, pp. 121–126, IEEE, 2016.

[20] J. Perelló, J. M. Gené, A. Pagès, J. A. Lazaro, and S. Spadaro, "Flex-grid/sdm backbone network design with inter-core xt-limited transmission reach," *Journal of Optical Communications and Networking*, vol. 8, no. 8, pp. 540–552, 2016.

[21] C. Rottondi, P. Boffi, P. Martelli, and M. Tornatore, "Routing, modulation format, baud rate and spectrum allocation in optical metro rings with flexible grid and few-mode transmission," *Journal of Lightwave Technology*, vol. 35, no. 1, pp. 61–70, 2016.

[22] R. Proietti, L. Liu, R. P. Scott, B. Guan, C. Qin, T. Su, F. Giannone, and S. B. Yoo, "3d elastic optical networking in the temporal, spectral, and spatial domains," *IEEE Communications Magazine*, vol. 53, no. 2, pp. 79–87, 2015.

[23] L. Delvalle, E. Alfonzo, and D. P. P. Roa, "Eons: An online rsa simulator for elastic optical networks," in *2016 35th International Conference of the Chilean Computer Science Society (SCCC)*, pp. 1–12, IEEE, 2016.

[24] R. Rumipamba-Zambrano, J. Perelló, A. Pagès, J. M. Gené, and S. Spadaro, "Influence of the spatial super channel guard-band width on the performance of dynamic flex-grid/sdm optical core networks," in *2016 18th International Conference on Transparent Optical Networks (ICTON)*, pp. 1–4, IEEE, 2016.

[25] M. Yang, Q. Wu, K. Guo, and Y. Zhang, "Evaluation of device cost, power consumption, and network performance in spatially and spectrally flexible sdm optical networks," *Journal of Lightwave Technology*, vol. 37, no. 20, pp. 5259–5272, 2019.

[26] R. Rumipamba-Zambrano, J. Perelló, J. M. Gené, and S. Spadaro, "On the scalability of dynamic flex-grid/sdm optical core networks," *Computer Networks*, vol. 142, pp. 208–222, 2018.

[27] R. Rumipamba-Zambrano, F.-J. Moreno-Muro, J. Perelló, P. Pavón-Mariño, and S. Spadaro, "Space continuity constraint in dynamic flex-grid/sdm optical core networks: an evaluation with spatial and spectral super-channels," *Computer Communications*, vol. 126, pp. 38–49, 2018.

[28] J. Wang, M. Shigeno, and Q. Wu, "Ilp models and improved methods for the problem of routing and spectrum allocation," *Optical Switching and Networking*, vol. 45, p. 100675, 2022.

[29] J. Wang, H. Xuan, Y. Wang, Y. Yang, and S. Liu, "Optimization model and algorithm for routing and spectrum assignment in elastic optical networks," in *2018 14th International Conference on Computational Intelligence and Security (CIS)*, pp. 306–310, IEEE, 2018.

[30] K. Morita and K. Hirata, "Dynamic spectrum allocation method for reducing crosstalk in multi-core fiber networks," in *2017 International Conference on Information Networking (ICOIN)*, pp. 686–688, IEEE, 2017.

[31] H. Tode and Y. Hirota, "Routing, spectrum and core assignment for space division multiplexing elastic optical networks," in *2014 16th International Telecommunications Network Strategy and Planning Symposium (Networks)*, pp. 1–7, IEEE, 2014.

[32] Y. Hirota, Y. Hatada, T. Watanabe, and H. Tode, "Dynamic spectrum allocation based on connection alignment for elastic optical networks," in *2015 10th Asia-Pacific Symposium on Information and Telecommunication Technologies (APSITT)*, pp. 1–3, IEEE, 2015.

[33] P. S. Khodashenas, J. M. Rivas-Moscoso, D. Siracusa, F. Pederzolli, B. Shariati, D. Klonidis, E. Salvadori, and I. Tomkos, "Comparison of spectral and spatial superchannel allocation schemes for sdm networks," *Journal of Lightwave Technology*, vol. 34, no. 11, pp. 2710–2716, 2016.

[34] J. Rivas-Moscoso, B. Shariati, A. Mastropaolo, D. Klonidis, and I. Tomkos, "Cost benefit quantification of sdm network implementations based on spatially integrated network elements," in *ECOC 2016; 42nd European Conference on Optical Communication*, pp. 1–3, VDE, 2016.

[35] S. Fujii, Y. Hirota, H. Tode, and K. Murakami, "On-demand spectrum and core allocation for multi-core fibers in elastic optical network," in *Optical Fiber Communication Conference*, pp. OTh4B–4, Optical Society of America, 2013.

[36] S. Fujii, Y. Hirota, and H. Tode, "Dynamic resource allocation with virtual grid for space division multiplexed elastic optical network," in *39th European Conference and Exhibition on Optical Communication (ECOC 2013)*, pp. 1–3, IET, 2013.

[37] A. Muhammad, G. Zervas, D. Simeonidou, and R. Forchheimer, "Routing, spectrum and core allocation in flexgrid sdm networks with multi-core fibers," in *2014 International Conference on Optical Network Design and Modeling*, pp. 192–197, IEEE, 2014.

[38] S. Fujii, Y. Hirota, H. Tode, and K. Murakami, "On-demand spectrum and core allocation for reducing crosstalk in multicore fibers in elastic optical networks," *J. Opt. Commun. Netw.*, vol. 6, pp. 1059–1071, Dec 2014.

[39] S. Fujii, Y. Hirota, T. Watanabe, and H. Tode, "Dynamic spectrum and core allocation with spectrum region reducing costs of building modules in aod nodes," in *2014 16th International Telecommunications Network Strategy and Planning Symposium (Networks)*, pp. 1–6, IEEE, 2014.

[40] A. Muhammad, G. Zervas, G. Saridis, E. H. Salas, D. Simeonidou, and R. Forchheimer, "Flexible and synthetic sdm networks with multi-core-fibers implemented by programmable roadms," in *2014 The European Conference on Optical Communication (ECOC)*, pp. 1–3, IEEE, 2014.

[41] Y. Li, N. Hua, and X. Zheng, "Routing, wavelength and core allocation planning for multi-core fiber networks with mimo-based crosstalk suppression," in *2015 Opto-Electronics and Communications Conference (OECC)*, pp. 1–3, IEEE, 2015.

[42] A. Muhammad, G. Zervas, and R. Forchheimer, "Resource allocation for space-division multiplexing: optical white box versus optical black box networking," *Journal of Lightwave Technology*, vol. 33, no. 23, pp. 4928–4941, 2015.

[43] R. Zhu, Y. Zhao, H. Yang, Y. Tan, H. Chen, J. Zhang, and J. P. Jue, "Dynamic virtual optical network embedding in spectral and spatial domains over elastic optical networks with multicore fibers," *Optical Engineering*, vol. 55, no. 8, p. 086108, 2016.

[44] R. Zhu, Y. Zhao, J. Zhang, H. Yang, Y. Tan, and J. P. Jue, "Multi-dimensional resource virtualization in spectral and spatial domains for inter-datacenter optical networks," in *2016 Optical Fiber Communications Conference and Exhibition (OFC)*, pp. 1–3, IEEE, 2016.

[45] H. Tode and Y. Hirota, "Routing, spectrum and core assignment on sdm optical networks," in *2016 Optical Fiber Communications Conference and Exhibition (OFC)*, pp. 1–3, IEEE, 2016.

[46] Y. Li, Y. Li, N. Hua, and X. Zheng, "Shared backup path protection in multi-core fiber networks with mimo-based crosstalk suppression," in *Optical Fiber Communication Conference*, pp. Tu2H–7, Optical Society of America, 2016.

[47] R. Zhu, Y. Zhao, H. Yang, Y. Tan, X. Yu, G. Gao, J. Zhang, N. Wang, and J. P. Jue, "Crosstalk-aware virtual optical network embedding (vone) in spatial division

multiplexing enabled elastic optical networks with multi-core fibers," in *ECOC 2016; 42nd European Conference on Optical Communication*, pp. 1–3, VDE, 2016.

[48] H. Tode and Y. Hirota, "Routing, spectrum, and core and/or mode assignment on space-division multiplexing optical networks," *Journal of Optical Communications and Networking*, vol. 9, no. 1, pp. A99–A113, 2017.

[49] Y. Zhao, R. Tian, X. Yu, J. Zhang, and J. Zhang, "An auxiliary graph based dynamic traffic grooming algorithm in spatial division multiplexing enabled elastic optical networks with multi-core fibers," *Optical Fiber Technology*, vol. 34, pp. 52–58, 2017.

[50] R. Rumipamba-Zambrano, F.-J. Moreno-Muro, P. Pavón-Marino, J. Perelló, S. Spadaro, and J. Solé-Pareta, "Assessment of flex-grid/mcf optical networks with roadm limited core switching capability," in *2017 International Conference on Optical Network Design and Modeling (ONDM)*, pp. 1–6, IEEE, 2017.

[51] F.-J. Moreno-Muro, R. Rumipamba-Zambrano, P. Pavón-Marino, J. Perelló, J. M. Gené, and S. Spadaro, "Evaluation of core-continuity-constrained roadms for flex-grid/mcf optical networks," *Journal of Optical Communications and Networking*, vol. 9, no. 11, pp. 1041–1050, 2017.

[52] B. Shariati, J. M. Rivas-Moscoso, D. M. Marom, S. Ben-Ezra, D. Klonidis, L. Velasco, and I. Tomkos, "Impact of spatial and spectral granularity on the performance of sdm networks based on spatial superchannel switching," *Journal of Lightwave Technology*, vol. 35, no. 13, pp. 2559–2568, 2017.

[53] Y. Tan, R. Zhu, H. Yang, Y. Zhao, J. Zhang, Z. Liu, Q. Qu, and Z. Zhou, "Crosstalk-aware provisioning strategy with Dedicated Path Protection for elastic multi-core fiber networks," in *Optical Communications and Networks (ICOCN), 2016 15th International Conference on*, pp. 1–3, IEEE, 2016.

[54] F. Pederzolli, D. Siracusa, J. M. Rivas-Moscoso, B. Shariati, E. Salvadori, and I. Tomkos, "Spatial group sharing for sdm optical networks with joint switching," in *2016 International Conference on Optical Network Design and Modeling (ONDM)*, pp. 1–6, IEEE, 2016.

[55] F. Pederzolli, D. Siracusa, B. Shariati, J. M. Rivas-Moscoso, E. Salvadori, and I. Tomkos, "Improving performance of spatially joint-switched space division multiplexing optical networks via spatial group sharing," *IEEE/OSA Journal of Optical Communications and Networking*, vol. 9, no. 3, pp. B1–B11, 2017.

[56] P. M. Moura and N. L. da Fonseca, "Routing, core and spectrum assignment based on connected component labelling for sdm optical networks," in *2016 IEEE International Conference on Communications (ICC)*, pp. 1–6, IEEE, 2016.

[57] L. Zhang, N. Ansari, and A. Khreishah, "Anycast planning in space division multiplexing elastic optical networks with multi-core fibers," *IEEE Communications Letters*, vol. 20, no. 10, pp. 1983–1986, 2016.

[58] M. N. Dharmaweera, L. Yan, M. Karlsson, and E. Agrell, "Nonlinear-impairments- and crosstalk-aware resource allocation schemes for multicore-fiber-based flexgrid networks," in *ECOC 2016; 42nd European Conference on Optical Communication*, pp. 1–3, VDE, 2016.

[59] C. Rottondi, P. Boffi, P. Martelli, M. Tornatore, and A. Pattavina, "Optimal resource allocation in distance-adaptive few-modes backbone networks with flexible grid," in *Asia Communications and Photonics Conference*, pp. AS4H–2, Optical Society of America, 2015.

[60] H. Huang, S. Huang, S. Yin, M. Zhang, J. Zhang, and W. Gu, "Virtual network provisioning over space division multiplexed optical networks using few-mode fibers," *IEEE/OSA Journal of Optical Communications and Networking*, vol. 8, no. 10, pp. 726–733, 2016.

[61] D. Siracusa, F. Pederzolli, D. Klonidisz, V. Lopezy, and E. Salvadori, "Resource allocation policies in sdm optical networks," in *2015 International Conference on Optical Network Design and Modeling (ONDM)*, pp. 168–173, IEEE, 2015.

[62] J. Wang, S. Chen, Q. Wu, Y. Tan, and M. Shigeno, "Solving the static resource-allocation problem in sdm-eons via a node-type ilp model," *Sensors*, vol. 22, no. 24, p. 9710, 2022.

[63] Q. Wu, J. Wang, S. Chen, and A. Kanai, "Resource allocation problem in multi-band space-division multiplexing elastic optical networks," in *2022 18th International Conference on Computational Intelligence and Security (CIS)*, pp. 225–228, IEEE, 2022.

[64] D. Siracusa, F. Pederzolli, P. Khodashenas, J. Rivas-Moscoso, D. Klonidis, E. Salvadori, and I. Tomkos, "Spectral vs. spatial super-channel allocation in sdm networks under independent and joint switching paradigms," in *2015 European Conference on Optical Communication (ECOC)*, pp. 1–3, IEEE, 2015.

[65] B. Shariati, P. S. Khodashenas, J. M. Rivas-Moscoso, S. Ben-Ezra, D. Klonidis, F. Jiménez, L. Velasco, and I. Tomkos, "Evaluation of the impact of different sdm switching strategies in a network planning scenario," in *Optical Fiber Communication Conference*, pp. Tu2H–4, Optical Society of America, 2016.

[66] B. Shariati, D. Klonidis, J. M. Rivas-Moscoso, and I. Tomkos, "Evaluation of the impact of spatial and spectral granularities on the performance of spatial superchannel switching schemes," in *2016 18th International Conference on Transparent Optical Networks (ICTON)*, pp. 1–4, IEEE, 2016.

[67] B. Shariati, D. Klonidis, D. Siracusa, F. Pederzolli, J. Rivas-Moscoso, L. Velasco, and I. Tomkos, "Impact of traffic profile on the performance of spatial superchannel switching in sdm networks," in *ECOC 2016; 42nd European Conference on Optical Communication*, pp. 1–3, VDE, 2016.

[68] Y. Zhao and J. Zhang, "Crosstalk-aware cross-core virtual concatenation in spatial division multiplexing elastic optical networks," *Electronics Letters*, vol. 52, no. 20, pp. 1701–1703, 2016.

[69] Z. Shi, Y. Zhao, X. Yu, Y. Li, J. Zhang, C. Liu, G. Zhang, and Z. Liu, "Contaminated area-based rsca algorithm for super-channel in flex-grid enabled sdm networks," in *Asia Communications and Photonics Conference*, pp. ATh2E–4, Optical Society of America, 2016.

[70] Q. Yao, H. Yang, Y. Zhao, R. Zhu, J. Zhang, and J. Wu, "Crosstalk-aware routing, spectrum, and core assignment in elastic optical networks with multi-core fibers," in *Asia Communications and Photonics Conference 2016*, p. ATh2C.1, Optical Society of America, 2016.

[71] Y. Tan, H. Yang, R. Zhu, Y. Zhao, J. Zhang, Z. Liu, Q. Ou, and Z. Zhou, "Distance adaptive routing, core and spectrum allocation in space division multiplexing optical networks with multi-core fibers," in *Asia Communications and Photonics Conference*, pp. AF2A–159, Optical Society of America, 2016.

[72] N.-P. Diamantopoulos, B. Shariati, and I. Tomkos, "On the power consumption of mimo processing and its impact on the performance of sdm networks," in *2017 Optical Fiber Communications Conference and Exhibition (OFC)*, pp. 1–3, IEEE, 2017.

[73] R. Rumipamba-Zambrano, J. Perelló, J. M. Gené, and S. Spadaro, "Capacity quantification of joint-switching-enabled flex-grid/sdm optical backbone networks," in *2017*

Optical Fiber Communications Conference and Exhibition (OFC), pp. 1–3, IEEE, 2017.

[74] "Transatlantic communications cable." Available: https://en.wikipedia.org/wiki.

[75] A. K. Dutta, N. K. Dutta, and M. Fujiwara, *WDM Technologies: Passive Optical Components*, vol. 2. Academic press, 2003.

[76] S. Arnon, J. Barry, G. Karagiannidis, R. Schober, and M. Uysal, *Advanced optical wireless communication systems*. Cambridge university press, 2012.

[77] R. Ramaswami, K. Sivarajan, and G. Sasaki, *Optical networks: a practical perspective*. Morgan Kaufmann, 2009.

[78] G. Shen and M. Zukerman, "Spectrum-efficient and agile co-ofdm optical transport networks: architecture, design, and operation," *IEEE Communications Magazine*, vol. 50, no. 5, pp. 82–89, 2012.

[79] M. Jinno, H. Takara, B. Kozicki, Y. Tsukishima, Y. Sone, and S. Matsuoka, "Spectrum-efficient and scalable elastic optical path network: architecture, benefits, and enabling technologies," *IEEE communications magazine*, vol. 47, no. 11, pp. 66–73, 2009.

[80] P. J. Winzer, "Spatial multiplexing: The next frontier in network capacity scaling," in *IET Conference Proceedings*, The Institution of Engineering & Technology, 2013.

[81] D. Richardson, J. Fini, and L. E. Nelson, "Space-division multiplexing in optical fibres," *Nature Photonics*, vol. 7, no. 5, p. 354, 2013.

[82] A. Ferrari, A. Napoli, J. K. Fischer, N. Costa, J. Pedro, N. Sambo, E. Pincemin, B. Sommerkohrn-Krombholz, and V. Curri, "Upgrade capacity scenarios enabled by multi-band optical systems," in *2019 21st International Conference on Transparent Optical Networks (ICTON)*, pp. 1–4, IEEE, 2019.

[83] A. Napoli, N. Calabretta, J. K. Fischer, N. Costa, S. Abrate, J. Pedro, V. Lopez, V. Curri, D. Zibar, E. Pincemin, *et al.*, "Perspectives of multi-band optical communication systems," in *2018 23rd Opto-Electronics and Communications Conference (OECC)*, pp. 1–2, IEEE, 2018.

[84] N. Sambo, B. Correia, A. Napoli, J. Pedro, L. Kiani, P. Castoldi, and V. Curri, "Network upgrade exploiting multi band: S-or e-band?," *Journal of Optical Communications and Networking*, vol. 14, no. 9, pp. 749–756, 2022.

[85] M. Jinno, "Spatial channel network (scn) architecture employing growable and reliable spatial channel cross-connects toward massive sdm era," in *2018 Photonics in Switching and Computing (PSC)*, pp. 1–3, IEEE, 2018.

[86] M. Jinno, "Opportunities, challenges, and solutions for spatial channel networks (scns) toward the sdm abundant era," in *2019 24th OptoElectronics and Communications Conference (OECC) and 2019 International Conference on Photonics in Switching and Computing (PSC)*, pp. 1–3, IEEE, 2019.

[87] M. Jinno, "Spatial channel network (scn): Opportunities and challenges of introducing spatial bypass toward the massive sdm era," *Journal of Optical Communications and Networking*, vol. 11, no. 3, pp. 1–14, 2019.

[88] M. Jinno, "Spatial channel cross-connect architectures for spatial channel networks," *IEEE Journal of Selected Topics in Quantum Electronics*, vol. 26, no. 4, pp. 1–16, 2020.

[89] M. Jinno, T. Kodama, and T. Ishikawa, "Feasibility demonstration of spatial channel networking using sdm/wdm hierarchical approach for peta-b/s optical transport," *Journal of Lightwave Technology*, vol. 38, no. 9, pp. 2577–2586, 2020.

[90] Z. Luo, S. Yin, L. Zhao, Z. Wang, W. Zhang, L. Jiang, and S. Huang, "Survivable routing, spectrum, core and band assignment in multi-band space division multiplexing-elastic optical networks," *Journal of Lightwave Technology*, vol. 40, no. 11, pp. 3442–3455, 2022.

[91] C. Metz, "Ip anycast point-to-(any) point communication," *IEEE Internet computing*, vol. 6, no. 2, pp. 94–98, 2002.

[92] the Fiber Optic Association, "Optical fiber." Available: https://www.thefoa.org.

[93] A. A. Saleh and J. M. Simmons, "All-optical networking—evolution, benefits, challenges, and future vision," *Proceedings of the IEEE*, vol. 100, no. 5, pp. 1105–1117, 2012.

[94] B. Zhu, L. Leng, A. Gnauck, M. Pedersen, D. Peckham, L. Nelson, S. Stulz, S. Kado, L. Gruner-Nielsen, R. Lingle, *et al.*, "Transmission of 3.2 tb/s (80× 42.7 gb/s) over 5200 km of ultrawave™ fiber with 100-km dispersion-managed spans using rz-dpsk format," in *2002 28TH European Conference on Optical Communication*, vol. 5, pp. 1–2, IEEE, 2002.

[95] M. Ali and J. Deogun, "Allocation of multicast nodes in wavelength-routed networks," in *ICC 2001. IEEE International Conference on Communications. Conference Record (Cat. No. 01CH37240)*, vol. 2, pp. 614–618, IEEE, 2001.

[96] S. Azodolmolky, M. Klinkowski, E. Marin, D. Careglio, J. S. Pareta, and I. Tomkos, "A survey on physical layer impairments aware routing and wavelength assignment algorithms in optical networks," *Computer networks*, vol. 53, no. 7, pp. 926–944, 2009.

[97] ITU-T, "Extension of rec. g.694.1," Dec 2011.

[98] W. Shieh and C. Athaudage, "Coherent optical orthogonal frequency division multiplexing," *Electronics letters*, vol. 42, no. 10, pp. 587–589, 2006.

[99] J. Armstrong, "Ofdm for optical communications," *Journal of lightwave technology*, vol. 27, no. 3, pp. 189–204, 2009.

[100] W. Shieh and I. Djordjevic, *OFDM for optical communications*. Academic Press, 2009.

[101] J. Armstrong and A. Lowery, "Power efficient optical ofdm," *Electronics letters*, vol. 42, no. 6, p. 1, 2006.

[102] W. Shieh, H. Bao, and Y. Tang, "Coherent optical ofdm: theory and design," *Opt. Express*, vol. 16, pp. 841–859, Jan 2008.

[103] G. Bosco, V. Curri, A. Carena, P. Poggiolini, and F. Forghieri, "On the performance of nyquist-wdm terabit superchannels based on pm-bpsk, pm-qpsk, pm-8qam or pm-16qam subcarriers," *Journal of Lightwave Technology*, vol. 29, no. 1, pp. 53–61, 2010.

[104] R. Schmogrow, S. Wolf, B. Baeuerle, D. Hillerkuss, B. Nebendahl, C. Koos, W. Freude, and J. Leuthold, "Nyquist frequency division multiplexing for optical communications," in *CLEO: Science and Innovations*, pp. CTh1H–2, Optical Society of America, 2012.

[105] P. Schindler, R. Schmogrow, S. Wolf, B. Bäuerle, B. Nebendahl, C. Koos, W. Freude, and J. Leuthold, "Full flex-grid asynchronous multiplexing demonstrated with nyquist pulse-shaping," *Optics Express*, vol. 22, no. 9, pp. 10923–10937, 2014.

[106] R. Rudnick, A. Tolmachev, D. Sinefeld, O. Golani, S. Ben-Ezra, M. Nazarathy, and D. M. Marom, "Sub-banded/single-sub-carrier drop-demux and flexible spectral shaping with a fine resolution photonic processor," in *2014 The European Conference on Optical Communication (ECOC)*, pp. 1–3, IEEE, 2014.

[107] M.-F. Huang, A. Tanaka, E. Ip, Y.-K. Huang, D. Qian, Y. Zhang, S. Zhang, P. N. Ji, I. B. Djordjevic, T. Wang, *et al.*, "Terabit/s nyquist superchannels in high capacity fiber field trials using dp-16qam and dp-8qam modulation formats," *Journal of lightwave technology*, vol. 32, no. 4, pp. 776–782, 2013.

[108] A. Bocoi, M. Schuster, F. Rambach, M. Kiese, C.-A. Bunge, and B. Spinnler, "Reach-dependent capacity in optical networks enabled by ofdm," in *2009 Conference on Optical Fiber Communication-incudes post deadline papers*, pp. 1–3, IEEE, 2009.

[109] M. Klinkowski and K. Walkowiak, "On performance gains of flexible regeneration and modulation conversion in translucent elastic optical networks with superchannel transmission," *Journal of lightwave technology*, vol. 34, no. 23, pp. 5485–5495, 2016.

[110] M. Klinkowski and K. Walkowiak, "A heuristic algorithm for routing, spectrum, transceiver and regeneration allocation problem in elastic optical networks," in *2016 18th International Conference on Transparent Optical Networks (ICTON)*, pp. 1–4, IEEE, 2016.

[111] B. Kozicki, H. Takara, T. Yoshimatsu, K. Yonenaga, and M. Jinno, "Filtering characteristics of highly-spectrum efficient spectrum-sliced elastic optical path (slice) network," in *Optical Fiber Communication Conference*, p. JWA43, Optica Publishing Group, 2009.

[112] Y. Wang, X. Cao, and Y. Pan, "A study of the routing and spectrum allocation in spectrum-sliced elastic optical path networks," in *2011 Proceedings Ieee Infocom*, pp. 1503–1511, IEEE, 2011.

[113] G. M. Saridis, D. Alexandropoulos, G. Zervas, and D. Simeonidou, "Survey and evaluation of space division multiplexing: From technologies to optical networks," *IEEE Communications Surveys & Tutorials*, vol. 17, no. 4, pp. 2136–2156, 2015.

[114] B. Li, L. Gan, S. Fu, Z. Xu, M. Tang, W. Tong, and P. P. Shum, "The role of effective area in the design of weakly coupled mcf: Optimization guidance and osnr improvement," *IEEE Journal of Selected Topics in Quantum Electronics*, vol. 22, no. 2, pp. 81–87, 2015.

[115] T. Hayashi, T. Taru, O. Shimakawa, T. Sasaki, and E. Sasaoka, "Characterization of crosstalk in ultra-low-crosstalk multi-core fiber," *Journal of Lightwave Technology*, vol. 30, no. 4, pp. 583–589, 2011.

[116] J. Sakaguchi, B. J. Puttnam, W. Klaus, Y. Awaji, N. Wada, A. Kanno, T. Kawanishi, K. Imamura, H. Inaba, K. Mukasa, *et al.*, "305 tb/s space division multiplexed transmission using homogeneous 19-core fiber," *Journal of Lightwave Technology*, vol. 31, no. 4, pp. 554–562, 2012.

[117] R. Ryf, A. Sierra, R.-J. Essiambre, A. Gnauck, S. Randel, M. Esmaeelpour, S. Mumtaz, P. Winzer, R. Delbue, P. Pupalaikis, *et al.*, "Coherent 1200-km 6× 6 mimo mode-multiplexed transmission over 3-core microstructured fiber," in *European Conference and Exposition on Optical Communications*, pp. Th–13, Optical Society of America, 2011.

[118] R. Ryf, R. Essiambre, A. Gnauck, S. Randel, M. A. Mestre, C. Schmidt, P. Winzer, R. Delbue, P. Pupalaikis, A. Sureka, *et al.*, "Space-division multiplexed transmission over 4200 km 3-core microstructured fiber," in *National Fiber Optic Engineers Conference*, pp. PDP5C–2, Optical Society of America, 2012.

[119] R. Ryf, N. Fontaine, B. Guan, R.-J. Essiambre, S. Randel, A. Gnauck, S. Chandrasekhar, A. Adamiecki, G. Raybon, B. Ercan, *et al.*, "1705-km transmission over coupled-core fibre supporting 6 spatial modes," in *2014 The European Conference on Optical Communication (ECOC)*, pp. 1–3, IEEE, 2014.

[120] R. Ryf, S. Randel, A. H. Gnauck, C. Bolle, A. Sierra, S. Mumtaz, M. Esmaeelpour, E. C. Burrows, R.-J. Essiambre, P. J. Winzer, *et al.*, "Mode-division multiplexing over 96 km of few-mode fiber using coherent 6 *times* 6 mimo processing," *Journal of Lightwave technology*, vol. 30, no. 4, pp. 521–531, 2011.

[121] S. Randel, R. Ryf, A. Sierra, P. J. Winzer, A. H. Gnauck, C. A. Bolle, R.-J. Essiambre, D. W. Peckham, A. McCurdy, and R. Lingle, "6× 56-gb/s mode-division multiplexed transmission over 33-km few-mode fiber enabled by 6× 6 mimo equalization," *Optics Express*, vol. 19, no. 17, pp. 16697–16707, 2011.

[122] R. Ryf, N. Fontaine, B. Guan, B. Huang, M. Esmaeelpour, S. Randel, A. Gnauck, S. Chandrasekhar, A. Adamiecki, G. Raybon, *et al.*, "305-km combined wavelength and mode-multiplexed transmission over conventional graded-index multimode fibre," in *2014 The European Conference on Optical Communication (ECOC)*, pp. 1–3, IEEE, 2014.

[123] N. K. Fontaine, R. Ryf, H. Chen, A. V. Benitez, J. A. Lopez, R. A. Correa, B. Guan, B. Ercan, R. P. Scott, S. B. Yoo, *et al.*, "30× 30 mimo transmission over 15 spatial modes," in *Optical Fiber Communication Conference*, pp. Th5C–1, Optical Society of America, 2015.

[124] T. Hayashi, T. Nagashima, K. Yonezawa, Y. Wakayama, D. Soma, K. Igarashi, T. Tsuritani, and T. Sasaki, "6-mode 19-core fiber for weakly-coupled mode-multiplexed transmission over uncoupled cores," in *Optical Fiber Communication Conference*, pp. W1F–4, Optical Society of America, 2016.

[125] R. Van Uden, R. A. Correa, E. A. Lopez, F. Huijskens, C. Xia, G. Li, A. Schülzgen, H. De Waardt, A. Koonen, and C. Okonkwo, "Ultra-high-density spatial division multiplexing with a few-mode multicore fibre," *Nature Photonics*, vol. 8, no. 11, p. 865, 2014.

[126] A. Muhammad, M. Furdek, G. Zervas, and L. Wosinska, "Filterless networks based on optical white boxes and sdm," in *ECOC 2016; 42nd European Conference on Optical Communication*, pp. 1–3, VDE, 2016.

[127] Y. Yang, X. Chen, H. Yan, B. Hua, J. Li, Y. Hao, Z. Chen, and Y. He, "A scattered-spectrum-scan routing and spectrum allocati2020on scheme for spatial-division-multiplexing optical networks based on blocking oxcs," in *Asia Communications and Photonics Conference*, pp. ATh2E–2, Optical Society of America, 2016.

[128] Y. Li, N. Hua, and X. Zheng, "A capacity analysis for space division multiplexing optical networks with mimo equalization," in *Optical Fiber Communication Conference*, pp. Th2A–15, Optical Society of America, 2017.

[129] S. Randel, P. J. Winzer, M. Montoliu, and R. Ryf, "Complexity analysis of adaptive frequency-domain equalization for mimo-sdm transmission," in *39th European Conference and Exhibition on Optical Communication (ECOC 2013)*, pp. 1–3, IET, 2013.

[130] T. Matsui, T. Sakamoto, Y. Goto, K. Saito, K. Nakajima, F. Yamamoto, and T. Kurashima, "Design of 125 μm cladding multi-core fiber with full-band compatibility to conventional single-mode fiber," in *2015 European Conference on Optical Communication (ECOC)*, pp. 1–3, IEEE, 2015.

[131] H. Takara, A. Sano, T. Kobayashi, H. Kubota, H. Kawakami, A. Matsuura, Y. Miyamoto, Y. Abe, H. Ono, K. Shikama, *et al.*, "1.01-pb/s (12 sdm/222 wdm/456 gb/s) crosstalk-managed transmission with 91.4-b/s/hz aggregate spectral efficiency," in *European Conference and Exhibition on Optical Communication*, pp. Th–3, Optical Society of America, 2012.

[132] P. S. Khodashenas, J. M. Rivas-Moscoso, B. Shariati, D. M. Marom, D. Klonidis, and I. Tomkos, "Investigation of spectrum granularity for performance optimization

of flexible nyquist-wdm-based optical networks," *Journal of Lightwave Technology*, vol. 33, no. 23, pp. 4767–4774, 2015.

[133] H. Yuan, M. Furdek, A. Muhammad, A. Saljoghei, L. Wosinska, and G. Zervas, "Space-division multiplexing in data center networks: on multi-core fiber solutions and crosstalk-suppressed resource allocation," *Journal of Optical Communications and Networking*, vol. 10, no. 4, pp. 272–288, 2018.

[134] M. Klinkowski and K. Walkowiak, "An efficient optimization framework for solving rssa problems in spectrally and spatially flexible optical networks," *IEEE/ACM Transactions on Networking*, vol. 27, no. 4, pp. 1474–1486, 2019.

[135] Online, "Gurobi v9.0.1." Available: http://www.gurobi.com, 2020.

[136] Online, "Gurobi v9.5.2." Available: http://www.gurobi.com, 2022.

[137] G. Shen, H. Guo, and S. K. Bose, "Survivable elastic optical networks: survey and perspective," *Photonic Network Communications*, vol. 31, pp. 71–87, 2016.

[138] H. M. Oliveira and N. L. da Fonseca, "Routing, spectrum and core assignment algorithms for protection of space division multiplexing elastic optical networks," *Journal of Network and Computer Applications*, vol. 128, pp. 78–89, 2019.

[139] E. E. Moghaddam, H. Beyranvand, and J. A. Salehi, "Crosstalk-aware resource allocation in survivable space-division-multiplexed elastic optical networks supporting hybrid dedicated and shared path protection," *Journal of Lightwave Technology*, vol. 38, no. 6, pp. 1095–1102, 2019.

[140] S. Paira, M. Chatterjee, and U. Bhattacharya, "On survivable energy-efficient and crosstalk-aware routing, spectrum and core allocation schemes for dynamic multiclass traffic in sdm-eons," *Optical Switching and Networking*, vol. 42, p. 100630, 2021.

[141] M. W. Przewozniczek, R. Goścień, P. Lechowicz, and K. Walkowiak, "Metaheuristic algorithms with solution encoding mixing for effective optimization of sdm optical networks," *Engineering Applications of Artificial Intelligence*, vol. 95, p. 103843, 2020.